Antidepressant action of optogenetic stimulation of serotonin-prefrontal cortical projections in chronically stressed female mice via hippocampal modulation

Alberto Francisco Fuentes Alvarenga

A thesis submitted to the Faculty of Medicine in partial fulfillment of the requirements for the Master's degree in Neuroscience

Department of Cellular and Molecular Medicine
Faculty of Medicine
University of Ottawa

Table of Contents

List of Tables ..... **v**

List of Figures ..... **vi**

List of abbreviations ..... **viii**

Acknowledgement ..... **x**

Contributions ..... **xi**

Abstract ..... **xii**

1. Introduction **1**

1.1 Major Depressive Disorder 1
1.2 Serotonin 2
1.3 Serotonin in MDD 3
1.4 Treatment options 5
1.4.1 Monoamine Oxidase Inhibitors 5
1.4.2 Tricyclic Antidepressants 5
1.4.3 Selective Serotonin Reuptake Inhibitor (SSRIs) 6
1.4.4 Electroconvulsive Therapy 7
1.4.5 Repetitive Transcranial Magnetic Stimulation 7
1.4.6 Deep Brain Stimulation 7
1.4.7 Transcranial Direct Current Stimulation 8
1.5 Chronic stress 8
1.6 Animal Models of Depression 10
1.6.1 Early life stress model 11
1.6.2 Social defeat model 11
1.6.3 Chronic restraint stress model 12
1.6.4 Chronic corticosterone (CORT) model 12
1.6.5 Unpredictable chronic mild stress (UCMS) 12
1.7 Novel approach-Optogenetic stimulation 13
1.8 Objectives and Rationale 15
1.9 Hypothesis 16

2. Methodology **18**

2.1 Animal handling and housing 18
2.2 Mouse line 18
2.3 Genotyping 18
2.4 Cohorts 19
2.5 Unpredictable Chronic Mild Stress (UCMS) 19
2.6 Optogenetic implantation and stimulation 21
2.6.1 Optical Fiber Implants 21
2.6.2 Surgery 21
2.6.3 Behaviour tests and ON/OFF Stimulation Paradigm 22
2.7 Phenotypical assessments 22
2.7.1 Coat state 23
2.7.2 Behavioral assays 23

2.7.2.a Elevated Plus Maze (EPM) test 23
2.7.2.b Open field (OF) test 24
2.7.2.c Tail suspension (TS) test 24
2.7.2.d Forced Swim Test (FST) 24
2.7.2.e Novelty-Suppressed Feeding (NSF) Test 24
2.7.2.f Naïve animals' behaviour tests 25
2.8 Magnetic Resonance Imaging 25
2.8.1 Hippocampal volumetric measurements 26
2.9 Brain sectioning 28
2.10 Immunofluorescent staining (FosB) 28
2.11 Immunofluorescence of 5-HT synaptic and triad structures 31
2.12 Imaging 31
2.13 FosB+ Cell quantification 32
2.14 Image analysis using Imaris 10.1 for synaptic triad formations 32
2.15 Statistical Analyses 33

3. Results 35

3.1 Behavioral changes 35
3.1.1 Coat state 35
3.1.2 Elevated Plus Maze 35
3.1.3 Open Field 38
3.1.4 Tail Suspension Test 40
3.1.5 Novelty Supressed Feeding 40
3.1.6 Forced Swim Test 40
3.2 Changes in Dorsal Raphe 43
3.2.1 Chronic activity changes in the DR 43
3.2.2 Serotonergic neurons 44
3.2.3 Chronic activity of serotonergic neurons 46
3.3 Chronic neuronal activity 48
3.4 Chronic excitatory neural activity 52
3.5 Chronic inhibitory neuronal activity 56
3.6 Hippocampal volume changes 60
3.7 5-HT projection changes (axonal volume and varicosity density) 62
3.8 5-HT synapse formation changes 69
3.9 Inhibitory and excitatory 5-HT triadic synapses 73

4. Discussion 81

4.1 Chronic stress promoted behaviours changes associated with depressive and anxiety like phenotypes 81
4.2 Optogenetic stimulation had antidepressant effects related to behavior in Pet-ChR2 mice 83
4.3 Optogenetic stimulation induced anxiogenic like behaviours 85
4.4 Chronic stress attenuated chronic activity throughout the brain 87
4.5 Chronic stress induced reduction in 5-HT synapses and reductions in excitatory and inhibitory 5-HT triadic synapses 89
4.6 Optogenetic stimulation increased serotonin activity and induced hippocampal activation 90

5. Conclusion 92
6. Future steps 97
Supplemental figures 98
References 99

List of Tables

Table 1. Schedule for UCMS protocol **20**

Table 2. Coordinates relative to bregma of areas assessed by immunofluorescence **28**

Table 3. Primary and secondary antibodies used for immunofluorescence staining **30**

Supplemental table 1. F and P values of all statistical comparisons **98**

List of Figures

Figure 1. Visual representation of methodological approach for UCMS and opto-stimulation. **27**

Figure 2. Deterioration in coat state and increased anxiety-like behaviours in EPM due to UCMS exposure. **37**

Figure 3. Increased anxiety-like behaviour in OF test of mice exposed to UCMS. **39**

Figure 4. Increased depressive-like behaviour in TST due to UCMS with robust antidepressant effect from opto-stimulation. **42**

Figure 5. Increased chronic activity of the dorsal raphe and decrease TPH+ cells due to stress. **45**

Figure 6. Significant increase of serotonergic chronic activity in dorsal raphe of optogenetic stimulated Pet-ChR2 mice. **47**

Figure 7. Significant chronic activity decreases due to UCMS, and chronic activity potentiation in CA1 shown by FosB staining. **49**

Figure 8. Chronic activity decreases shown by FosB quantification due to UCMS exposure. **51**

Figure 9. Significant decrease of chronic excitatory activity due to UCMS in CG and PrL, and potentiation of MSN and CA1 due to opto-stimulation. **53**

Figure 10. Excitatory chronic activity changes shown by CaMKIIα+/FosB+ co-localization and quantification. **55**

Figure 11. Significant decrease in chronic inhibitory activity shown by the quantification of the co-localization of GAD67+/FosB+ cells staining induced by UCMS. **57**

Figure 12. Decreases in inhibitory chronic activity shown by GAD67+/FosB+ co-localization and quantification. **59**

Figure 13. Decrease in hippocampal volume of chronically stressed compared to unstressed mice. **61**

Figure 14. Representative images of 5-HT axonal volume and density of varicosities of the CG shown by the reconstruction of SERT immuno-stained sections using Imaris 64x 10.1. **63**

Figure 15. UCMS induced region-specific decrease of 5-HT axonal volume. **66**

Figure 16. UCMS induced region-specific decrease of 5-HT varicosities. **68**

Figure 17. UCMS induced decrease in 5-HT excitatory synaptic contacts. **71**

Figure 18. UCMS induced decrease in 5-HT inhibitory synaptic contacts. **72**

Figure 19. Sections were stained with SERT, synaptophysin (synaptic marker), and postsynaptic marker PSD95 or GD67 to visualize 5-HT triads. **74**

Figure 20. Decrease of presynaptic excitatory triads. **76**

Figure 21. Changes in presynaptic inhibitory triads. Sections were stained with SERT, synaptophysin (synaptic marker), and postsynaptic marker GAD67 to visualize inhibitory triads. **77**

Figure 22. Changes in postsynaptic excitatory triads. Sections were stained with SERT, synaptophysin (synaptic marker), and postsynaptic marker PSD95 to visualize excitatory triads. **79**

Figure 23. Changes in postsynaptic inhibitory triads. Sections were stained with SERT, synaptophysin (synaptic marker), and postsynaptic marker GAD67 to visualize inhibitory triads. **80**

Figure 24. Optogenetic stimulation microcircuitry. **96**

List of abbreviations

5-HT Serotonin; 5-hydroxytryptamine

5-HIAA 5-hydroxyindoleacetic acid

5-HTP 5-Hydroxytryptophan

5-HT1A Serotonin 1A receptor

ANOVA Analysis of variance

BLA Basolateral amygdala

CG Cingulate Gyrus

ChR2 Channelrhodopsin

DG Dentate Gyrus

DR Dorsal raphe

EC Entorhinal cortex

EPM Elevated plus maze

FST Forced swim test

IL Infralimbic

LSN Lateral septum

MDD Major Depressive Disorder

MO Medial Orbital Cortex

mPFC medial Prefrontal cortex

MR Median raphe

MSN Medial septum

NAc Nucleus accumbens

NSF Novelty Suppressed Feeding

OF Open field test

Pet-ChR2 Pet-Channelrhodopsin

PrL Prelimbic

SERT Serotonin transporter

SSRI Selective serotonin reuptake inhibitor

TPH Tryptophan hydroxylase

TS Tail suspension

WT Wild type

Acknowledgement

First and foremost, I would like to thank God for this incredible opportunity; for the intelligence, strength, and encouragement throughout all the challenging moments. I am truly grateful for His unconditional grace.

I would like to thank Dr. Paul R. Albert for his continues support and guidance in my master's degree. I would also like to thank all past and current members of Dr. Albert's lab for training me and helping me in my research. I would like to extend a special thank you to Dr. Faranak Vahid-Ansari for her tremendous support and her help with optogenetic surgery and behaviour in this research project.

I am also very thankful with my thesis advisory committee, Dr. Mario Tiberi and Dr. Hsiao-Huei Chen for their constant help in my research.

I would like to thank my family for their unwavering love and support, they have been of tremendous help and an enormous blessing.

Contributions

This research project was completed with the help of Dr. Paul R. Albert (PRA), Dr. Faranak Vahid-Ansari (FVA), and Mireille Daigle (MD).

PRA and FVA developed the theoretical framework for this research. MD supported with animal breeding and genotyping. FVA performed opto-implantation and stimulation; performed animal behavioral tests. AFFA contributed to brain sample preparation and immunostaining; completed data extraction; wrote the paper with inputs from all contributors. PRA, FVA, AFFA contributed to the interpretation of results and provided critical feedback for analysis.

Abstract

Major depressive disorder is twice as prevalent in females. Selective Serotonin Reuptake Inhibitors are the first line of treatment; however, only 30% of patients remit with a 6-8-week latency.

We used Unpredictable Chronic Mild Stress model of depression in female mice and opto-genetically targeted serotonin projections at medial prefrontal cortex (mPFC) to assess new treatment options.

Using transgenic Cre-mediated expression of light-sensitive channelrhodopsin-2 in serotonin neurons, mice were bilaterally stimulated in the mPFC during behavioural testing.

UCMS induced anxiety/depression-like phenotypes with reductions of TPH+/FosB+ cells and reduction of serotonin axons, varicosities, and synaptic contacts. Opto-stimulation reversed behavioral effects in tail suspension and increased the chronic activation of serotonin neurons and CA1 pyramidal cells.

UCMS induced depression/anxiety-like phenotypes in female mice that can be partly reversed by bilateral opto-stimulation of 5-HT projections to the mPFC, activating serotonin neurons and inducing hippocampal activity, resulting in activation of a mini-circuitry connecting mPFC–hippocampus–DR.

1. Introduction

1.1 Major Depressive Disorder

Major Depressive Disorder (MDD) is a psychiatric disorder with a global prevalence of about 1 in 5 people (Vahid-Ansari and Albert, 2021). It is a major contributor to the global burden of disease and according to the World Health Organization (WHO) it is the second-leading cause of disability in the world, projected to be the first by 2030 (Karrouri et al., 2021).

The current guidelines of the Diagnostic and Statistical Manual of Mental Disorders, 5th Edition (DSM-5), states that a person must present five of the following symptoms to be clinically diagnosed with MDD; persistent low mood, anhedonia, anergia, feelings of guilt or worthlessness, lack of energy, poor concentration, appetite changes, psychomotor retardation or agitation, and sleep disturbance (Bains and Abdijadid, 2023). In particular, depressed mood or anhedonia causing social or occupational impairment must be present (Bains and Abdijadid, 2023). It is noteworthy that MDD can lead to high levels of suicidality, which indicates how important research in MDD is. Not only do people with MDD account for 87% of completed suicides, but 53% of depressed subjects have suicidal ideation and 31% of them attempt suicide (Cai et al., 2021). Current antidepressant treatments have been shown to lack efficiency and efficacy, especially the gold standard Selective Serotonin Reuptake Inhibitors (SSRIs), which adds to the challenges faced by MDD patients (Vahid-Ansari and Albert, 2021).

Most importantly understanding the full pathophysiology of MDD still remains a challenge, making it very difficult to treat effectively. Based on the DSM-5 criteria, clinical depression symptomatology is diverse and heterogeneous (Vahid-Ansari and Albert, 2021); appetite and sleep changes support a diagnosis of depression regardless of whether patients report an increase or a decrease (Lynall and McIntosh, 2023). Furthermore, research has shown that the neurobiology of

MDD suggests abnormal hypothalamic-pituitary-adrenal (HPA) axis activity (Pariante and Lightman, 2008), oxidative and nitrosative stress (Maes et al., 2011), and immune-inflammatory responses (Zolfaghari et al., 2021). Additionally, most research points towards involvement of an impairment in neurotransmission of monoamine systems, more specifically the serotonergic system (Vahid-Ansari and Albert, 2021). Furthermore, genome-wide association studies have identified 178 genetic risk loci and more than 200 genes that may be responsible for increased risk of MDD (Flint, 2023). In addition, MDD affects almost twice as many females compared to males, the WHO predict that 5% of men and 9% of women will experience a depressive disorder in a given year (Lohoff, 2010).

All together this demonstrates how complex clinical MDD is. There is evidence to show that 1) MDD interacts with many neuronal and hormonal systems at the same time, 2) affects males and females differently, and 3) there is unknown genetic component; three criteria that add to the complexity of the disease. Nonetheless, interestingly chronic stress seems to be a shared environmental risk factor for developing MDD.

1.2 Serotonin

Serotonin (5-HT) is a monoamine neurotransmitter that is widely implicated in control of mood and emotion (Delgado, 2000). 5-HT neurons originate in the raphe nuclei of the midbrain where they extend to produce the largest and most complex efferent system in the brain (Berger et al., 2009). The most caudal raphe projects mainly to the spinal cord and cerebellum (Berger et al., 2009), while the more rostral raphe, including the dorsal raphe nucleus (DR) and the medial raphe nucleus (MR), project to cortical and hippocampal/amygdala regions respectively (Ren et al., 2018). Serotonergic fibres are in proximity to nearly every cell of the brain, and consequently

serotonin regulates nearly all behaviours including but not limited to mood, perception, reward, anger, aggression, appetite, memory, sexuality, and attention (Berger et al., 2009).

Interestingly the serotonin system shows a high degree of plasticity even in adulthood, presumably the system must be able to adapt given its wide range of functions. The extensive ascending and descending 5-HT network forms synaptic and non-synaptic contacts that aid 5-HT modulate brain function through 14 different receptor subtypes (Vahid-Ansari and Albert, 2021). Serotonin can also grow and form axons through pathfinding and arborization functions (Vahid-Ansari and Albert, 2021) that help 5-HT neurons regrow following injury even in adulthood (Zahrai et al., 2020; Jin et al., 2016). In addition to conventional synaptic communication, the serotonin system can also release 5-HT from varicosities into the extracellular space through a process known as volume transmission (Vahid-Ansari and Albert, 2021). This non-synaptic release of 5-HT acts like paracrine transmission of serotonin to surrounding populations of neurons and glia (Vahid-Ansari and Albert, 2021). Closely apposing synapses may be modulated by serotonin through volume transmission, consequently disrupting the serotonin system may have broad pathological consequences as seen in MDD.

The complexity of the serotonin system makes it difficult to study; however, its role in MDD has been shown by many research groups.

1.3 Serotonin in MDD

The long-held monoamine theory of depression proposes that the pathophysiological basis of depression relies on depletion of serotonin, norepinephrine (NE), and/or dopamine (DA) in the Central Nervous System (CNS) (Delgado, 2000). This theory was supported by the mechanism of action of common antidepressants that showed that effective antidepressant medications aimed to elevate levels of these monoamines in the brain. It was later reported that levels of the major

serotonin metabolite 5-hydroxyindoleacetic acid were lower in the cerebrospinal fluid of MDD diagnosed patients, and particularly suicide attempters or completers compared to normal controls (Delgado, 2000). This discovery, although not always consistent in all studies, pointed towards serotonin possibly being the major neurotransmitter involved in the etiology of MDD. Researchers also reported that the number of serotonin transporter sites and thus the uptake of serotonin can be reduced in the platelets of depressed individuals (Healy and Leonard, 1987). The effect of decrease serotonin receptors is specific to MDD and is not mechanistically shared in patients with mania, Alzheimer's disease, fibromyalgia, and atypical depression (Nemeroff and Owens, 2009; Delgado, 2000).

Moncrieff et al. (2022) presented a systematic umbrella review to show that serotonin research does not provide consistent evidence of an association between serotonin and depression, and no foundation to support the hypothesis that depression is caused by lowered serotonin activity or concentration (Moncrieff et al., 2023). However, this is not completely accurate given the inconsistent association of studies in the review paper. Stressing the precise inability of comparison between methodologies, among the selected studies, which reached the expected outcome of substantial heterogeneity in results (Albert and Blier, 2023).

Furthermore, clinically it has been shown that deficits in serotonergic transmission, like reduction of serotonin neurons and their projections, are characteristic in MDD patients. It has also been reported that increase 5-HT autoinhibition is associated with MDD and impaired antidepressant response (Jans et al., 2007; Delgado, 2000). Post-mortem brain tissue from depressed individuals also showed reduced 5-HT innervation. These observations were also reported in pre-clinical research using animal models (Delgado, 2000). Repeatedly, stress rodent models of depression

have shown changes in 5-HT innervation as seen in the human post-mortem brain tissue (Vahid-Ansari and Albert, 2021)

Ultimately, Young et al. (1989) showed that depression in humans can be triggered by a decrease in 5-HT. They used acute tryptophan depletion to reduce the level of serotonin in a transient and reversible manner in a primate model using monkeys (Young et al., 1989), which was also conducted in humans (Leyton et al., 1997). Given 5-HT synthesis is entirely dependent on the bioavailability of its precursor essential amino acid tryptophan, the research group was able to deplete the brain of serotonin stores by administering a tryptophan-free amino acid drink (Delgado, 2000).

1.4 Treatment options

Pharmacological interventions are the first line of defense against MDD, especially the widely prescribed SSRIs (Bains and Abdijadid, 2023). Different classes of antidepressant medications have been shown to differ in effectiveness and risk of adverse effects (Cipriani et al., 2018).

1.4.1 Monoamine Oxidase Inhibitors

The first antidepressant medications were monoamine oxidase inhibitors, which act by blocking the monoamine oxidase enzyme to inhibit the breakdown of norepinephrine, serotonin, dopamine, and tyramine. Thus, increasing their concentration in the synaptic cleft and allowing them to more strongly influence synapses (Sub Laban and Saadabadi, 2024). Nonetheless, these medications were shown to have hepatotoxicity and lead to hypertensive crisis (especially due to direct drug interactions with foods that contain tyramine) that can result in lethal intracranial hemorrhages (Karrouri et al., 2021). As a result, it is now exclusively prescribed for patients who have not responded to several other pharmacotherapies.

1.4.2 Tricyclic Antidepressants

In 1957 tricyclic antidepressants (TCA) were introduced for clinical use. They function by inhibiting the reuptake of monoamine neurotransmitters serotonin and norepinephrine, which modulates mood, attention, and pain (Moraczewski et al., 2024). They have been shown to be superior to SSRIs for patients with severe forms of MDD and consequently they are generally reserved for patients that cannot respond to first-line drug treatments (Karrouri et al., 2021).

1.4.3 Selective Serotonin Reuptake Inhibitor (SSRIs)

The most widely used antidepressant drugs are SSRIs, mainly due to the fact that they can be as effective as TCAs for treating depression while causing fewer adverse effects (Karrouri et al., 2021). They can elicit sexual and digestive related side-effects; nevertheless, they have a good tolerability profile (Cipriani et al., 2005). This is why most current guidelines recommend SSRIs as the first-line treatment for MDD (Karrouri et al., 2021).

Their mechanism of action relies on their ability to block the serotonin transporter protein (SERT) to inhibit the reuptake of 5-HT into the presynaptic serotonin neuron (Beyer and Cremers, 2008). Consequently, acute treatment with SSRIs results in a transient increase in 5-HT in both the nerve terminals and cell body region (serotonergic target areas and raphe). However, increased 5-HT concentration hyperactivates the 5-HT1A autoreceptor that through negative feedback inhibition from the raphe attenuates 5-HT neuronal firing (Turcotte-Cardin et al., 2019). Subsequent chronic SSRI treatment desensitizes the 5-HT1A autoreceptor, which disinhibits the 5-HT neuron resulting in enhanced firing and successive 5-HT release (Albert and Lemonde, 2004; Piñeyro and Blier, 1999). The desensitization period, one of the mechanisms by which SSRIs promote recovery, requires chronic treatment of at least 3-4 weeks to increase 5-HT concentration and improve depressive behaviours (Vahid-Ansari et al., 2019; Vahid-Ansari and Albert, 2018). More notable is the fact that even when about 50% of patients will respond initially to SSRIs only 30% will

achieve a remission state (Vahid-Ansari and Albert, 2018). This raises the question on the reliability of these medications as it shows severe disadvantages in terms of efficacy and efficiency. The possible side effects and the delayed pharmacologic effect may reduce patient's adherence, in turn, leading to worsening depressive states.

Depression can also be treated with somatic brain stimulation treatments that include electroconvulsive therapy (ECT), repetitive transcranial magnetic stimulation (rTMS), deep brain stimulation (DBS), and transcranial direct current stimulation (tDCS), among others.

1.4.4 Electroconvulsive Therapy

ECT is arguably the most effective treatment modality in psychiatry. It has been shown to reduce the number of hospital readmissions and lighten the burden of depression, which leads to a better quality of life (Karrouri et al., 2021). It works through administering electrical current to the skull to induce a generalized tonic-clonic seizure (Kritzer et al., 2023). This induces changes in the brain chemistry, and neural activity and connectivity that lead to a range of clinical effects with a broad therapeutic spectrum of action (Deng et al., 2024).

1.4.5 Repetitive Transcranial Magnetic Stimulation

rTMS is a type of biological stimulation that affects brain metabolism and neuronal electrical activity (Karrouri et al., 2021). It is usually targeted to stimulate the left dorsolateral prefrontal cortex (DLPFC) region by the production of high and low-intensity magnetic fields that ultimately modulate cortical excitability (Mann and Malhi, 2024; Lan et al., 2016)

1.4.6 Deep Brain Stimulation

DBS has been shown to significantly improve antidepressant resistant depression in approximately 40-60% of patience after 6 months (Mayberg et al., 2005; Van Der Wal et al., 2020). For this

treatment electrodes are implanted, and electrical impulses are administered to modulate brain activity. The implant location is generally the subcallosal cingulate gyrus (SCG), which lies in the Brodmann area 25 (subgenual cingulate region) (Mayberg et al., 2005) and parts of 24 and 32, is the portion of the cingulum that lies ventral to the corpus callosum (Hamani et al., 2011). Research has shown its effectiveness as it can modulate behavioral effects and mood, with significant impact in anhedonia, as early as one week after beginning of treatment (Karrouri et al., 2021). However, the full mechanism by which it promotes depressive relief is still elusive given that the electrical impulses activate all the neurons within the SCG.

1.4.7 Transcranial Direct Current Stimulation

tDCS is a non-invasive neuromodulation technique that uses two surface scalp electrodes that promote non-convulsive current to affect cortical areas of the brain by modulating cerebral blood flow, metabolism, and brain-derived neurotrophic factors (Blumberger et al., 2015).

1.5 Chronic stress

Although the exact etiology of MDD is yet to be fully understood there is clear evidence that chronic exposure to stress is an etiological environmental risk factor (Richter-Levin and Xu, 2018). This is mainly commenting on the effects from psychological and physical stress that highlight elements of inescapability and/or uncontrollability (Cohen et al., 2007).

Psychological stress can be acute or chronic, and it can change the brain's architecture, molecular profile, and its neurochemistry. Stress can cause neuronal circuitry imbalance subserving impairment in cognition, decision making, anxiety, and mood that can either increase or decrease expression of behavioral states (McEwen, 2017). Neural imbalances can affect neuroendocrine, autonomic, immune, and metabolic mediators which can ultimately affect systemic physiology. Short-term effects of stress may be adaptive due to the high plastic capacity of the brain (as acute

stress can be beneficial in preparation for a flight or fight response); however, maladaptive changes in neural circuitry may persist if stress is chronic in nature (McEwen, 2017). Chronic stress can lead to atrophy of the brain mass and decrease its weight, which ultimately leads to changes in response to stress, cognition, and memory (Yaribeygi et al., 2017). Chronic stress has also been shown to lead to neuronal anatomical changes as it causes dendritic shrinkage and loss of spines especially in the hippocampus and (McEwen, 1999) prefrontal cortex (McEwen, 2017).

These neuronal changes may come from the intertwined activity of metabolic pathways where hormones and neurons come together. In response to chronic stress, cortical areas of the brain transmit impulses to the hypothalamus through the limbic system. Neurotransmitters such as serotonin, norepinephrine, and acetylcholine are released, where cells of the paraventricular nucleus (PVN) are activated and in turn synthesize and secrete corticotropin releasing hormone (CRH) (Yang et al., 2015). CRH enters the hypothalamic portal venous system and stimulates corticotrophs in the anterior pituitary gland to synthesis proopiomelanocortin (POMC) which subsequently cleaves to produce adrenocorticotropic hormone (ACTH) and alpha melanocyte stimulation hormone (α-MSH). ACTH stimulates zone fasciculate and reticularis of the adrenal cortex to produce glucocorticoids (GCs) which together with catecholamine are the main stress hormones. These stress mediators can cross the blood-brain barrier and modulate processes in the CNS and neuroendocrine system (Yang et al., 2015). Thus, GCs affect a plethora of brain functions like survival of neurons, neurogenesis, hippocampal size, and emotion (Yang et al., 2015). Importantly, the hippocampus is a critical site that is strongly implicated in glucocorticoid negative feedback regulation. Thus, impaired hippocampus function can lead to dysregulated stress axis and stress sensitivity (Meaney et al., 2010) that ultimately decreases 5-HT release. Neuronal damage in turn can release damage-associated signaling molecules which create a feed forward

loop that accelerates peripheral inflammation. Peripheral inflammation in turn exacerbates neuroinflammation through several mechanisms including disruption of the blood–brain barrier, immune cellular trafficking, and activation of glial cells. Remarkably, activated glial cells release cytokines, chemokines, and reactive oxygen and nitrogen species into the extra-synaptic space. These mediators can dysregulate neurotransmitter systems, unbalancing the excitatory to inhibitory ratio, and disrupting neural circuitry plasticity and adaptation (Hassamal, 2023). This highlights the extremely complicated mechanism and very fine interplay between systems in the pathophysiology of depression.

CRH projections have also been shown to activate the monoamine system as an important adaptive measure in response to stress, which reinforces the monoamine hypothesis of depression (Flügge et al., 2004). Despite the fact that an active monoamine system enables the brain to react to stressors by reorganizing neuronal networks (Flügge et al., 2004), chronic hyperactivity as a response to chronic stress may lead to MDD psychopathologies.

1.6 Animal Models of Depression

It has been well established that the precise neurobiological mechanism of MDD is extremely complex due to the many systems involved and the heterogeneity of the symptomatology. Research on MDD is also extremely complex. Using patient tissue is very complicated: as 1) peripheral tissues from patient such as blood may have limited value to inform brain changes (Wang et al., 2017) and 2) postmortem brain samples from human subjects are scarce and carry many confounding factors. Confounding variables include the patient's history with antidepressants, the postmortem interval, and pH of the brain (Wang et al., 2017). Furthermore, the majority of postmortem tissue available comes from depressed individuals who committed suicide, which may confound insight into the neurobiological mechanisms of the disease (Wang

et al., 2017). To overcome these challenges, research focuses on animal models that aid in mimicking neuropsychiatric disorders and allow researchers to selectively examine neural circuitry with molecular and cellular pathways (Wang et al., 2017).

Effective animal models are assessed on three basic constructs 1) face validity, which is the ability of the model to successfully phenotypically mimic human conditions; 2) construct validity, that indicates that the process of inducing the pathological manifestations in the model are similar to human conditions; and 3) predictive validity, which assesses the sensitivity of model-induced pathophysiology to respond to pharmacological interventions that are effective in the human condition (Nestler and Hyman, 2010; Wang et al., 2017). Neuroscience research tends to lean towards animal models using rodents, especially mice. These animals are chosen for their ease of reproduction and relatively simple procedures to alter their genetic information.

The most common rodent models of depression are:

1.6.1 Early life stress model

Which relies on the basis that adverse events in early life substantially affect the development of psychiatric illnesses later in life (Wang et al., 2017). The most common procedure is to separate the pups from the mother in maternal separation stress which has been shown to have long-lasting effects on emotionality and stress responsiveness. This model imitates how children that may have experienced childhood abuse and parental neglect have considerably higher probabilities of developing emotional and mental illnesses, like anxiety and depression (Cui et al., 2020).

1.6.2 Social defeat model

This model uses social conflict to develop emotional and psychological stress in rodents. Social stress is involved in the development of depression and other psychopathology in humans (Wang et al., 2017). The model relies on an aggressive male dominant rodent that attacks a less aggressive

rodent. The repeatedly defeated rodent shows important depressive-like characteristics like anhedonia, decreased sexual behavior, increased defensive behavior, increased anxiety, changes in circadian rhythmicity, alterations in feeding and body weight, sleep disturbances, and impaired immune functions (Wang et al., 2017).

1.6.3 Chronic restraint stress model

As its name suggests, rodents are restrained for a minimum of 2 hours for at least 14 to 21 days. Restrain is a very establish source of stress that mimics daily repetition of a stressful job, social or financial stress, familial stress, or day to day stresses that are repeated (Wang et al., 2017). This type of model has been shown to result in depressive like behaviours in rodents and induce damage to pyramidal cells in the CA3, increased corticosteroid levels, and apoptotic cell death.

1.6.4 Chronic corticosterone (CORT) model

Unlike other models this one relies on pharmaceutical induction of chronic stress by administering CORT. It is a well-established pharmacological stressor (Dieterich et al., 2019) that mimics an hyperactivated HPA axis that naturally leads to CORT secretion (Berger et al., 2019). CORT treated animals have been shown to display higher immobility duration in forced swim test, increase anhedonia in sucrose preference test and hyponeophagia in novelty supressed feeding (Berger et al., 2019). CORT can also inhibit hippocampal neurogenesis (David et al., 2009).

1.6.5 Unpredictable chronic mild stress (UCMS)

The UCMS model of depression involves daily exposure to low-intensity random stressors over several weeks. This protocol has been shown to induce physiological symptoms like hypercortisolemia and hypertension; and neurological symptoms like anhedonia and learned helplessness (Frisbee et al., 2015), clinically manifested in MDD (Frisbee et al., 2015). Interestingly it is one of the few models where rodents respond to chronic, but not acute, treatment

of common monoaminergic antidepressants (Nollet, 2021). It has also been shown to respond to the rapid acting antidepressant Ketamine, the N-methyl-D-aspartate (NMDA) receptor antagonist (Frisbee et al., 2015). It is for these reasons that this model is an established translationally relevant model for inducing behavioral symptoms associated with clinical depression that demonstrates face, construct, and predictive validity.

1.7 Novel approach-Optogenetic stimulation

Common antidepressants have been shown to lack efficacy and efficiency, in addition to multiple side effects. New somatic treatments have been shown to be more effective than pharmaceuticals; however, we still do not fully understand the entire wiring mechanism by which they exert their action, especially due to the lack of stimulatory specificity in neuronal populations. Consequently, this research project will aim to understand how stimulation of serotonergic projections in the mPFC can elicit an antidepressant response. This will be done using optogenetic stimulation.

Optogenetic stimulation enables researchers to activate or inhibit the activity of specific neuronal populations using light and light-sensitive proteins (opsins) that are introduced into the organism through genetic techniques. Optogenetics allows single gene encoding of light-activated channels that work through regulation of ion-conductance or biochemical signaling proteins (Kim et al., 2017). It is well accepted that neuronal circuits are highly diverse and complex. Thus targeting specific cell types or projections is a crucial step in studying them. This was enabled by optogenetics and the development of efficient strategies of introducing light sensitive proteins. These strategies are either viral aided implantation through axonal transduction or retrograde propagation (Kim et al., 2017) or transgenic mouse lines that use genetic promoters and recombinase mechanisms to knock-in the genetic modification (Ting and Feng, 2013).

All together optogenetic stimulation combines the temporal and spatial precision of light pulses over specific cellular targets and aid in coupling cellular behaviour with light (Mei and Zhang, 2012). Most importantly, it allows for fast and reliable neuronal activity manipulation in intact brain circuits, essential for studying complex neuronal circuits. Compared to somatic treatments for MDD, like rTMS and DBS, optogenetics stimulates specifically-targeted neurons that express the opsin, whereas magnetic or electrical stimulation affects diverse local, afferent, axonal fibers, and even somas near the electrodes (Mei and Zhang, 2012).

In our research we will be using the opsin, channelrhodopsin-2 (ChR2) a light-gated cation channel that is activated with blue light (~470 nm) that causes influx of Na+ ions which depolarizes the specific neuron, in our case serotonin related neurons (Boyden et al., 2005).

Most research involving optogenetics and the expression of ChR2 use viral transduction for genetic manipulation. A viral vector that drives ChR2 expression can be delivered directly into specific brain regions with robust transduction efficacy and limited tissue damage. Adeno-associated viruses (AAVs) are normally used, as lentivirus vectors do not appear to spread as effectively as AAV vectors and preferentially transduce to excitatory neurons (Cardin et al., 2010).

On the other hand, targeted expression of genes to specific cell types can be robustly achieved with the Cre–loxP system which introduces Cre into the driver line under the control of a gene-specific promoter. In turn the reporter line directs Cre-dependent expression of the transgene (in our model we are using the Pet-1 promoter, specific for serotonin neurons, and ChR2, as our light-sensitive opsin). Genetically, Cre-mediated recombination between two loxP sites deletes the STOP cassette flanked by the loxP sites and induces transgene expression (Zeng and Madisen, 2012). This method promotes opsin expression in the entire system controlled by the specific genetic promoter with a lower concentration of opsin expression compared to AAV induction.

1.8 Objectives and Rationale

This research project aimed to understand the effects of serotonin activation in a chronic stress model of depression. A transgenic mouse model was used to examine the potential antidepressant effects of targeting serotonergic projections in the medial prefrontal cortex (mPFC) through optogenetic stimulation.

Due to the considerable sex differences in the diagnostic of MDD and given most MDD pre-clinical research is male focused (researchers tend to only use male animal models of depression), this research mainly focused on female animals to try to elucidate the neurological and behavioural effects of chronic stress in female depression. Additionally due to the overwhelming evidence that chronic exposure to stress leads to MDD and the abundant research that has shown the effectiveness of UCMS in developing depressive-like phenotypes comparable to MDD in mice, we decided to study UCMS in the context of female depression. We assessed 1) behavioural changes that validate depression-like phenotype in female mice and 2) neurological effects elicited due to stress, mainly on the chronic activity of serotonergic, excitatory, and inhibitory neurons. In addition, we also assessed serotonergic axonal and varicosity density, and synaptic changes. Finally, to evaluate the therapeutic effect of increased serotonergic activity in MDD we stimulated serotonergic projections in the mPFC, more specifically the cingulate gyrus (CG) (the mouse equivalent location of the SCG), using optogenetic stimulation. Translationally, this mimics the effect of DBS with a more precise delivery, given that we only stimulated the serotonin system and achieved similar effects seen in the antidepressant response elicited by common antidepressant pharmaceuticals. Ultimately, we looked into the possibility of promoting an antidepressant response, while bypassing the delay effect of common SSRIs.

Despite the evidence to support the crucial role of the serotonergic system in the development of MDD pathology and its subsequent role in antidepressant response, little research has been done to understand what direct activation of the serotonin system does through optogenetic stimulation. Ohmura et al. (2020) showed that optogenetic stimulation of serotonin cells in the DR exerted antidepressant-like effects in a naïve mouse model (Ohmura et al., 2020). For their experiment they used a tetracycline-controlled transcription activator, limiting ChR2 expression to 5-HT neurons (cell bodies) through the tryptophan hydroxylase 2 promoter (Ohmura et al., 2014). However, Ohmura et al. did their research in normal mice and not in a depression model. The results shown by Ohmura et al. are supported by unpublished research from Zhang et al. (2019) where he showed that optogenetic stimulation of serotonin cells in the DR (using the Pet-1 promoter for ChR2 induction under a Cre-lox system) has antidepressant-like effects in a post-stroke depression model ("Canadian Stroke Congress 2019 Abstract Supplement," 2019).

Unlike both of these studies, our research will use the UCMS model of depression to try to understand the potential antidepressant action of serotonergic activation of cortical projection in female mice. More importantly we will focus on serotonergic projections to cortical areas of the brain, in an attempt to mimic SSRI action in a more targeted and rapid time scale. Trying to combine the mechanism of action seen in cognitive behavioural therapy (CBT) (where CBT increases cortical excitatory activity that trickles down to limbic brain regions) and SSRI treatment (that modulates the activity of limbic brain regions through serotonin by DR activation) (Warner-Schmidt, 2013).

1.9 Hypothesis

I hypothesize that UCMS will induce behavioural changes associated with depressive-like phenotypes and that these changes will be accompanied by neuronal chemical and architectural

changes as a response to chronic exposure to stress, in female mice. I also hypothesize that stimulating serotonergic projections to the CG will promote an antidepressant response by potentially tonically increasing the chronic activity of the entire serotonin system which will modulate the activity of the limbic system, likely through serotonin neurotransmission and volumetric transmission. This antidepressant response will be seen in behavioral changes associated with antidepressant activity and probably through recovery of neuronal damage elicited by chronic stress.

2. Methodology

2.1 Animal handling and housing

The University of Ottawa Animal Care Committee approved all experimental procedures in accordance with guidelines established by the Canadian Council of Animal Care. 10-week-old female and male mice were maintained on a reverse 12/12h light/dark cycle with *ad libitum* access to food and water. Animals were grouped housed prior to optogenetic implantation surgery and single-housed post-surgery to avoid detachment of opto-stimulation implants and remained single-housed during behavioural testing.

2.2 Mouse line

The experimental mouse line was generated through a Cre-lox system. Pet-Cre (C57BL/6N-Tg (Fev-cre)1Esd/J) mice, that contain the Cre construct fused to the Pet-1 (also called *Fev)* promoter, were crossed with flx-stop-ChR2YFP (ChR2-H134R-YFP) mice that express channelrhodopsin-yellow fluorescent protein (YFP) fusion protein flanked by loxP sites with the YFP integrated downstream as a marker for channelrhodopsin expression. This generated heterozygous Pet-ChR2 wt/flx mice (+/- hemi), which were interbred to generate homozygous Pet-ChR2 flx/flx mice (-/- hemi) and wild-type (+/+ hemi) mice. All animals in this project were Pet-Cre hemi and cohorts differed on the presence or absence of channelrhodopsin.

The Pet-1 promoter was used as it is a transcription factor exclusively expressed in serotonin neurons, hence this resulted in mice expressing ChR2 in serotonin neurons only (Wyler et al., 2016).

2.3 Genotyping

DNA was extracted from ear tissue samples taken at three weeks of age, using the REDExtract-N-Amp Tissue PCR kit (Millipore Sigma) and genotyping of target protein was done using 1X One-Taq Mastermix (New England Biolabs) and 2 pmol of each respective PCR primer and conditions: Pet-cre: CRE-P1L, 5'-GCC TGC ATT ACC GGT CGA TGC AAC G-3' and CRE-P2R, 5'-AAA TCC ATC GCT CGA CCA GTT TAG TTA CCC -3'. Cycling conditions were: 2 min at 94°C, and 12 cycles of 94°C for 30 sec, 68°C for 30 sec -0.5°C/cycle, 68°C for 45 sec, followed by 20 cycles of 94°C for 30 sec, 62°C for 30 sec, 68°C for 45 sec a final elongation of 5 min at 68°C. The expected PCR product is 643bp.

ROSA26 (ChR2): RR711, 5'-GCA CTT GCT CTC CCA AAG TC-3', RR712, 5'-GGG CGT ACT TGG CAT ATG AT-3'and RR713, 5'-CTT TAA GCC TGC CCA GAA GA -3'. Cycling conditions were: 2 min at 94°C, and 33 cycles of 94°C for 30 sec, 64°C for 30 sec, 68°C for 30 sec, and a final elongation of 5 min at 68°C. The expected PCR products are 252bp and 495bp.

2.4 Cohorts

In this study, we used three cohorts of PetCre-CHR2 mice. I) Naïve mice that served as our control group. These were genetically identified mainly as ChR2 +/+ and ChR2 +/- mice (n=13) Naïve mice were not chronically stressed, nor subjected to optogenetic implant surgery. II) WT mice (+/+ hemi) served as a control group for opto-stimulation and underwent through the stress protocol and were opto-implanted and stimulated during behavioral test, but lacking ChR2 did not response to opto-stimulation (n=5). III) Pet-ChR2 mice served as our experimental line. This cohort was subjected to chronic stress and opto-stimulated during behaviour (n=12). These were Pet-Cre-ChR2 flx/flx mice (-/- hemi) mice, therefore expressed channelrhodopsin in the serotonin system and could respond to opto-stimulation.

2.5 Unpredictable Chronic Mild Stress (UCMS)

A total of 19 mice (13 Pet-ChR2 (12 females and 1 male) and 6 WT (5 females and 1 male)) were subjected to daily randomized stressors for 6 weeks (**Table 1.**). Stressors were mild in nature and relatively short in time, ranging from 1 minute to 24 hours. One stressor was chosen randomly each day to avoid repetition of the same stressor for at least three consecutive days to discourage adaptation.

Table 1. Schedule for UCMS protocol

Days/ Weeks	Monday	Tuesday	Wednesday	Thursday	Friday	Saturday	Sunday
1	shaking-1 min in a bag	450 Lux (3 hrs)	tilted cage (3 hrs)	restraint (3 hrs)	dirty rat bedding (3 hrs)	24 hrs light on	24 hrs regular cycle
2	shaking-1 min in a bag	dirty rat bedding (3 hrs)	restraint (3 hrs)	450 Lux (3 hrs)	tilted cage (3 hrs)	24 hrs light on	24 hrs regular cycle
3	shaking-1 min in a bag	tilted cage (3 hrs)	450 Lux (3 hrs)	dirty rat bedding (3 hrs)	restraint (3 hrs)	24 hrs light on	24 hrs regular cycle
4	shaking-1 min in a bag	dirty rat bedding (3 hrs)	tilted cage (3 hrs)	restraint (3 hrs)	450 Lux (3 hrs)	24 hrs light on	24 hrs regular cycle
5	shaking-1 min in a bag	450 Lux (3 hrs)	restraint (3 hrs)	tilted cage (3 hrs)	dirty rat bedding (3 hrs)	24 hrs light on	24 hrs regular cycle
6	shaking-1 min in a bag	dirty rat bedding (3 hrs)	450 Lux (3 hrs)	restraint (3 hrs)	tilted cage (3 hrs)	24 hrs light on	24 hrs regular cycle

Additionally, mice underwent surgery before being subjected to five behavioural tests, according to the experimental timeline (**Figure 1.a**). Both the surgery and behavioral tests in addition to being single-housed are considered sources of continues stress. Consequently, even though the chronic stress paradigm was followed for six weeks, mice were under social isolation stress during the entirety of the project. On the other hand, to maintain a control mouse group, Naïve mice were

not subjected to the chronic stress, nor where they single-housed. The only source of stress was that they followed the same battery of behavioural tests.

2.6 Optogenetic implantation and stimulation

2.6.1 Optical Fiber Implants

To make the fiber implants, 15-20 mm of optic fiber wire (FT200EMT - 0.39 NA, Ø200 µm Core Multimode Optical Fiber; ThorLabs) was stripped of its insulation and cleaned with 100% ethanol. Using a ruby DualScribe, the optic fiber was cut approximately 9.7mm (after considering the depth needed to reach the CG and length of the ferrule itself (6.5mm)) prior to inserting it into the flat end of the ferrule (PFP LC 1.25mm OD Multimode Ceramic Zirconia with inner bore of 230 µm; Precision Fiber Products), making sure the flattest end of the fiber went in first, until the end of the fiber protruded slightly from the round end of the ferrule. The fiber was fixed in place with epoxy and allowed to dry overnight. The dried implants were then polished on 4 different polishing sheets (with grit sizes of 5, 3, 1, and 0.1 µm). Implants were tested using an optical power meter (ThorLabs; PM20) and only those with measured power over 3 mW/mm^2 and displaying a concentric light pattern were used.

2.6.2 Surgery

Surgery for optical fiber implantation was performed on both WT and Pet-ChR2 mice. Mice were anaesthetized in a chamber by inhalation with 5% isoflurane with oxygen flowing at 2 mL/min. Unresponsive mice were fixed in stereotaxic device and kept under anesthesia with isoflurane at 2% and oxygen flow at 1.5-2mL/min during the surgery. Once the scalp was carefully opened anterior-posterior (AP), dorsal-ventral (DV), and medial-lateral (ML) positions in reference to bregma were recorded. Final implantation coordinates in the bilateral cingulate gyrus (CG) were AP +1.95; ML+/- 0.4; DV -1.25. Implantation was done bilaterally and consequently, given the

size of the implant, one implant was introduced straight (left) and the other one at an angle of 10º (right). Implants were secured with dental cement and scalp was closed with Vetbond. Post-surgery and 4 hours later mice were administered subcutaneous Buprenorphine. Post-surgical care also included recovery in incubator at 37ºC and the incision was covered with topical Bupivacaine. Implant location was confirmed with MRI (**Figure 1.b-c**)

2.6.3 Behaviour tests and ON/OFF Stimulation Paradigm

Mice underwent optogenetic stimulation during each behavioral test to induce activation of ChR2 in 5-HT neurons. WT and Pet-ChR2 cohorts were connected to the opto-stimulation apparatus. Each behaviour test was divided into three equal parts, except for the NSF test where animals were stimulated all through the test. Animals were stimulated only during the second third of each test, according to experimental timeline (**Figure 1.a**). During the first and last third of each test animals were kept connected to the commutator; however, no light was being transmitted. This was done in order to: 1) eliminate confounding factors as we gathered a baseline period during each behavioral test of animals being connected to the apparatus but not receiving any stimulation, 2) assess the acute effects in behaviour of stimulating the serotonin system through 5-HT CG projecting, and 3) the possible lasting effect of stimulation in said behaviors. Stimulation was administered (during behaviour testing) bilaterally in the CG through a high-performance optical fiber (0.66 NA; Plexon) using a 465 nm blue LED (PlexBright Compact Led Module; Plexon) at 20 Hz for 10 ms LED pulses (duration of stimulation was dependant on the behaviour test and is discussed in more detail within the behavioral assays). All animals underwent behaviour testing with the same parameters, except the naïve cohort that was not attached or exposed to opto-stimulation.

2.7 Phenotypical assessments

2.7.1 Coat state

Mice that were subjected through the UCMS protocol were tested for seven weeks (once per week) to assess the physical changes associated with depression and anxiety like phenotypes. Coat state was scored with either 1 or 2, where 1 was a tidy well-kept (smooth and clear) coat and 2 was a dirty unkept (bristling with spikes) coat.

2.7.2 Behavioral assays

Behavioral testing was conducted in all three cohorts one week after both WT and Pet-ChR2 cohorts had opto-implantation surgery to allow for proper healing time. Mice were transferred to the behaviour testing rooms 1h prior to the beginning of each test (10:00 AM) to allow for habituation. Testing was performed under white light illumination except for the forced swim test (FST), which was performed under red light. All animals were 18 weeks at the start of behavioral testing and all tests were done in accordance with the **experimental timeline** and completed within 10 days.

2.7.2.a Elevated Plus Maze (EPM) test

Mice were placed in the center of an elevated two-arm plus maze that measures 20 (high) x 6 (wide) x 75 (long) cm^3 (Noldus). The arms of the maze are crossed, one of the arms has an open platform and the other one has a closed platform with walls that are 20 cm tall, with an overhead illumination (100-110 Lux) and a camera. For the experiment, mice were placed in the center of the maze adjusting the head to point towards the closed arm and were allowed to explore the maze for 15 min; opto-stimulated mice were stimulated 5 min OFF – 5 min ON – 5 min OFF, in accordance with the opto-stimulation procedure. Mouse movements were recorded, and the time spent in both closed and open arms, distance and velocity were determined (Ethovision 10, Noldus IT, RRID:SCR_000441).

2.7.2.b Open field (OF) test

Mice were placed in a corner of an empty arena measuring 45 cm long in each side and 45 cm high. The tested mouse was allowed to explore the new environment for a total of 15 min (in accordance with the opto-stimulation paradigm; 5 min OFF – 5 min ON – 5 min OFF) with ambient light level of 300 Lux. Mouse movements were videotaped and the time spent in the outside and inside of a center (24 × 24 cm) of the OF arena along with the total distance moved and velocity were analyzed (Ethovision 10, Noldus IT)

2.7.2.c Tail suspension (TS) test

Mice were suspended by their tail, that was secured with tape to a horizontal bar, for 9 min (in accordance with the opto-stimulation paradigm; 3 min OFF – 3 min ON – 3 min OFF) in a mouse TS box (Med Associates). The automated detection device (ENV-505TS Load-Cell Amplifier) was used to record immobility time, and processed through Med Associates software (Ethovision XT, Noldus IT).

2.7.2.d Forced Swim Test (FST)

Each mouse was placed in a clear plastic cylinder 22 cm in diameter and 37 cm deep filled with 4 L of water at 23°C. The test ran for 15 min (in accordance with the opto-stimulation paradigm; 5 min OFF – 5 min ON – 5 min OFF). Animals were videotaped from the side of the cylinder under red light illumination to quantify the duration of immobility time using an automated video-tracking software form Med Associates (Ethovision XT).

2.7.2.e Novelty-Suppressed Feeding (NSF) Test

Animals were food deprived for 16 h. After a 3-min habituation period, mice were placed in a new cage and were then individually placed in an arena (45 cm long on each side and 45 cm high, with 300 Lux ambient light intensity) with a food pellet in the center. The latency for mice to start eating

the pellet was recorded manually, and immediately after mice approached the food or after 10 min passed (which ever came first) they were removed from the arena and placed in their home cage where the latency to approach food and the amount of food consumed in 5 min was recorded. This was the only test that animals were stimulated throughout the whole procedure.

2.7.2.f Naïve animals' behaviour tests

To assess the effect of chronic stress it was necessary to compare naïve parameters with pre-stimulatory periods of each test from the WT and Pet-ChR2 cohorts. Accordingly, Naïve data was extracted from the beginning part of their tests which was the equivalent to the pre-stimulatory third of the total experiment for the stimulated (WT and Pet-ChR2) animals, keeping data sets comparable to the same amount of time.

2.8 Magnetic Resonance Imaging

Magnetic resonance imaging (MRI) was done to visualize and measure hippocampal volume to assess volumetric changes in vivo. To do this, six mice (WT and Pet-ChR2, n=3/each) were followed through chronic stress and opto-stimulation. Taking scans at three different time points; pre-stress, post-stress, and after opto-stimulation, as highlighted in experimental timeline (**Figure 1.a**). This was done to assess the differences in hippocampal volume due to exposure to chronic stress and assess the potential changes occurring post opto-stimulation. A 7T GE/Agilent MRI (Milwaukie, WI, USA) machine was used at the University of Ottawa Preclinical Imaging Core Facility. Animals were anesthetized with isoflurane/O_2 mixture induced at 3% and maintained at 1.5% isoflurane.

Serial scans were acquired with 300-μm thickness using a fast spin echo pulse sequence with repetition time of 4500 ms with effective echo time of 13 ms rendering a field of view of 3 cm

with a matrix size of 256 x 256. The overall thickness per scanned frame was 300 μm with 15 averaged images/scan and a scan time of 30 minutes with an axial (transverse) image orientation. After the MRI scans animals were returned to their home cage and remained under observation until recovery from anesthesia.

2.8.1 Hippocampal volumetric measurements

Volumetric measurements of hippocampal area were performed by manually tracing the hippocampus structure which encompassed the hippocampus proper (CA1, 2, and 3) and DG (as shown in (**Figure 1.d.1-d.2)**. This was done by two independent assessors who were blinded to the sample identity. To assess differences between dorsal and ventral hippocampus MRI scans were segmented using the stack to images function in FIJI (64-bit, ImageJ 2.9.0). This generated 22-24 individual images from which seven sections were selected encompassing dorsal and ventral hippocampus within 1.7 to 2.98 mm relative to bregma, respectively. Hippocampal volume was calculated by multiplying the individual sections' area by the thickness of the interval between sections (300 μm) and adding the seven consecutive scans used per animal.

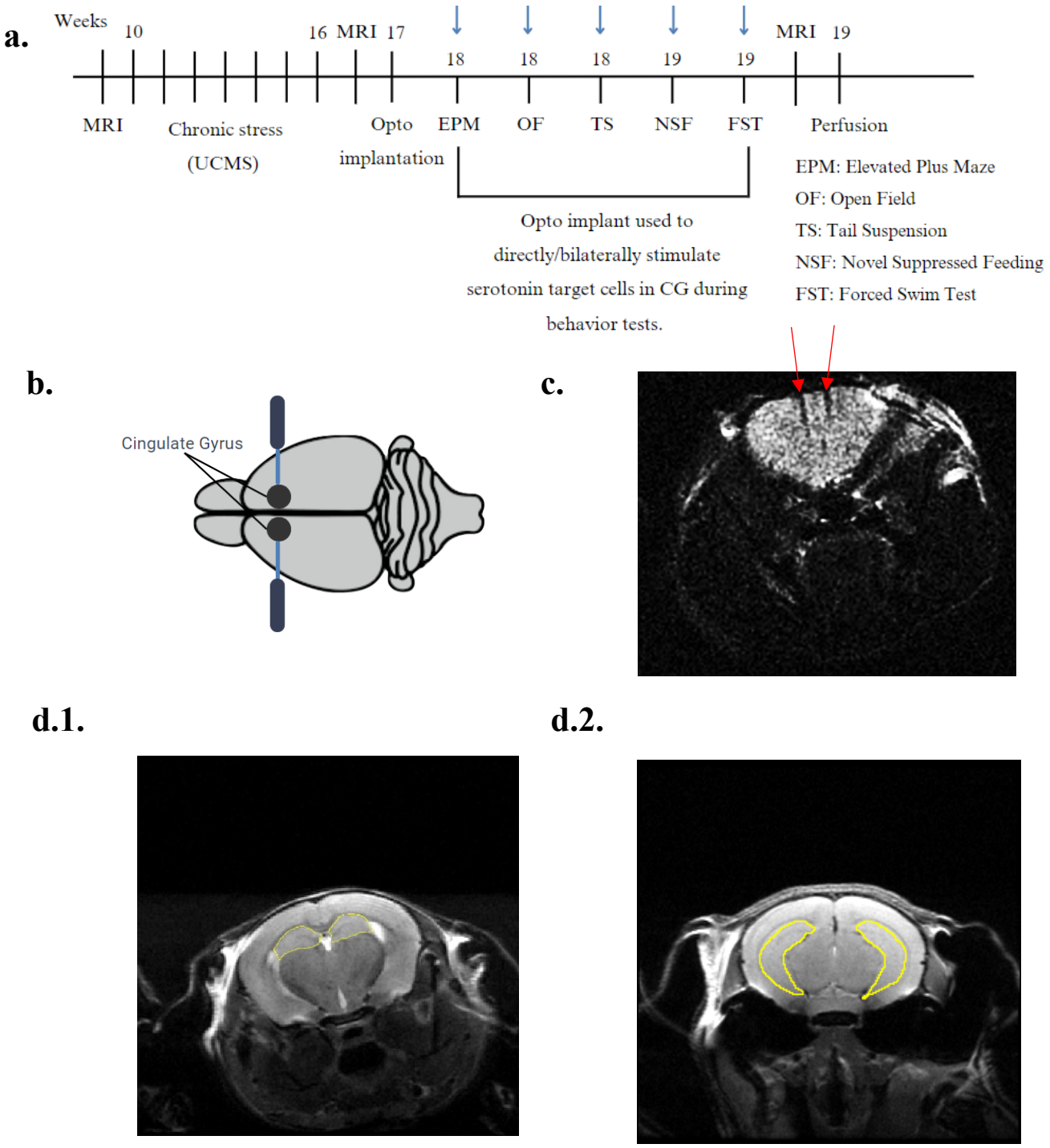

Figure 1. Visual representation of methodological approach for UCMS and opto-stimulation. a. Experimental timeline, with timepoints of MRI data acquisition. Blue arrows in behavior tests show opto-stimulation periods for WT and Pet-ChR2 mice (only stimulated during the second third of each test). b. cartoon representation of bilateral opto-implantation on CG. c. MRI showing exact opto-implants highlighted by red arrow. d. representative images of hippocampal volumetric measurements for d.1. dorsal and d.2. ventral hippocampus.

2.9 Brain sectioning

Mice were euthanized 24 h after the last behavioral test to avoid acute activation following the last test. They were anesthetized by lethal injection (0.01 ml/g, i.p.) of sodium pentobarbital (Somnitol; MTC Pharmaceuticals) and perfused by cardiac infusion of cold 30 ml PBS and then 25 ml 4% paraformaldehyde. Extracted whole brains were cryoprotected with 20% sucrose for three days and subsequently frozen at -65°C in 2-methylbutane (Thermo Fisher Scientific; 03551-4) and kept in -80 °C. Coronal brain sections, 25 µm thick were prepared using the cryostat (HM 525 NX-2210) using coordinates indicated in **Table 2**. Slices were thaw-mounted on Superfrost slides (Thermo-Fisher, 1255015) and kept at -20°C. For immunohistochemistry protocols, brains from four different mice for the three different conditions (Naïve, WT and Pet-ChR2) were selected and brain sections from the forebrain, hippocampal and dorsal nuclei regions were stained.

Table 2. Coordinates relative to bregma of areas assessed by immunofluorescence

Brain area	CG	PrL	IL	MO	NAc	LSN	MSN	CA1	CA2/3	DG	BLA	EC	DR	MR
Bregma (mm)	2.1/1.7	2.1/1.7	2.1/1.7	2.1/1.9	1.5/1.1	0.7/0.5	0.7/0.5	−1.3/−1.7	−1.3/−1.7	−1.3/−1.7	−2.06/−2.3	−2.06/−2.3	−4.5/−4.72	−4.5/−4.72

CG, cingulate cortex; PrL prelimbic; IL, infralimbic; MO, medial orbital cortex; NAc, nucleus accumbens; LSN, lateral septal nucleus; CA1, CA2/3, hippocampus regions; DG, dentate gyrus; EC, entorhinal cortex; DR, dorsal raphe; MR, median raphe

2.10 Immunofluorescent staining (FosB)

For chronic activity (FosB) studies, a two-day immunofluorescent staining protocol was followed. Sections were washed in PBS (3 × 10 min) prior to being blocked for 1h in PBS with 10% normal donkey serum (NDS), and 0.3% Triton X-100, followed by overnight incubation at 4°C with

primary antibodies (**TABLE 3**). The sections were then washed in PBS (3 × 10 min) and incubated for 1 h in the solution to the corresponding secondary antibodies (**TABLE 3**) and 4′,6-diamido-2-phenylindole (DAPI, Thermo Fisher Scientific #D1406, RRID AB_2629482, 1:15,000) at 22°C.

Table 3. Primary and secondary antibodies used for immunofluorescence staining

	Host	Dilution	Company	Catalogue #	RRID
Primary antibody					
FosB	R	1/100	ThermoFisher Scientific	MA5-15056	AB_10983364
CamKIIα	G	1/250	ThermoFisher Scientific	PA5-19128	AB_10986857
GAD 67	M	1/500	Millipore Sigma	MAB5406	AB_2278725
TPH	SH	1/500	Millipore Sigma	ab1541	AB_90754
Gephyrin	R	1/1000	Abcam	ab32206	AB_2112628
SERT	R	1/1000	Millipore Sigma	PC177L-100UL	AB_10697452
PSD95	M	1/1000	Abcam	ab2723	AB_303248
Synaptophysin	M	1/500	Millipore Sigma	MAB5258	AB_95185
Secondary antibody					
Anti-rabbit 488	D	1/1000	ThermoFisher Scientific	A-21206	AB_2535792
Anti-goat 647	D	1/200	ThermoFisher Scientific	A-21447	AB_2535864
Anti-mouse cy3	D	1/250	Jackson ImmunoResearch Labs	715-165-150	AB_2340813
Anti-sheep cy3	D	1/200	Jackson ImmunoResearch Labs	713-165-003	AB_2340727
Anti-rabbit 568	G	1/2000	ThermoFisher Scientific	A-11036	AB_10563566
Anti-rabbit 488	G	1/1000	ThermoFisher Scientific	A11034	AB_2576217
Anti-mouse Cy5	G	1/1000	Abcam	AB6563	AB_955068
Anti-mouse 405	G	1/100	ThermoFisher Scientific	A-31553	AB_221604
Monovalent F(ab) (anti-rabbit)	G	1/100	Jackson ImmunoResearch Labs	115-007-003	AB_2338476
Monovalent F(ab) (anti-mouse)	G	1/100	Jackson ImmunoResearch Labs	111-007-003	AB_2337925

R= rabbit; G= goat; M= mouse, SH= sheep; D= donkey

2.11 Immunofluorescence of 5-HT synaptic and triad structures

To quantify 5-HT innervation, immunofluorescence was done for SERT at dilutions indicated in **Table 3.** Brain sections (25 µm) were incubated at 22°C for 1h in blocking solution (4% normal goat serum, 1% BSA, 0.3% Triton X-100%, and 0.05% Tween20 in 1X PBS) and then with rabbit anti-SERT (1/1000) and mouse anti-PSD95 (1/1000) antibodies diluted in blocking solution for 24h at 4°C. The sections were then washed in blocking solution (3 × 10 min) and incubated in goat anti-rabbit-Alexa488 (1/1000) and goat anti-mouse-Cy5 (1/1000) diluted in blocking solution for 4 h at room temperature. Slices were then washed in blocking solution (3 × 10 min) followed by 1X PBS three (10 min) washes. To block the free binding sites from the first labeling round slices were incubated in a mixture of 5% normal mouse serum (NMS) and 10% normal rabbit serum (NRS) diluted in blocking solution for 1h at room temperature prior to being washed 3 x 10 min in blocking solution. Slices were then incubated in goat anti-mouse (1/100) and goat anti-rabbit (1/100) monovalent F(ab) antibody fragments diluted in 1X PBS for 1 h at 22°C, then washed 3 × 10 min in blocking solution. For the second stage of the immunolabeling process, slices were incubated in a combination of rabbit anti-gephyrin (1/1000) and mouse anti-synaptophysin (1/500) diluted in blocking solution for 24 h at 4°C. After three washes in blocking solution, slices were incubated in a mixture of goat anti-rabbit-Alexa 568 (1/2000) and goat anti-mouse-Alexa405 (1/750) diluted in blocking solution for 4 h. Slices were then washed in blocking solution (3 × 10 min) followed by 1X PBS (3 x 10 min).

2.12 Imaging

Images for chronic activity studies (FosB data) were acquired on the inverted microscope AxioObserver 7 (Zeiss, 491912-0001-000) using the Zen blue 3.0 Pro software (Zeiss). All images were taken at 20x magnification using the Plan-Apochromat lens (NA 0.8).

Confocal laser scanning images for triadic synapses within SERT-positive axon structures were acquired using the Zeiss LSM 880 AxioObserver Z1 with AiryScan microscope. All images were taken at 63x magnification using a Plan-Apochromat oil-immersed lens (NA 1.4). Z-stacks of each area of interest were set with a spacing of 0.3 µm apart and given the region of interest template size was 134.95 × 134.95 × 15.6µm it resulted on 53 stacks per image. Imaging was conducted using ZenBlack 2.3 software, where channels were set to image sequentially using the adjustable emission band path to avoid overlaps in the emission/excitation wavelength. This was done as follows: Alexa 568 was first excited through the laser diode 561 nm with an emission band path set to 569–657 nm. Alexa 488 nm was then visualized using the Argon laser with the 480 nm line that has an emission band path of 493–604 nm. Finally, Alexa 405 and Alexa 647 were imaged together using the HeNe 633 nm laser and the diode 405 nm laser combined with the emission band path of 410–501 and 638–745 nm, respectively.

2.13 FosB+ Cell quantification

For chronic activity studies (FosB) images were transferred to Fiji (64-bit, ImageJ 2.9.0).

The number of FosB positive cells was counted manually under 20x magnification images of 25 µm thick slices. Nuclear FosB+ staining was confirmed with nuclear DAPI staining and colocalization was quantified by those FosB+ signals surrounded with GAD67 or CamKIIα which were quantified as FosB/GAD67+ or FosB/CamKIIα+. FosB+ and marker+ cells were quantified per area of interest per section, after which mean values were then averaged (n=4 per condition). The same procedure was done for FosB/tryptophan hydroxylase (TPH)+ for DR sections, where FosB+/TPH+ cells were quantified at four different levels per mouse (n=4).

2.14 Image analysis using Imaris 10.1 for synaptic triad formations

Images acquired from triad staining were processed using Imaris x64 10.1. SERT-positive fibers were reconstructed into 3D images using the surfacing function of Imaris. These parameters were used to calculate SERT+ axonal volume in reference to total tissue volume (calculated to 284749 µm given the thickness and area of the images acquired) and density of SERT+ varicosities per tissue volume. Using the masking function of the software the intra-fiber labeling was removed to conserve positive stained synaptophysin signals outside of SERT+ axons (Syn^{out}). By then masking the outside synaptophysin signal, the synaptophysin fluorescent signal outside of the created SERT surfaces was removed to only identify synaptophysin within the SERT+ fibers and quantify the putative serotonergic synaptic boutons (Syn^{in}). The spotting detection tool was then used to reconstruct the signals from gephyrin (Geph), PSD95, Syn^{in}, and Syn^{out}, in order to identify the serotonergic boutons that were in contact with either inhibitory synapses or excitatory synapses. The detection of spots was set to 0.6 µm diameter and above. The chosen size is based on the fact that each z-stack is 0.3 µm apart, thus this ensured that each spot is present in at least two confocal optical slices. This corresponded to a spot present in 3D space, consequently excluding artifacts from imaging. Finally, the spot colocalization tool was used to label either Syn^{in}/PSD95 or Syn^{in}/Geph spot pairs, within a distance of 0.6 µm between spots among pairs. This aided in identifying pairs of putative serotonergic contacts with either excitatory or inhibitory synapses, respectively. Syn^{in} boutons that were then located within 0.6 µm of Syn^{out}/Geph (corresponding to a serotonergic synaptic bouton in close apposition to an inhibitory synapse) or Syn^{out}/PSD95 (corresponding to a serotonergic synaptic bouton in close apposition to an excitatory synapse) spots pairs were labeled to quantify serotonergic inhibitory and excitatory triads.

2.15 Statistical Analyses

All analyses were done using the Statistical Package for the Social Sciences (GraphPad Prism version 9.4.1 for Windows, GraphPad Software, La Jolla, CA, USA; www.graphpad.com; RRID:SCR_002798). All data is expressed as mean ± SEM, where $p \leq 0.05$ was used as the threshold for significance. One-way analysis of variance was performed for data comparing Naïve, WT, and Pet-ChR2 animals, for which the Tukey's post-hoc test was also performed for multiple comparisons. Except for MRI data that was analyzed through a t-test (Mann-Whitney). All F and P values are described in **supplemental table 1**.

3. Results

3.1 Behavioral changes

Mice were treated with light stimulation during each behavioral test. Consequently, by the time they were sacrificed, Pet-ChR2 and WT had received five sessions of opto-stimulation with WT mice as negative controls. Tests were chosen to study both anxiety- and depressive-like phenotypes. Accordingly, EPM, NSF, and OF were used to test anxiety-like behaviours and, FST and TST were used to assess depressive-like behaviours. Results from each test according to the timeline are discussed separately, comparing unstressed naïve mice to stressed WT mice for the effect of stress, and WT to Pet-ChR2 mice for the effect of opto-stimulation. To avoid confounding factors naïve behavioral test data was compared to stimulated periods from WT and Pet-ChR2 mice.

3.1.1 Coat state

Coat state was used to monitor phenotypic changes associated with chronic depression-like behaviours particularly for the UCMS protocol since it was first introduced in male rats (Nollet, 2021). In our research female mice subjected to UCMS already presented deterioration of coat state after just four weeks, going from a score of 1 to an average score of 1.842 by week five. By week seven all animals showed the maximum score of 2 **(Figure 2.a)**, indicating that UCMS as a chronic stress paradigm resulted in a depressive-like phenotype.

3.1.2 Elevated Plus Maze

When comparing unstressed (naive) to stressed (WT and Pet-ChR2, pre-stimulation) there is a significant decrease in open arm duration that translated to a significant increase in closed arm duration. This suggest that UCMS promotes anxiety-like behaviours. The effect of opto-

stimulation is not evident when comparing WT and Pet-ChR2 mice, possibly because this was the first stimulation session **(Figure 2.b.2 and b.3)**.

Light also influenced distance moved within the maze. This parameter showed a proportional decrease after opto-stimulation that appeared more pronounced in the WT animals, this trend may suggest a resilience of Pet-ChR2 to freezing upon light stimulation **(Figure 2.b.1)**.

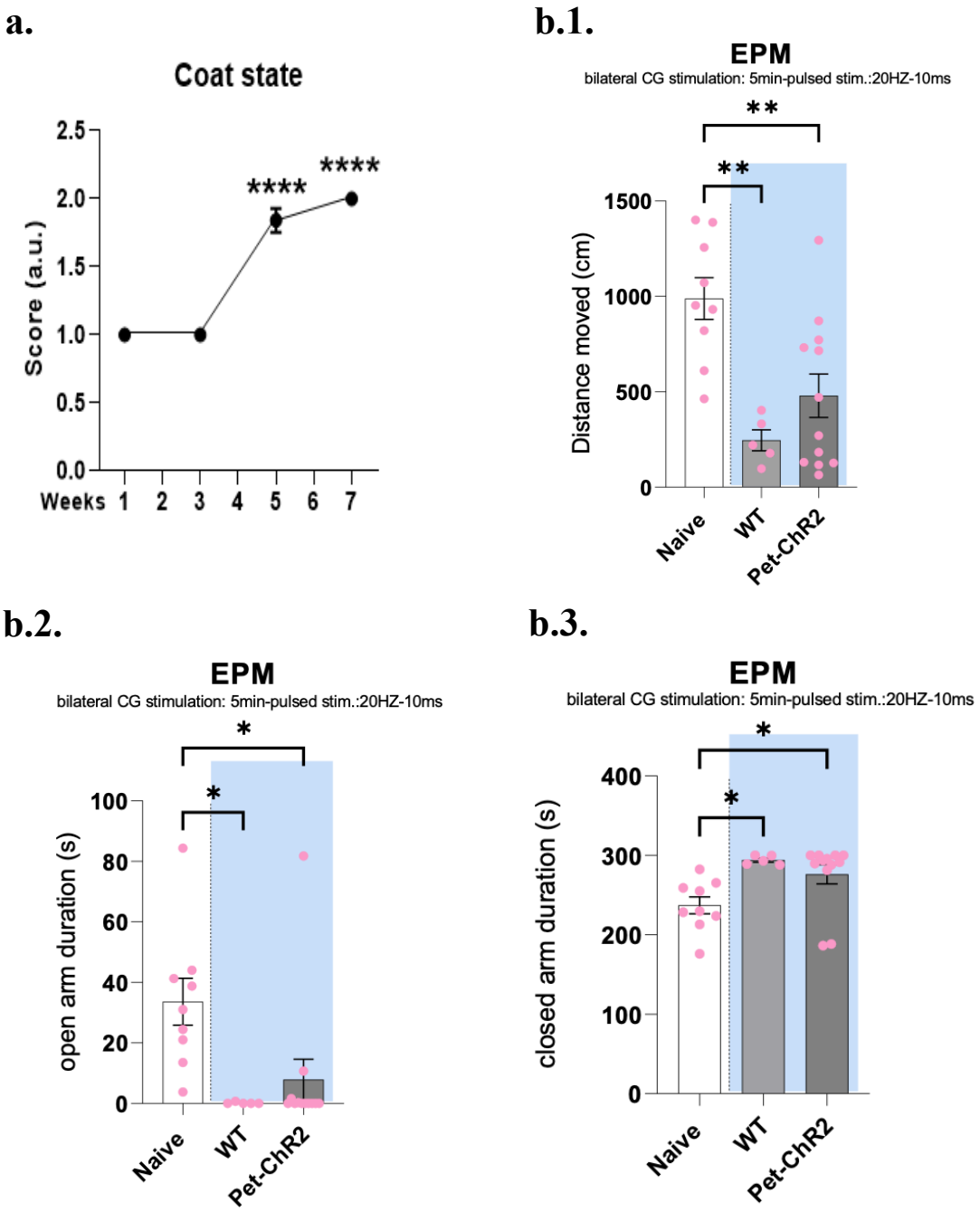

Figure 2. Deterioration in coat state and increased anxiety-like behaviours in EPM due to UCMS exposure. **a**. coat state measurement in UCMS exposed mice. **b**. EPM results **b.1**. distance moved within the EPM apparatus. **b.2**. Changes in open arm and **3**. closed arm duration. Blue bar shows period of stimulation in stimulate cohorts. Data presented as mean ± SEM. Significant differences were analysed using one-way ANOVA and post-hoc Tukey test; *p < 0.05, **p < 0.01, ***p < 0.001, ****p < 0.0001.

3.1.3 Open Field

UCMS exposed mice (WT and Pet-ChR2) showed significant decreased in distanced moved compared to naïve mice, suggesting that light induced freezing behaviour was still present by the second stimulatory session **(Figure 3.a.3)**. Naive animals had a significant greater large and small center duration than WT and Pet-ChR2 **(Figure 3.a.1 and a.2)**. Results therefore demonstrated that six weeks of UCMS according to the OF test promotes anxiety-like behaviours in female mice. Optogenetic stimulation had no significant effect when comparing stimulated Pet-ChR2 to WT mice, both for either small or large centre duration. However, a possible trend towards increased small and large center duration in some mice was seen in the Pet-ChR2 cohort. This may be an early effect of light stimulation, where some animals were able to respond rapidly and reached large center duration times like the average time shown by naïve mice.

a.1.

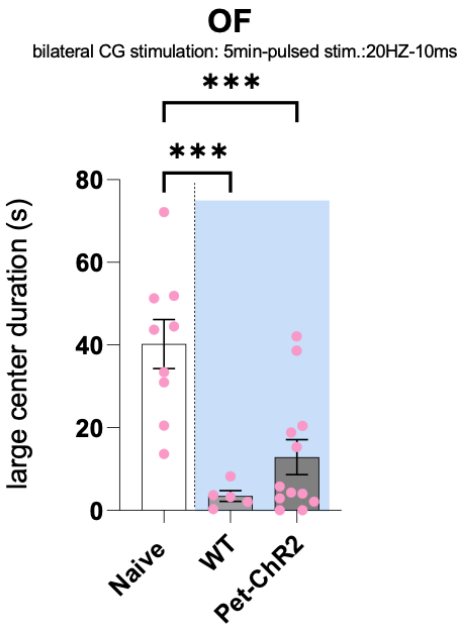

a.2.

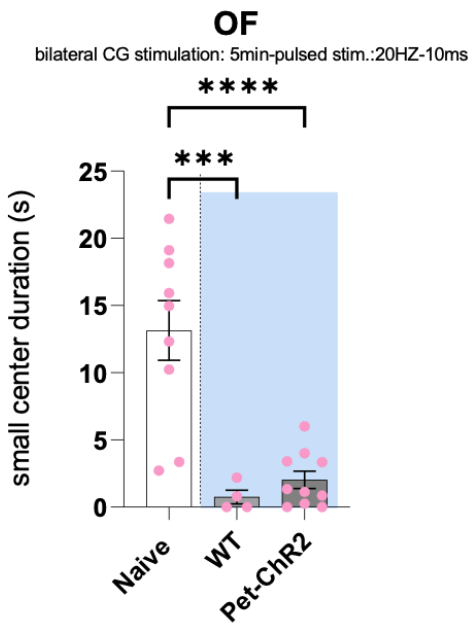

a.3.

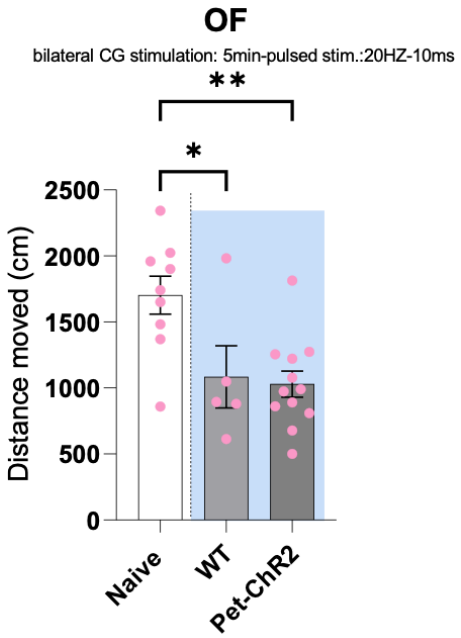

Figure 3. Increased anxiety-like behaviour in OF test of mice exposed to UCMS. **a.1.** large and **2.** small center duration in the OF arena. **3.** distance moved. Blue bar shows period of stimulation in stimulated cohorts. Data presented as mean ± SEM. Significant differences were analysed using one-way ANOVA and post-hoc Tukey test; *p < 0.05, **p < 0.01, ***p < 0.001, ****p < 0.0001.

3.1.4 Tail Suspension Test

Depression-like phenotypes were examined using the TST. This test was conducted for nine minutes total, thus stimulatory periods for WT and Pet-ChR2 lasted for the middle three minutes. There was a significant increase in immobility duration in the stressed WT mice compared to the unstressed naïve mice indicating that chronic stress in the form of UCMS and subsequent behavioral testing and mouse manipulation resulted in a depression-like phenotype. Interestingly, opto-stimulation significantly reversed this phenotype decreasing the immobility duration to a similar level seen in naive animals, indicating an antidepressant effect of opto-stimulation in this test **(Figure 4.a)**.

3.1.5 Novelty Supressed Feeding

In the NSF test, chronic stress did not alter the latency to feed in the open field arena (the unfamiliar location) **(Figure 4.b.1)** or the home cage (the control non-stressful environment) **(Figure 4.b.2)**, comparing unstressed naïve mice to stressed WT or Pet-ChR2 mice.

Furthermore, light stimulation did not have any effect on latency to feed in WT or Pet-ChR2.

The latency to feed in home cage was strongly reduced compared to the unfamiliar arena, demonstrating that lack of appetite was not a confounding factor when analysing the results. Altogether, there was no significant difference across all groups between scenarios indicating that motivation to feed did not differ between groups.

3.1.6 Forced Swim Test

The final behavioral test was the FST. Interestingly, (stressed) WT mice had a lower immobility duration than the naïve group (observable trend but not significant), suggesting that WT mice had a reduced depression-like response. Untreated Pet-ChR2 mice showed similar levels of immobility duration compared to naive animals. Upon light stimulation, both WT and Pet-ChR2 cohorts

showed similar immobility duration although in the post-stimulatory epoch the Pet-ChR2 cohort showed increased immobility **(Figure 4.c.1)**.

Interestingly stressed mice showed decreased velocity compared to unstressed mice **(Figure 4.c.2)**. This light induced freezing response, could account for the slight increase in immobility and may reflect increased anxiety in these mice post-stress. It may also indicate that female mice were struggling due to the added weight from the opto-stimulation apparatus.

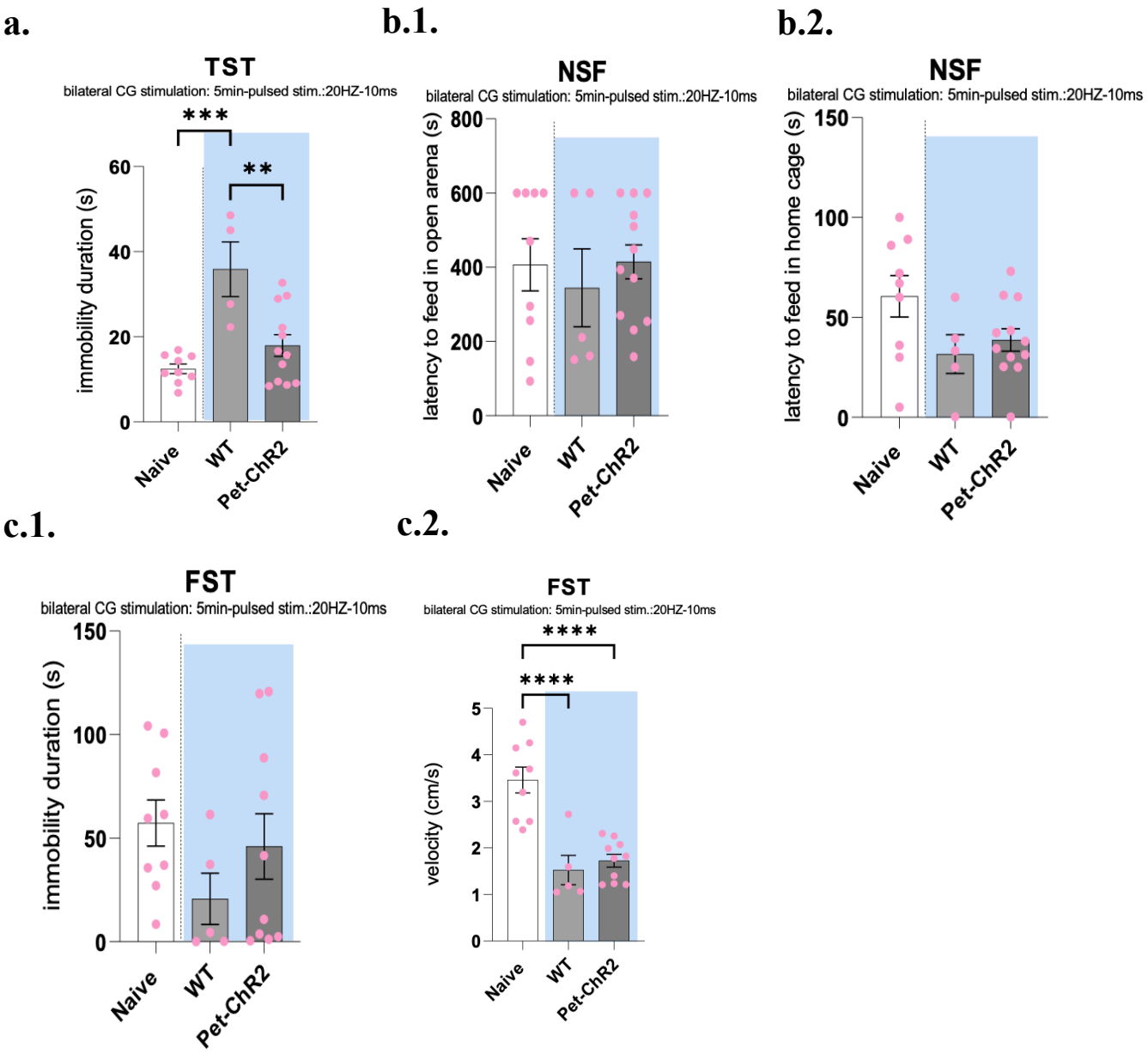

Figure 4. Increased depressive-like behaviour in TST due to UCMS with robust antidepressant effect from opto-stimulation. Changes seen in NSF and FST. **a.** TST showed significant changes in immobility duration in UCMS exposed animals and opto-stimulated mice. **b.** NSF test with no changes in **1.** open field arena or **2.** home cage. **c.1.** immobility duration of FST with no significant changes and **2.** decrease velocity of opto-stimulated mice in the FST apparatus. Blue bar shows period of stimulation in stimulate cohorts. Data presented as mean ± SEM. Significant differences were analysed using one-way ANOVA and post-hoc Tukey test; *$p < 0.05$, **$p < 0.01$, ***$p < 0.001$, ****$p < 0.0001$.

3.2 Changes in Dorsal Raphe

For opto-stimulation, light fibers were implanted in the mPFC at the CG, thus the light beam may also have reached further down within the mPFC to activate serotonin projections to the Prl and IL, sub-divisions of the mPFC. The mPFC communicates with serotonin neurons of the DR, which project widely throughout the corticolimbic system to impact anxiety and depression behaviour. To assess chronic brain activation patterns FosB-positive cells were quantified and colocalization with neuronal markers, used to identify cell types, was measured. Analysis was done in forebrain regions, hippocampal regions, and the dorsal raphe nucleus, regions that were the most enriched in FosB staining and implicated in chronic stress response. Opto-stimulation was directed to serotonin neuron projections, thus the DR (region where the serotonin system originates) was studied using TPH+ expression to identify serotonin cell bodies. Secondly, in hippocampus and mPFC excitatory and inhibitory neuronal activity was identified through the co-staining with CamKIIα+ and GAD67+ cells, respectively.

3.2.1 Chronic activity changes in the DR

Total FosB-positive cells were quantified in three sub-regions of the DR: the dorsal (DDR), lateral (LDR) and ventral (VDR). Comparing naïve to WT mice, no significant changes in FosB+ cells were seen in the three regions of the DR, suggesting that chronic stress did not affect chronic cellular activity in the DR. Importantly there was a significant increase in FosB+ cells after stressed animals were subjected to the optogenetic paradigm. FosB+ cell number was significantly increased in the Pet-ChR2 animals in the DDR showing double the amount of that shown by naïve or stressed WT animals **(Figure 5.a.1)**.

The same trend was seen in the VDR **(Figure 5.a.2)** where there was a significant increase in FosB+ cells in optogenetically-stimulated stressed Pet-ChR2 compared to naïve animals. Finally,

the LDR showed no significant changes between cohorts **(Figure 5.a.3)**. Thus, optogenetic stimulation of the mPFC induced a sub-region-specific activation of DR cells, mainly in the dorsal and ventral DR.

3.2.2 Serotonergic neurons

To analyse changes in the serotonin system TPH was used as an immunohistochemical marker for 5-HT cells. A reduction was observed in the number of TPH+ cells in the DDR and VDR of WT animals compared to naive animals **(Figure 5.b.1 and b.2.)**, with a similar trend in the LDR **(Figure 5.b.3)** that was not statistically significant. In all three subregions of Pet-ChR2's DR the loss of TPH+ cells were no longer significant compared to naïve mice, suggesting optogenetic stimulation partially restore the stress-induced loss of TPH expression.

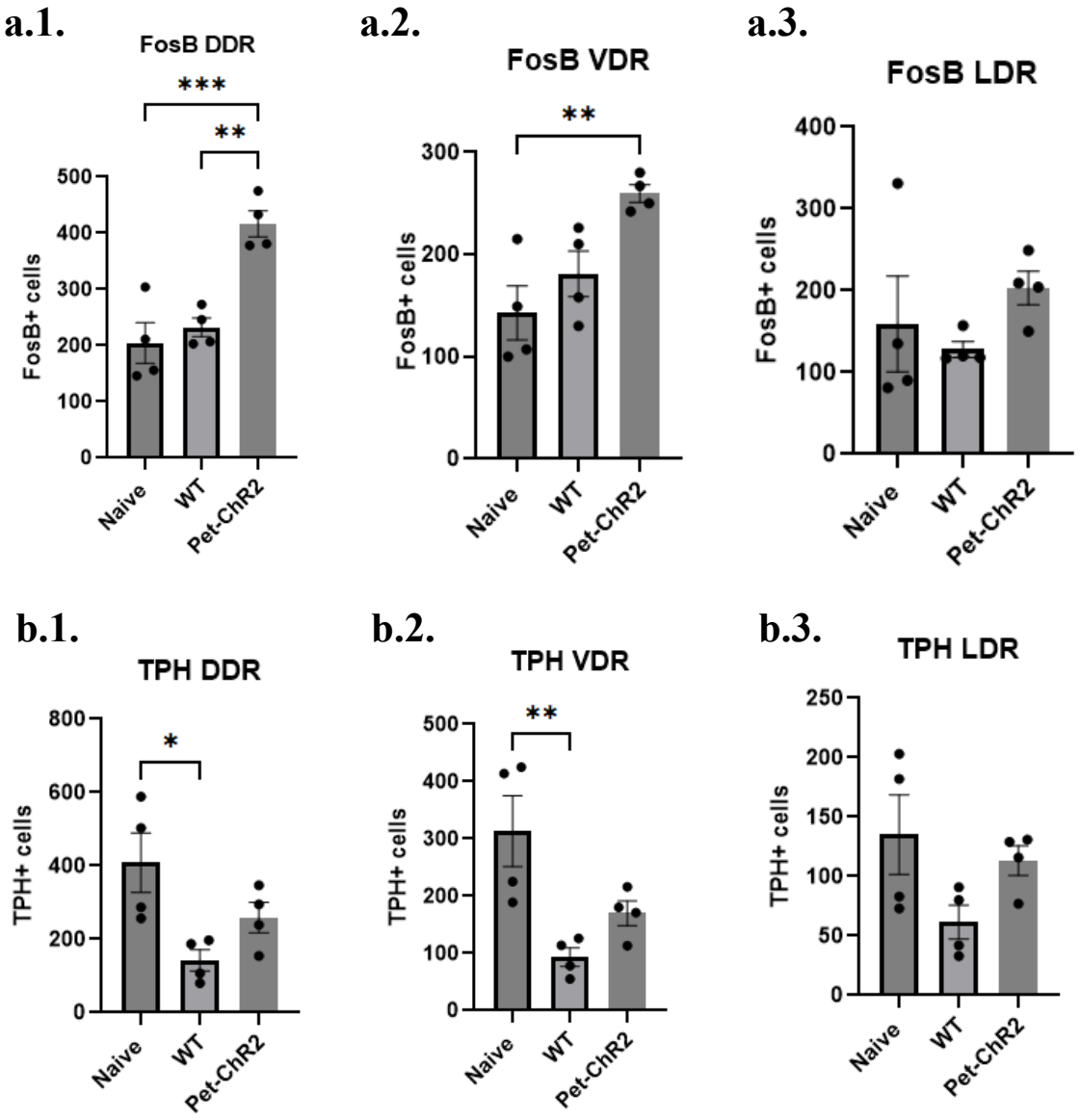

Figure 5. Increased chronic activity of the dorsal raphe and decrease TPH+ cells due to stress. DR was divided into three subregions dorsal (DDR), ventral (VDR) and later (LDR). **a.1.2.3.** Images were quantified for FosB in three subregions. **b.1.2.3.** Images were quantified for TPH in three subregions. Data presented as mean ± SEM; n=4 per group and quantification is taken from 4 different levels of the DR. Significant differences were analysed using one-way ANOVA and post-hoc Tukey test; *$p < 0.05$, **$p < 0.01$, and ***$p < 0.001$.

3.2.3 Chronic activity of serotonergic neurons

The co-localization of TPH+/FosB+ staining in the DR was quantified to assess changes in chronic activity of 5-HT neurons. Comparing naïve to stressed WT mice showed that the number of TPH+/FosB+ cells remained the same in all three sub-regions of the DR, indicating that chronic stress did not affect the overall activity of 5-HT neurons, despite the reduced number of TPH+ cells **(Figure 6.b.1, b.2. and b.3.)**. However, very surprisingly, comparing Pet-ChR2 to WT mice showed that optogenetic stimulation after chronic stress induced a significant increase in the co-localization of TPH and FosB. The most robust effect was in the DDR **(Figure 6.b.1)**, most likely due to the higher density of TPH+ cells. Importantly, significant increases in TPH+/FosB+ co-localization were seen in all subregions. This suggests that optogenetic stimulation of serotonergic projections in the mPFC significantly increased the chronic activity of the whole serotonin system by activating serotonin cell bodies. The optogenetic stimulation in fact potentiated the chronic activity of serotonin neurons in all subregions, more than doubling the number of TPH+/FosB+ in Pet-ChR2 animals compared to the naïve or stressed WT cohorts, and this difference is apparent in the representative epifluorescence images **(Figure 6.a.)**.

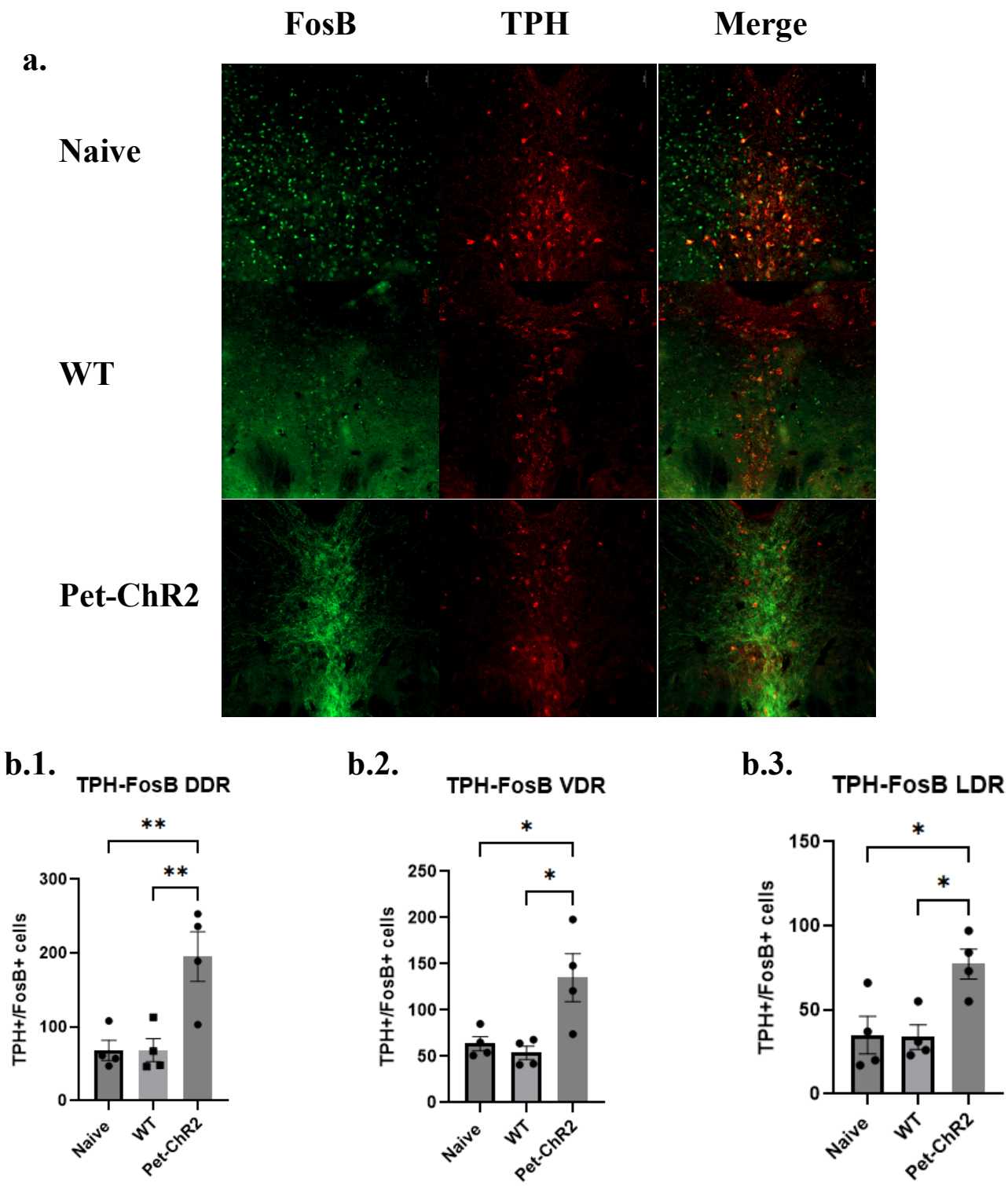

Figure 6. Significant increase of serotonergic chronic activity in dorsal raphe of optogenetic stimulated Pet-ChR2 mice. DR was divided into three subregions dorsal (DDR), ventral (VDR) and later (LDR). **a.** Representative images of FosB and TPH immunostaining in DR. **b.1.2.3.** Images were quantified for dual-labelled cells. Scale bar shows 50 µm. Data presented as mean ± SEM; n=4 per group and quantification is taken from 4 different levels of the DR. Significant differences were analysed using one-way ANOVA and post-hoc Tukey test; *$p < 0.05$ and **$p < 0.01$.

3.3 Chronic neuronal activity

Chronic brain activation patterns in the forebrain and hippocampal regions showed an effect of chronic stress.

Exposure to chronic stress had the strongest effect on the IL and NAc **(Figure 7.b. and c)**. These regions showed a significant decrease of FosB+ cells in the WT mice compared to the naïve cohorts **(Figure 7.a.)**. This suggests a dampening of chronic brain activity due to UCMS. Interestingly, optogenetic stimulation had a robust effect in the hippocampal region CA1 **(Figure 7.d.)**. Pet-ChR2 mice showed a significant three-fold increase in FosB+ cell number when comparing unstressed to stressed mice, showing a robust effect of opto-stimulation on the chronic activity of the hippocampus.

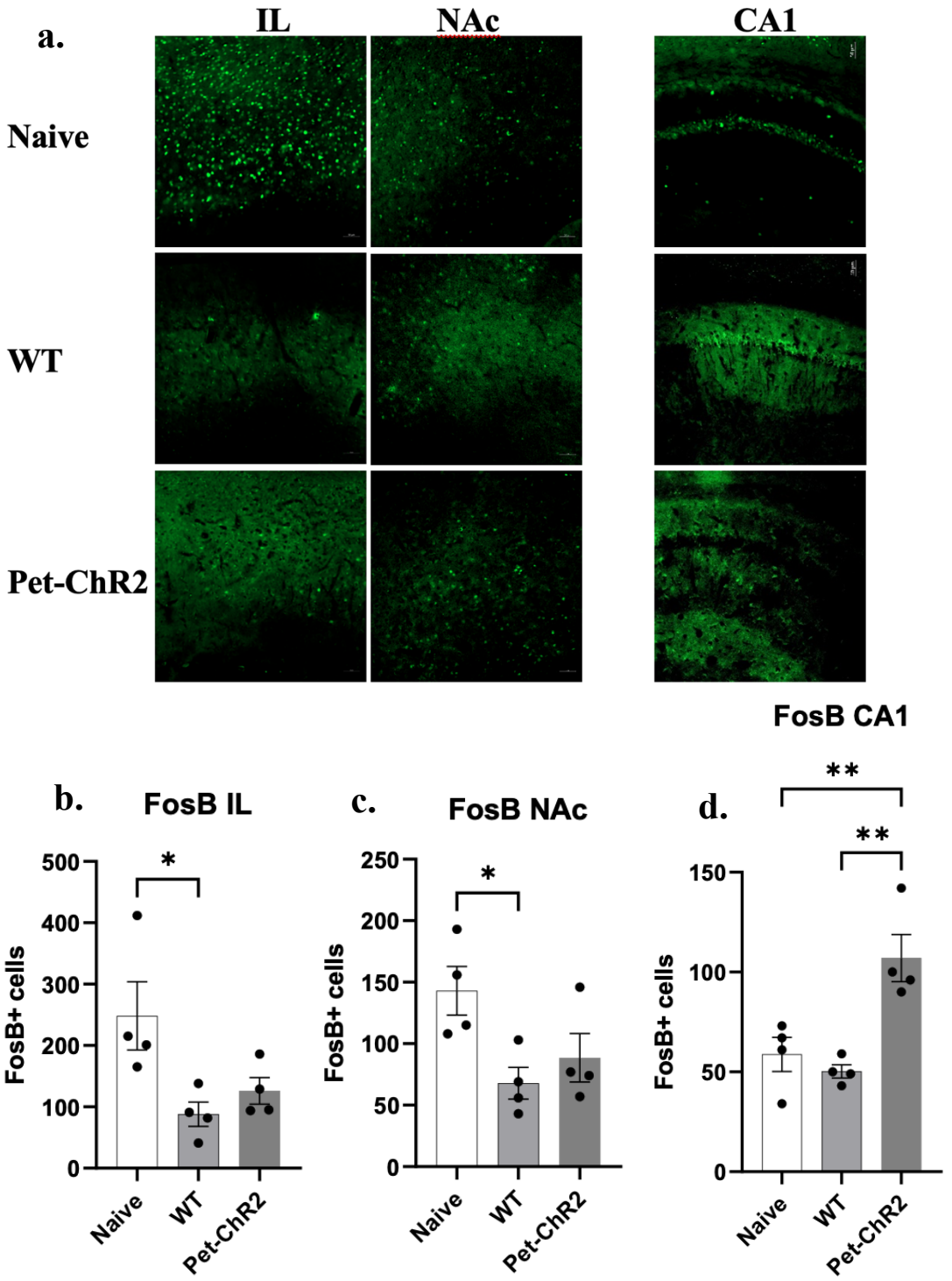

Figure 7. Significant chronic activity decreases due to UCMS, and chronic activity potentiation in CA1 shown by FosB staining. **a.** Representative images of FosB immunostaining in IL, NAc, and CA1. Images were quantified for FosB+ cells and UCMS induced changes were seen in **b.** IL and **c.** NAc; opto-stimulation induced recovery was seen in **d.** CA1 is shown. Scale bar shows 50 µm. Data presented as mean ± SEM; n=4 per group. Significant differences were analysed using one-way ANOVA and post-hoc Tukey test; *$p < 0.05$ and **$p < 0.01$.

The effect of UCMS seen in the IL and NAc was mimicked in other brain regions however the differences in FosB+ cells between WT and naïve mice were not significant.

A decrease in FosB+ cell quantification after chronic stress was seen in the CG, PrL, MO, and LSN **(Figure 8.)**. The CG showed a 50% reduction, the biggest decrease out of the four regions **(Figure 8.a.)**. The hippocampal regions CA2-3, DG, BLA, and EC showed a similar trend, where chronically stressed WT mice showed decreased FosB+ cell quantification **(Figure 8.)**.

The effect of opto-stimulation seen in CA1 was also seen in PrL **(Figure 8.b.)**, although not significant. To a lesser extent FosB+ cell quantification increased in the Pet-ChR2 cohort compared to the stressed WT mice in MO, NAc, IL, EC, BLA, CA2-3, and LSN **(Figure 8.)**. Curiously, Pet-ChR2 mice in the CG showed the same level of FosB+ cells as WT mice, and DG showed a lower cell quantification in opto-stimulated mice compared to WT. This may allude to the inability of opto-stimulation to fully recover the lost chronic activity in these brain regions.

Lastly, the MSN showed the same level of FosB+ cells in all three groups **(Figure 8.e.)**.

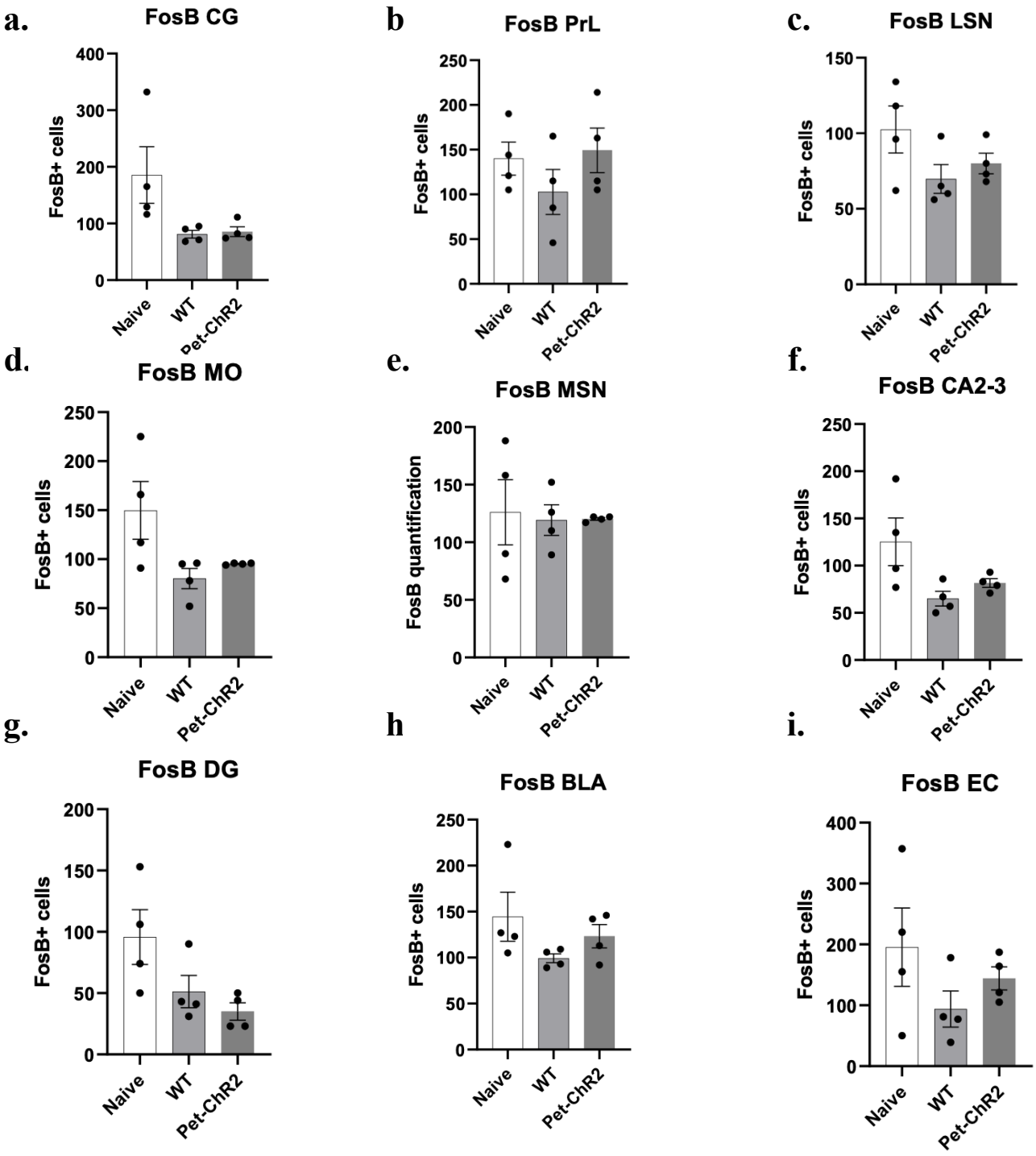

Figure 8. Chronic activity decreases shown by FosB quantification due to UCMS exposure. Data presented as mean ± SEM; n=4 per group. Significant differences were analysed using one-way ANOVA and post-hoc Tukey test.

3.4 Chronic excitatory neural activity

The co-localization of CamkIIα+/FosB+ was used as readout of the chronic activity of excitatory neurons. Within the mPFC, they showed a clear difference between unstressed vs stressed animals. Within the CG and PrL **(Figure 9.a. and b.)** a significant reduction of CamkIIα+/FosB+ co-localization was seen in WT vs. naïve mice, due to UCMS exposure. This stress-induced reduction of the chronic activity of excitatory neurons may contribute to the phenotypes seen in behavioral testing.

Optogenetic stimulation significantly increased the number of CamkIIα+/FosB+ cells in MSN and CA1 **(Figure 9.c.2. and c.3.)**, when comparing WT to Pet-ChR2 mice, suggesting that opto-stimulation had modulatory effects through activation of excitatory neurons. Both regions showed a higher CamkIIα+/FosB+ co-localization in the Pet-ChR2 mice even when compared to naïve animals **(Figure 9.c.1.)**. The strongest effect of opto-stimulation was seen in the CA1 which indicates that chronic activity of pyramidal CA1 neurons was robustly potentiated after the paradigm of opto-stimulation of 5-HT neuronal projections to the mPFC and may explain the antidepressant-like behavioral changes seen in TST.

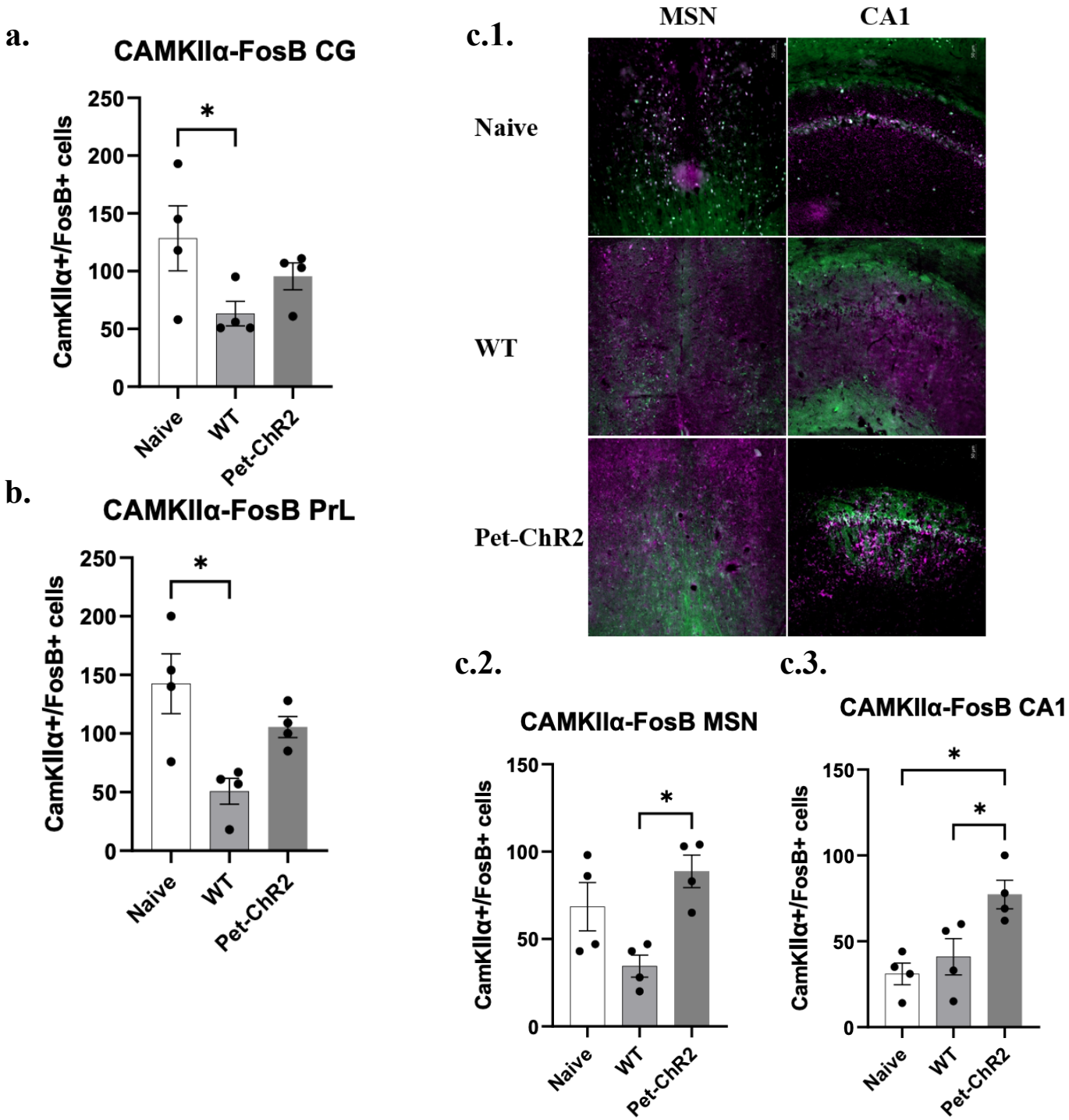

Figure 9. Significant decrease of chronic excitatory activity due to UCMS in CG and PrL, and potentiation of MSN and CA1 due to opto-stimulation. With quantification of the co-localization of CaMKIIα+/FosB+ cells staining. UCMS induced changes were seen in **a.** CG and **c.** PrL; opto-stimulation induced recovery was seen in **c.2.** MSN and **c.3.** CA1. **c.1.** Representative images of MSN and CA1 with CaMKIIα+/FosB+ immunostaining. Scale bar shows 50 µm. Data presented as mean ± SEM; n=4 per group. Significant differences were analysed using one-way ANOVA and post-hoc Tukey test; *$p < 0.05$.

Other regions in the brain showed the same trend towards decreased excitatory chronic activity due to UCMS. However, these changes were not significantly different. The IL, MO, NAc, MSN, CA2-3, BLA, and EC all showed a trend towards decreased CamkIIα+/FosB+ co-localization in the WT mice compared to naïve mice **(Figure 10.)**. On the other hand, UCMS induced increased CamkIIα+/FosB+ co-localization in the DG **(Figure 10.e.)**.

Opto-stimulation showed an overall trend towards increased chronic activity of excitatory neurons. In CG and PrL the co-localization of CamkIIα+/FosB+ cells in the Pet-ChR2 cohort were no longer statistically different from naïve **(Figure 9.a. and b.)**. Additionally, the IL, MO, and BLA cell quantification showed that Pet-ChR2 mice expressed the same levels of CaMKIIα+/FosB+ co-localization as the unstressed cohort (Naive animals) **(Figure 10.)**. Surprisingly, in the NAc and EC **(Figure 10.c. and g.)**, the opto-stimulated Pet-ChR2 animals showed a higher number of CaMKIIα+/FosB+ cell quantification than the naive group, although the difference between WT and Pet-ChR2 was not significant. This showed a trend towards increased excitatory chronic activity that may become significant with the addition of more mice.

Interestingly, CA2-3 **(Figure 10.d)** showed that opto-stimulation of Pet-ChR2 mice failed to change CamkIIα+/FosB+ co-localization number from the stressed-induced decrease seen in the WT mice. Furthermore, the DG **(Figure 10.e.)** showed a decrease in CamkIIα+/FosB+ cells compared to WT. The results seen in these regions may suggest that stronger or longer opto-stimulation may be needed to see a full recovery of excitatory neural activity.

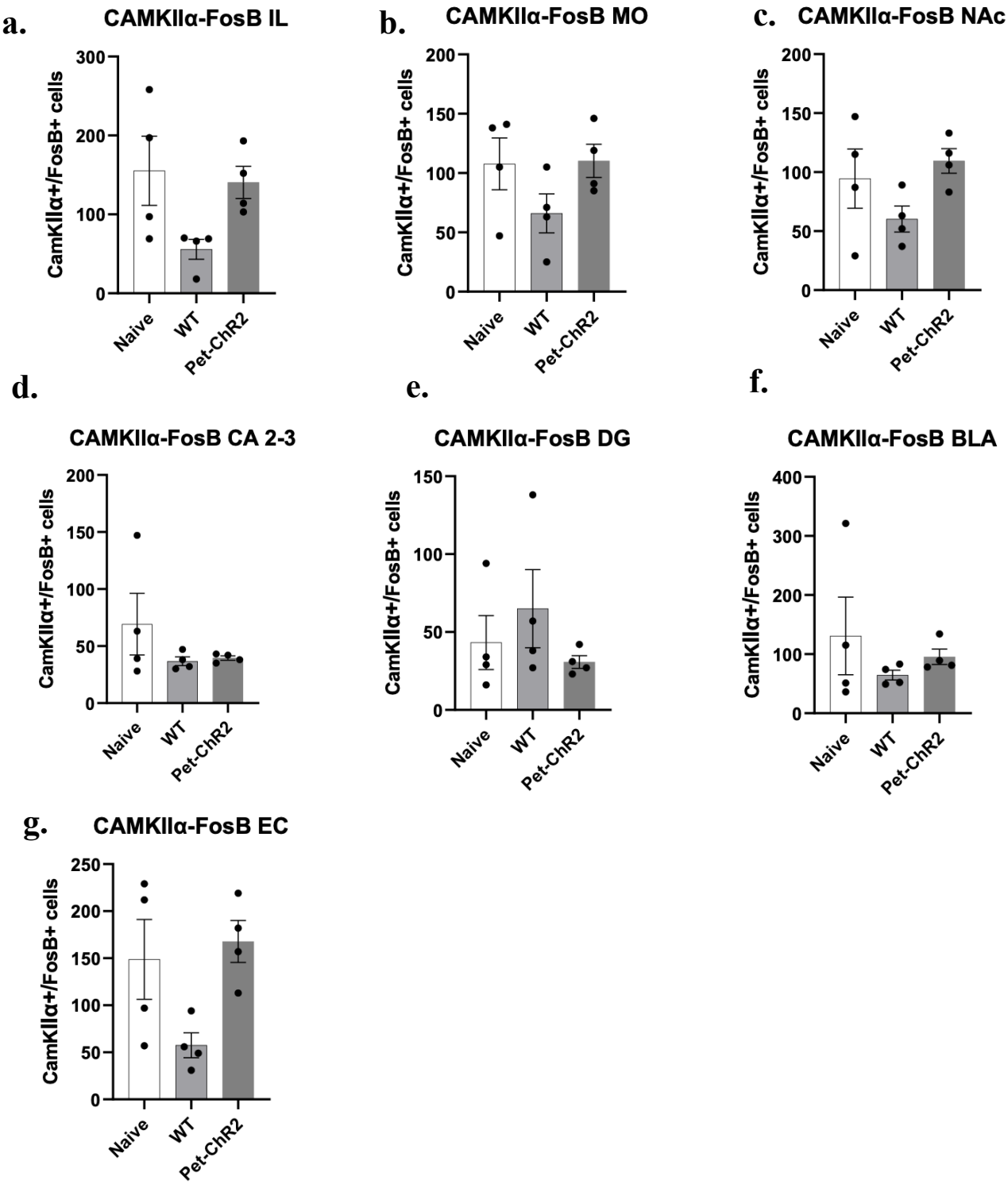

Figure 10. Excitatory chronic activity changes shown by CaMKIIα+/FosB+ co-localization and quantification. Data presented as mean ± SEM; n=4 per group. Significant differences were analysed using one-way ANOVA and post-hoc Tukey test; *p < 0.05, **p < 0.01, ***p < 0.001, ****p < 0.0001.

3.5 Chronic inhibitory neuronal activity

The effect of chronic stress and opto-stimulation on inhibitory GABAergic interneurons was assessed through the co-localization of GAD67 and FosB.

Chronic exposure to stress resulted in significant decreased chronic activity of inhibitory neurons. This was seen in IL, MO, CA2-3, BLA, and EC **(Figure 11.)** that showed decreased GAD67+/FosB+ cell quantification in the WT cohort compared to naïve mice. The strongest effect of UCMS was seen in the MO **(Figure 11.b.)** and EC **(Figure 11.e.1 and 2.)**.

In this chronic activity parameter, opto-stimulation did not significantly change GAD67+/FosB+ cell quantification in any brain region.

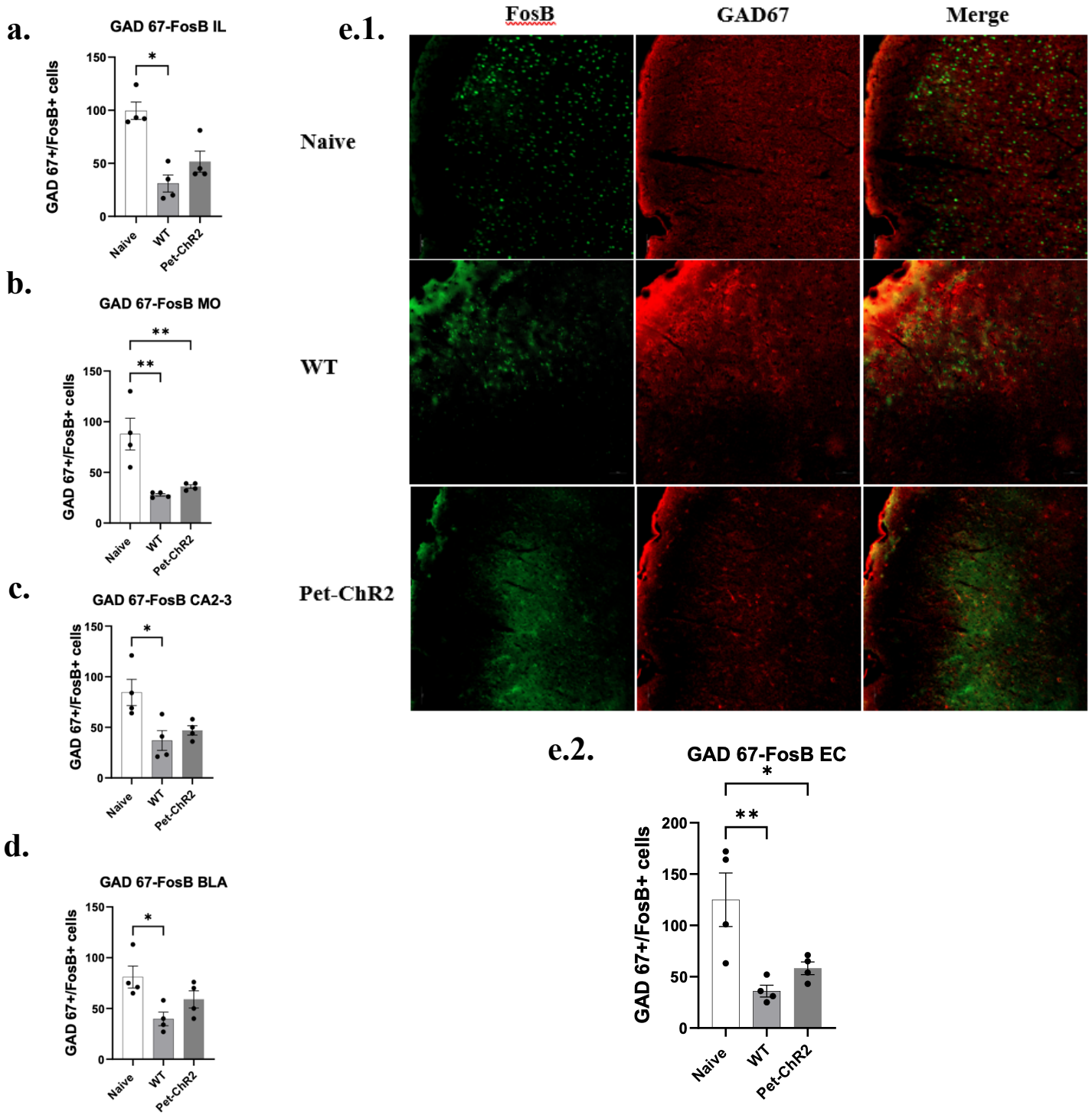

Figure 11. Significant decrease in chronic inhibitory activity shown by the quantification of the co-localization of GAD67+/FosB+ cells staining induced by UCMS. **e.1.** Representative images of EC with GAD67+/FosB+ immunostaining. Scale bar shows 50 µm. Data presented as mean ± SEM; n=4 per group. Significant differences were analysed using one-way ANOVA and post-hoc Tukey test; *$p < 0.05$ and **$p < 0.01$.

Other regions showed non-significant changes due to UCMS with chronically stressed animals (WT) having a lower number of GAD67+/FosB+ cells than unstressed (naive) mice. This was seen in CG, PrL, NAc, MSN, LSN, CA1, and DG **(Figure 12.)**. The biggest decrease was seen in the NAc and DG **(Figure 12.c. and g.)**.

Opto-stimulated mice showed increased trends of GAD67+/FosB+ cells in PrL, IL, NAc, MSN, LSN, EC, and BLA **(Figure 12.)**. Whereas in the PrL region **(Figure 12.b.)**, opto-stimulation induced higher GAD67+/FosB+ co-localization, with quantification being comparable to naïve animals. Interestingly, in the CG, MO, CA1, and CA2-3 **(Figure 12.)** Pet-ChR2 mice had a similar GAD67+/FosB+ cell quantification compared to WT mice. This may show that opto-stimulation was unable to recover the damage from chronic stress exposure. Moreover, the DG showed a lower GAD67+/FosB+ co-localization in opto-stimulated (Pet-ChR2) mice compared to stressed (WT) mice which may suggest that in this region opto-stimulation was not able to stop the effect from UCMS exposure.

All together FosB data showed that UCMS had a significant negative effect on the chronic activity of IL and NAc. Additionally inhibiting the excitatory chronic neuronal activity of CG and PrL, and dampening the inhibitory neural activity of IL, MO, CA2-3, BLA, and EC.

Contrariwise, opto-stimulation was able to recover chronic activity in CA1 and potentiate excitatory neural activity in MSN and CA1.

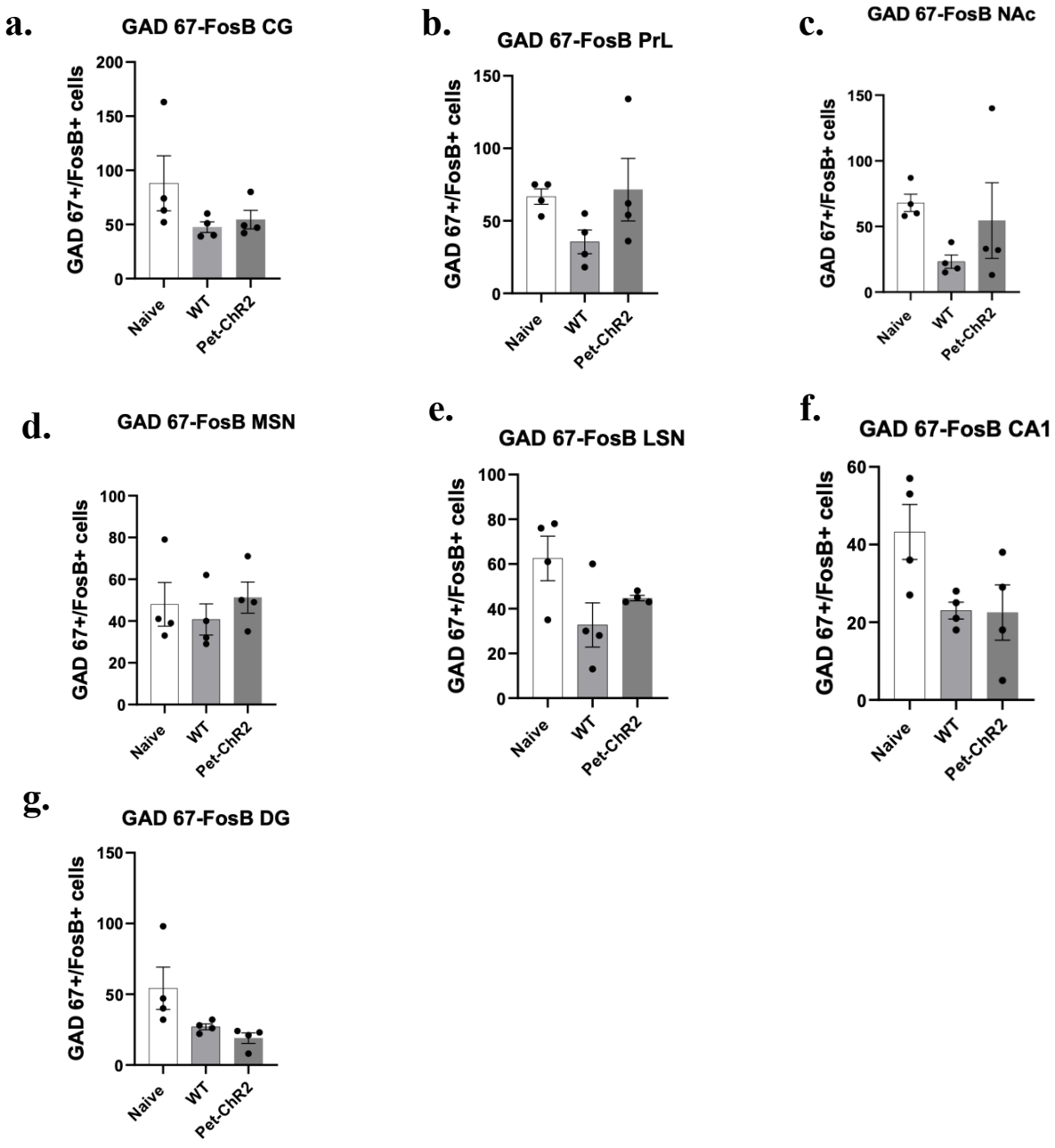

Figure 12. Decreases in inhibitory chronic activity shown by GAD67+/FosB+ co-localization and quantification. Data presented as mean ± SEM; n=4 per group. Significant differences were analysed using one-way ANOVA and post-hoc Tukey test.

3.6 Hippocampal volume changes

To fully understand the actions of chronic stress and optogenetic stimulation, volumetric data from the hippocampus was compared between the left and right side, dorsal and ventral sections, in WT and Pet-ChR2, under the following conditions: 1) unstressed, 2) stressed, and 3) stimulated mice. These comparisons did not show any differences between groups. However, pooling the data together, to assess the effect of stress alone and compare unstressed vs. stressed mice adding both left and right hippocampi, showed a significant decrease of hippocampal volume in the stressed mice. This is in line with what other working groups have highlighted, both in animal and human studies (McEwen, 1999). Chronic stress resulted in a decrease in hippocampal volume **(Figure 13.)**. There was no effect of optogenetic stimulation, thus optogenetic stimulation of the 5-HT projections in the CG may not be sufficient for recovery of hippocampal volume following chronic stress. However, additional mice may be necessary to fully address this issue.

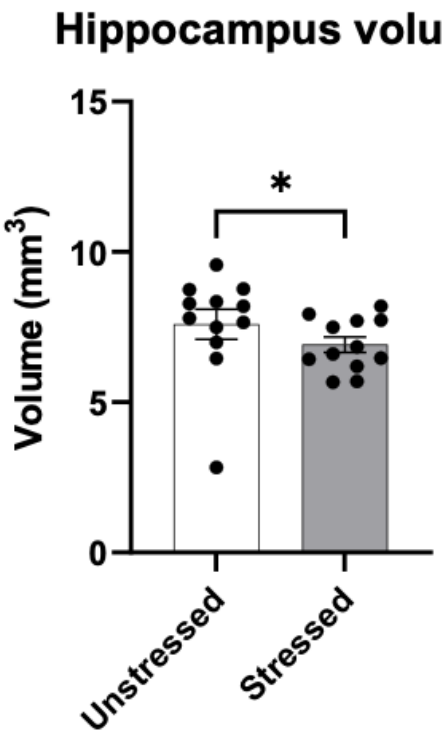

Figure 13. Decrease in hippocampal volume of chronically stressed compared to unstressed mice. Volume changes were assessed by manually tracing seven individual sections from an MRI scan per animal, multiplying individual surface areas by the thickness of the scan (300 µm) and adding the results together. Data presented as mean ± SEM; n=6 per group with values for left and right. Significant differences were analysed using T-test (Mann-Whitney); *$p < 0.05$.

3.7 5-HT projection changes (axonal volume and varicosity density)

Serotonergic axonal volume and the number of putative serotonergic boutons were examined by quantifying the 3D distribution obtained from the reconstruction of SERT immunostaining in specific stress-sensitive regions of interest revealed using FosB staining, as shown in the representative images in **Figure 14**. The actions of both chronic stress and optogenetic stimulation was studied in the context of 1) the changes in serotonergic axonal volume and 2) the density of SERT+ varicosities. The axonal volume and varicosity density were normalized to the template volume (284748.5 μm^3) obtained from the size of the confocal Z-stacks (53 stacks, 0.3 μm apart).

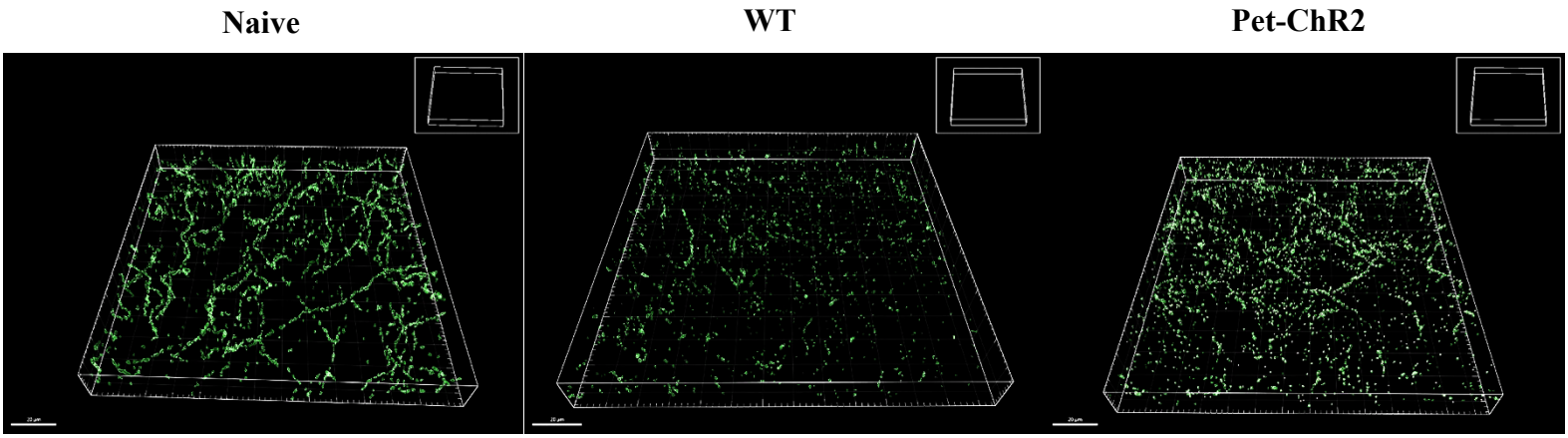

Figure 14. Representative images of 5-HT axonal volume and density of varicosities of the CG shown by the reconstruction of SERT immuno-stained sections using Imaris 64x 10.1.

Chronic stress decreased axonal volume in almost every region studied, while optogenetic stimulation was unable to significantly recover the lost axonal volume. In the mPFC, the CG showed a significant reduction between naïve vs. WT. However, optogenetic stimulation induced an observable but non-significant increase of SERT+ axonal volume that was no longer different from naïve tissue **(Figure 15.a.)**. The PrL showed a more marked reduction of SERT+ axonal volume in both WT and Pet-ChR2 cohorts **(Figure 15.b.)**. The IL showed a trend towards reduction; however, this was the only region examined where the decrease in axonal volume was not significant in either of the chronically stressed groups **(Figure 15.c.)**.

The NAc, EC, and MR all showed the same level of significant decrease after chronic stress between naïve vs. WT mice **(Figure 15.d., g., and i)**. It was only in the EC where the significant decrease of SERT+ axonal volume was maintained in the Pet-ChR2 mice when compared to naïve levels. The MR showed a slight recovery of the lost SERT+ axonal volume which was also seen in the CG. Nonetheless, the NAc showed similar levels of axonal volume in Pet-ChR2 vs. WT.

Both the BLA and DR showed a more pronounced stress-associated decrease of SERT+ axonal volume and processes density, respectively, in both stressed cohorts (WT and Pet-ChR2) compared to the naïve **(Figure 15.f. and h.)**.

The LSN region showed the most significant decrease of SERT+ axonal volume in both stress cohorts compared to the naïve cohort **(Figure 15.e.)**.

Overall, the strongest difference in naïve vs. stressed cohorts was seen in LSN, BLA, and DR, which was a direct effect of chronic exposure to stress in the form of UCMS. Optogenetic stimulation as unable to recover axonal lost and levels of axonal volume shown by Pet-ChR2 mice were similar to those seen in WT cohort. Expect for the CG and MR. The CG was the region with

the optogenetic implant, thus received more direct stimulation which may explain the upwards trend towards recovery of the lost axonal volume due to chronic stress. The increase in MR may suggest that the cortical stimulation is in turn prompting the raphe nuclei recovery of lost axonal volume; however, greater n value would be needed to verify this.

In the hippocampal region of the brain the CA1, CA2-3, and DG subregions were examined separately. The MRI data showed decreased volume in the hippocampal region. For MRI quantification it was necessary to use sections that contained dorsal and ventral areas of the hippocampus to assess specific subregions of change. Consequently, for axonal volume and density of varicosities quantification was conducted in four different sections that contained four different levels of the hippocampus. Ensuring that two slides showed dorsal hippocampus, and two slides showed ventral sections of the hippocampus.

All three subregions of the hippocampus CA1, CA2-3 and DG showed the same trend with significant decrease of SERT+ axonal volume in chronic stressed cohorts, both WT and Pet-ChR2 mice. As seen in most areas studied, optogenetic stimulation did not alter axonal volume. Thus, Pet-ChR2 mice showed the same level of significant decrease compared to the Naïve cohort **(Figure 15.j., k., and l.)**.

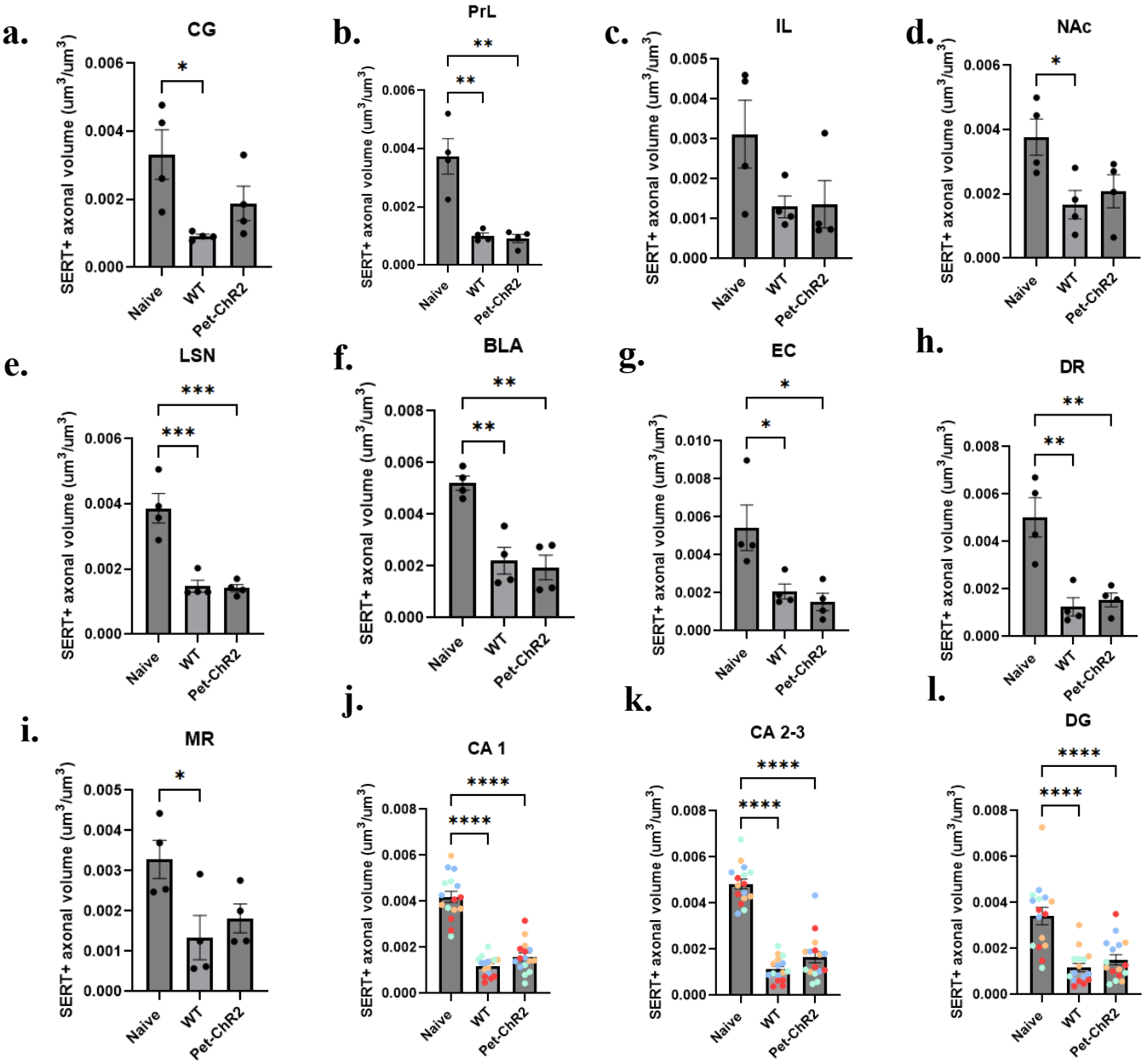

Figure 15. UCMS induced region-specific decrease of 5-HT axonal volume. Shown by the reconstruction and analysis of SERT immuno-stained sections using Imaris 64x 10.1. Axonal volume was normalized to tissue volume of the template. Data presented as mean ± SEM; n=4 per group. Hippocampus (CA1, CA2-3, DG) quantification was taken from 4 different levels of n=4 represented by four different colours, that showed no significant differences amongst levels. Significant differences were analysed using one-way ANOVA and post-hoc Tukey test; *$p < 0.05$, **$p < 0.01$, ***$p < 0.001$, ****$p < 0.0001$.

Varicosity density numbers generally reflected a chronic stress-induced reduction, as seen in axonal volume **(Figure 16.)**. However, some regions showed no change in varicosity density. The IL showed little change in varicosity density after chronic stress in both WT and Pet-ChR2 mice compared to naïve **(Figure 16.ac.)**. The hippocampal sections also showed the same trend, except the DG where the reduction of varicosity density in Pet-ChR2 mice was less significant than in the WT mice suggesting a partial effect of opto-stimulation **(Figure 16.l.)**. Nonetheless, overall similar results were seen for the density of varicosities, indicating that chronic stress reduces SERT+ varicosities and opto-stimulation does not greatly affect this change.

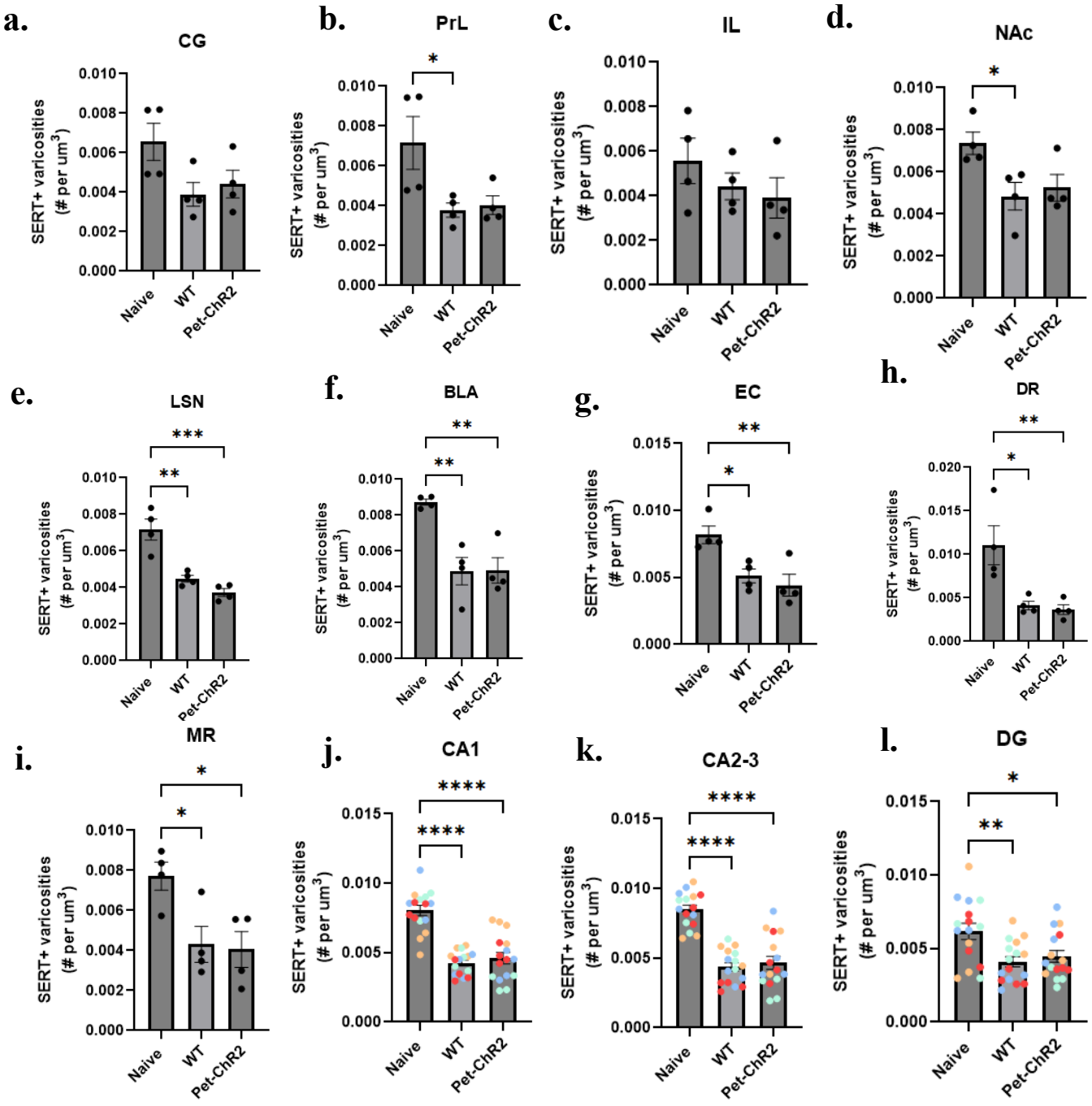

Figure 16. UCMS induced region-specific decrease of 5-HT varicosities. Shown by the reconstruction and analysis of SERT immuno-stained sections using Imaris 64x 10.1. Density of varicosities was normalized to tissue volume. Data presented as mean ± SEM; n=4 per group. Hippocampus (CA1, CA2-3, DG) quantification was taken from 4 different levels of n=4 represented by four different colours, that showed no significant differences amongst levels. Significant differences were analysed using one-way ANOVA and post-hoc Tukey test; *$p < 0.05$, **$p < 0.01$, ***$p < 0.001$, ****$p < 0.0001$.

3.8 5-HT synapse formation changes

Using synaptophysin as a marker of presynaptic release sites within the SERT+ axons, we quantified 5-HT boutons closely apposed to both neurochemical excitatory and inhibitory synapses. Proximity within 0.6 μm of serotonergic boutons and presynaptic endings of excitatory (PSD 95+) and inhibitor (Gephyrin+) terminals were identified, to quantify 5-HT synapses to inhibitory and excitatory synaptic sites. For quantification purposes of full triadic information, synaptophysin positive molecules that were in close apposition to either PSD95 (neuronal excitatory marker) or gephyrin (neural inhibitory marker) were selected. After which the co-localization of either co-localized syn in+ (synaptophysin within the SERT+ axon) and PSD95 or Geph with syn out+ (synaptophysin outside the SERT+ axon), corresponding to presynaptic terminals of either PSD95+ or Geph+ neurons, was determined. Consequently, two different parameters were measured. The density of 5-HT synapses with inhibitory and excitatory synapses and the full 5-HT triadic synapses to comment on the excitatory and inhibitory synapses that are modulated by serotonergic transmission.

Regions of the mPFC showed decrease excitatory and inhibitory contacts in WT mice compared to naïve levels. The CG, IL, and NAc **(Figure 17 and 18.a., c., and d.)** showed a decreasing trend in excitatory contacts. A stress-associated reduction was also seen for inhibitory contacts in the CG, which showed a significant decrease in the WT vs. naïve. Optogenetic stimulation showed increasing trends in CG and NAc in both excitatory and inhibitory contacts but not in IL. There was a significant reduction in excitatory and inhibitory contacts in both chronically stressed cohorts in the PrL region **(Figure 17 and 18.b.)**, where optogenetic stimulation was unable to recover them.

The LSN, BLA, EC, and DR **(Figure 17 and 18.e., f., g., and h.)** showed the same decreasing trend of both excitatory and inhibitory contacts after chronic stress compared to naïve mice. The LSN showed this decrease to be significant in excitatory contacts. All regions showed no recovery effect of optogenetic stimulation and WT vs. Pet-ChR2 cohorts showed similar levels of excitatory and inhibitory contacts, expect in the EC where Pet-ChR2 mice showed non-significant lower levels of both types of contacts compared to WT.

Hippocampal regions CA1, CA2-3, and DG **(Figure 17 and 18.j., k., and l.)** showed significant decreases in excitatory and inhibitory contacts following chronic stress. Pet-ChR2 mice showed similar levels of excitatory and inhibitory synapses as WT mice in these regions.

Interestingly, the MR **(Figure 17 and 18.i.)** showed a trend towards decrease excitatory and inhibitory synapses in the WT group compared to the naïve; however, opto-stimulated mice (Pet-Chr2) showed slightly higher levels of synaptic density than naïve mice. Further mice would be needed to confirm this.

UCMS induced lower levels of excitatory and inhibitory synaptic contacts brain wide, and optogenetic stimulation was not enough to recover normal levels of synaptic density. Nonetheless, a slight trend is observable in the MR and more stimulation might be needed to see significant changes.

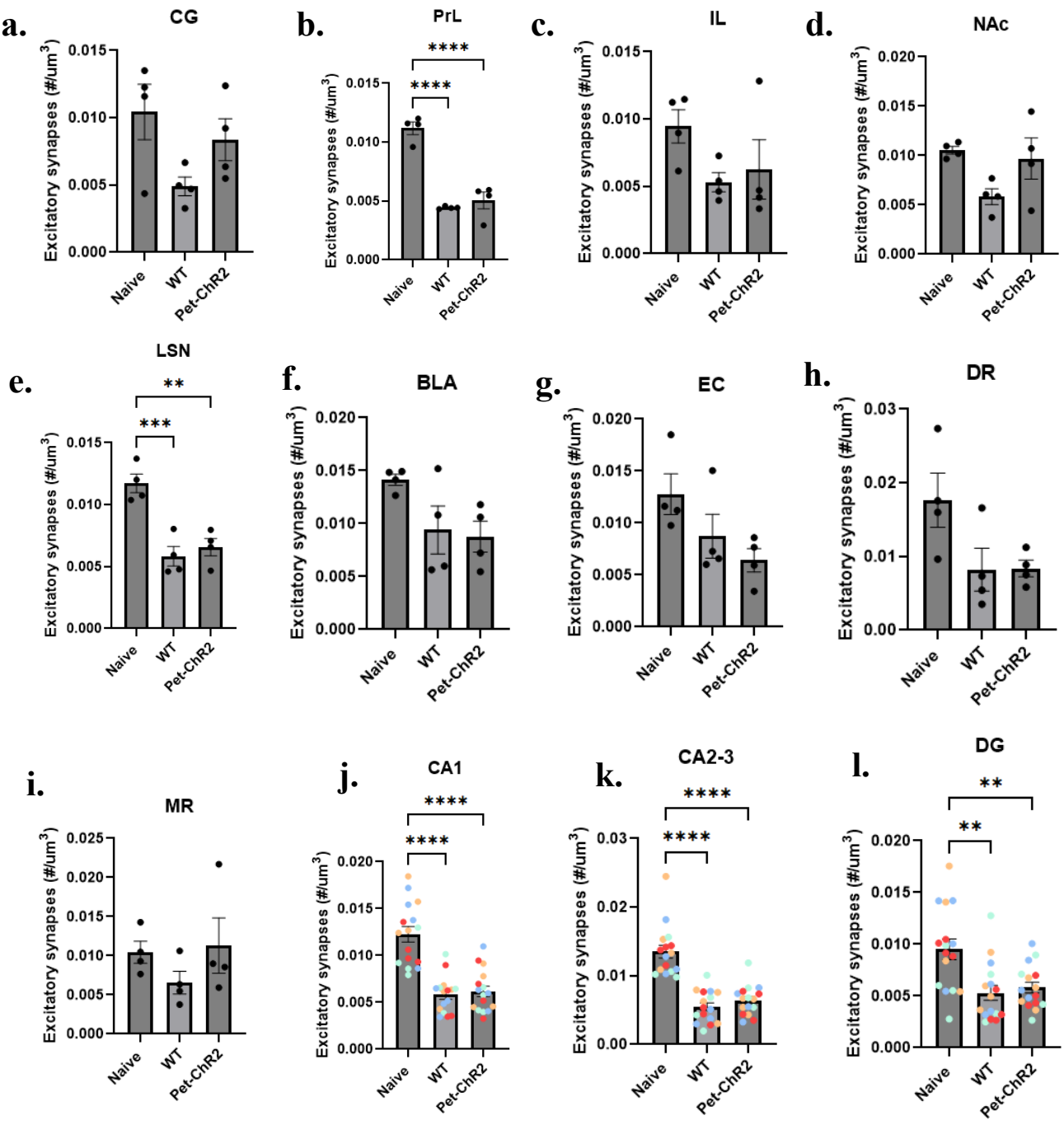

Figure 17. UCMS induced decrease in 5-HT excitatory synaptic contacts. SERT, synaptophysin, and PSD95 were co-stained and SERT-synaptophysin+ boutons within 0.6 µm of PSD95+ puncta were quantified and normalized to tissue volume. Data presented as mean ± SEM; n=4 per group. Hippocampus (CA1, CA2-3, DG) quantification was taken from 4 different levels of n=4 represented by four different colours, that showed no significant differences amongst levels. Significant differences were analysed using one-way ANOVA and post-hoc Tukey test; *$p < 0.05$, **$p < 0.01$, ***$p < 0.001$, ****$p < 0.0001$.

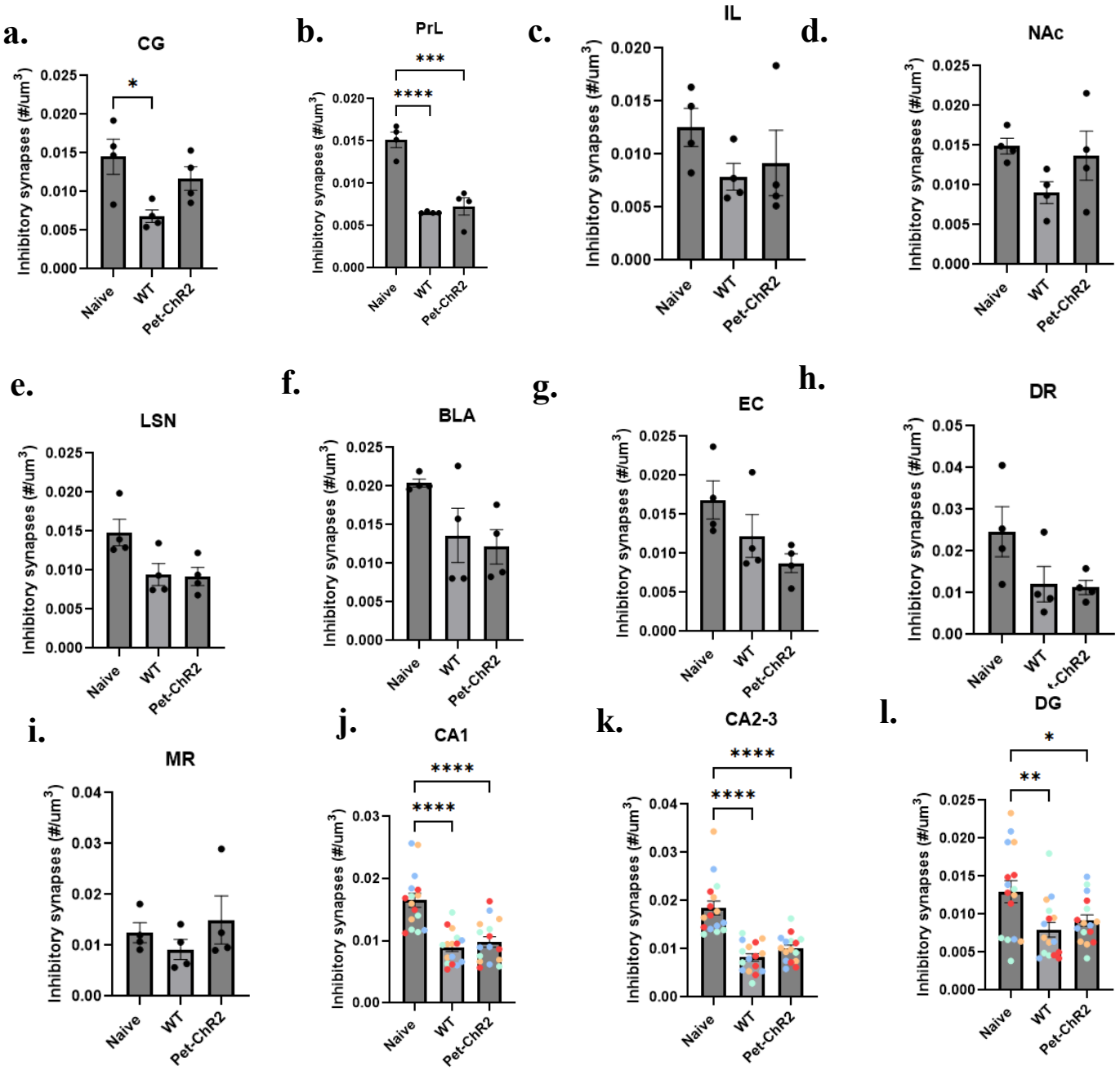

Figure 18. UCMS induced decrease in 5-HT inhibitory synaptic contacts. SERT, synaptophysin, and GAD67 were co-stained and SERT-synaptophysin+ boutons within 0.6 µm of GAD67+ puncta were quantified and normalized to tissue volume. Data presented as mean ± SEM; n=4 per group. Hippocampus (CA1, CA2-3, DG) quantification was taken from 4 different levels of n=4 represented by four different colours, that showed no significant differences amongst levels. Significant differences were analysed using one-way ANOVA and post-hoc Tukey test; *$p < 0.05$, **$p < 0.01$, ***$p < 0.001$, ****$p < 0.0001$.

3.9 Inhibitory and excitatory 5-HT triadic synapses

Excitatory and inhibitory triads were reconstructed from the staining of SERT, synaptophysin (presynaptic marker) and postsynaptic markers PSD95 or Gephyrin, in Imaris as shown in **Figure 19 a.** and **b.** which also shows representative images of the PrL region.

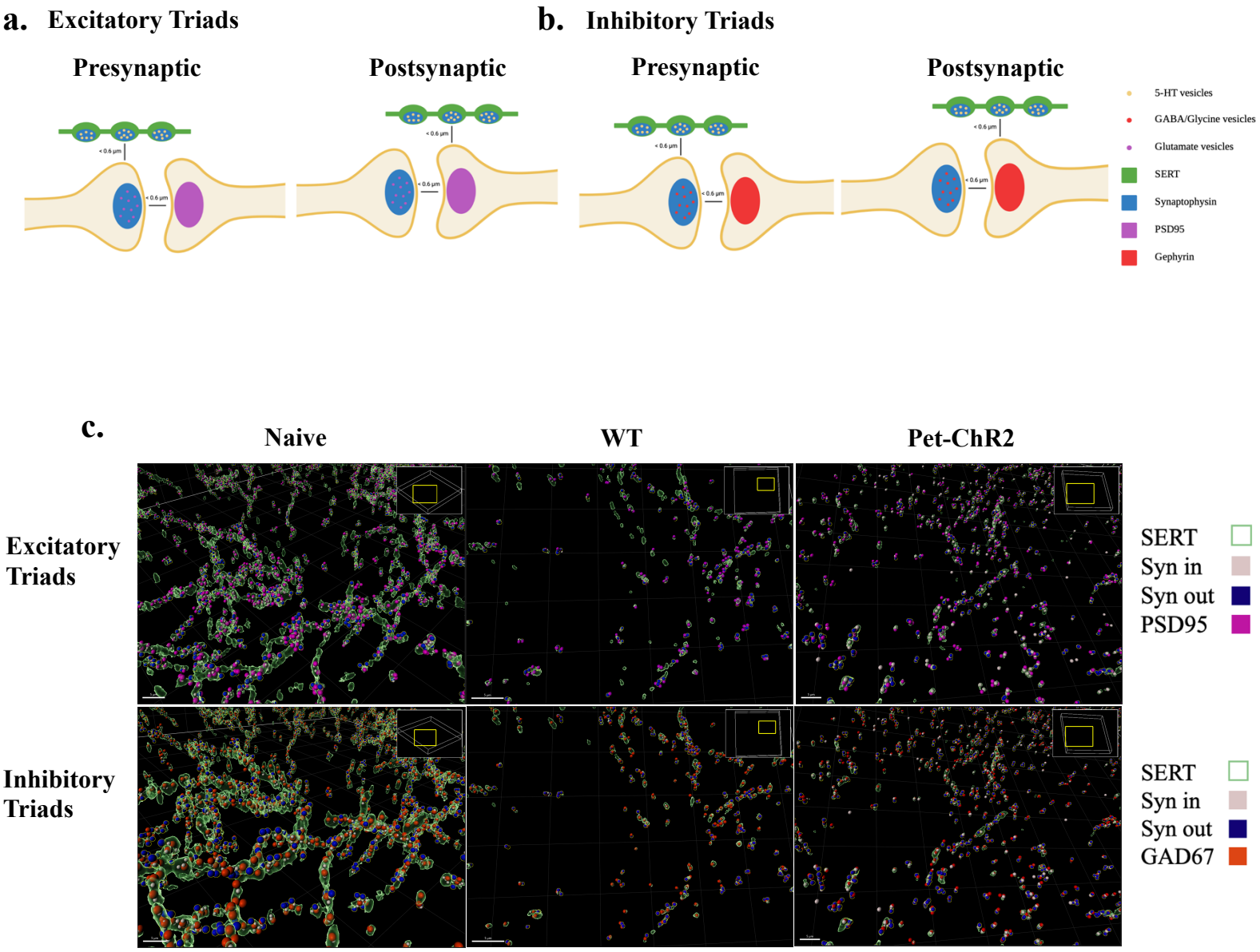

Figure 19. Sections were stained with SERT, synaptophysin (synaptic marker), and postsynaptic marker PSD95 or GD67 to visualize 5-HT triads. Models showing **a.** excitatory and **b.** inhibitory pre- and post-synaptic triads. **c.** representative images of excitatory and inhibitory triads in the PrL. Excitatory 5-HT triads identified through Syn in/SERT+ boutons within 0.6 µm of excitatory synapses (SERT-/synaptophysin+ boutons within 0.6 µm of PSD95+ puncta); and Inhibitory 5-HT triads, identified through Syn in/SERT+ boutons within 0.6 µm of inhibitory synapses (SERT-/synaptophysin+ boutons within 0.6 µm of GAD67+ puncta) were quantified and normalized to tissue volume.

Excitatory and inhibitory presynaptic triads were reduced in the CG, PrL, IL, and NAc **(Figure 20 and 21.a., b., c., and d.)** in chronically stressed mice, when comparing WT or Pet-ChR2 to naïve mice. Only the PrL region showed a significant decrease in excitatory contacts in WT but not Pet-ChR2 mice **(Figure 20.b.)**. In both, the CG and NAc optogenetic stimulation showed an increasing trend of presynaptic density in both excitatory and inhibitory triads. Whereas the PrL and IL showed no difference between WT and Pet-ChR2.

The LSN, DR, CA1, CA2-3, and DG all showed the same trend in excitatory and inhibitory presynaptic triad changes **(Figure 20 and 21.e., h., j., k., and l.)**. A decrease in both parameters was seen in WT group compared to the naïve, where Pet-ChR2 mice showed the same levels as WT cohort. This decrease was significant in presynaptic excitatory triads of the LSN, CA1, and CA2-3. The CA2-3 showed the most pronounced decrease in presynaptic excitatory triads and was the only region where the decrease in presynaptic inhibitory triads was also significant.

The BLA showed a trend towards decrease presynaptic density of both excitatory and inhibitory triads after chronic stress in the WT group, that persisted in the opto-stimulated Pet-ChR2 mice **(Figure 20 and 21.f.)**.

The EC showed the same levels of presynaptic triads in the naïve and WT group **(Figure 20 and 21.g.)** which was also seen in the MR **(Figure 20 and 21.i.)**. Interestingly Pet-ChR2 mice showed opposite action of opto-stimulation in both regions. In the EC Pet-ChR2 showed a slight decrease of both excitatory and inhibitory triads, but the MR showed a slight increase of both presynaptic triads.

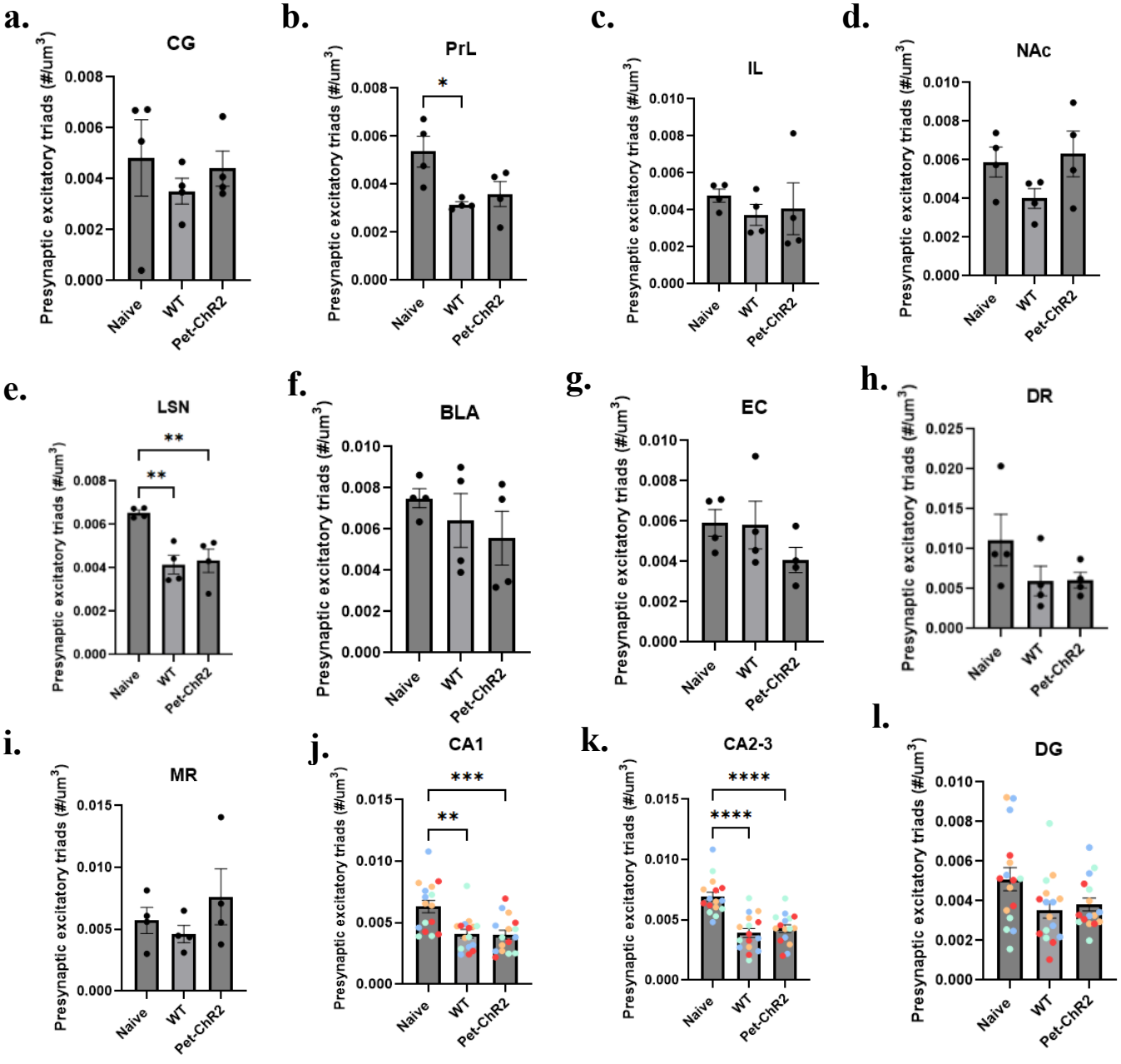

Figure 20. Decrease of presynaptic excitatory triads. Sections were stained with SERT, synaptophysin (synaptic marker), and postsynaptic marker PSD95 to visualize excitatory triads. Presynaptic excitatory 5-HT triads; identified through Syn in/SERT+ boutons within 0.6 µm of excitatory synapses (SERT-/synaptophysin+ boutons within 0.6 µm of PSD95+ puncta), were quantified and normalized to tissue volume. Data presented as mean ± SEM; n=4 per group. Hippocampus (CA1, CA2-3, DG) quantification was taken from 4 different levels of n=4 represented by four different colours, that showed no significant differences amongst levels. Significant differences were analysed using one-way ANOVA and post-hoc Tukey test; *$p < 0.05$, **$p < 0.01$, ***$p < 0.001$, ****$p < 0.0001$.

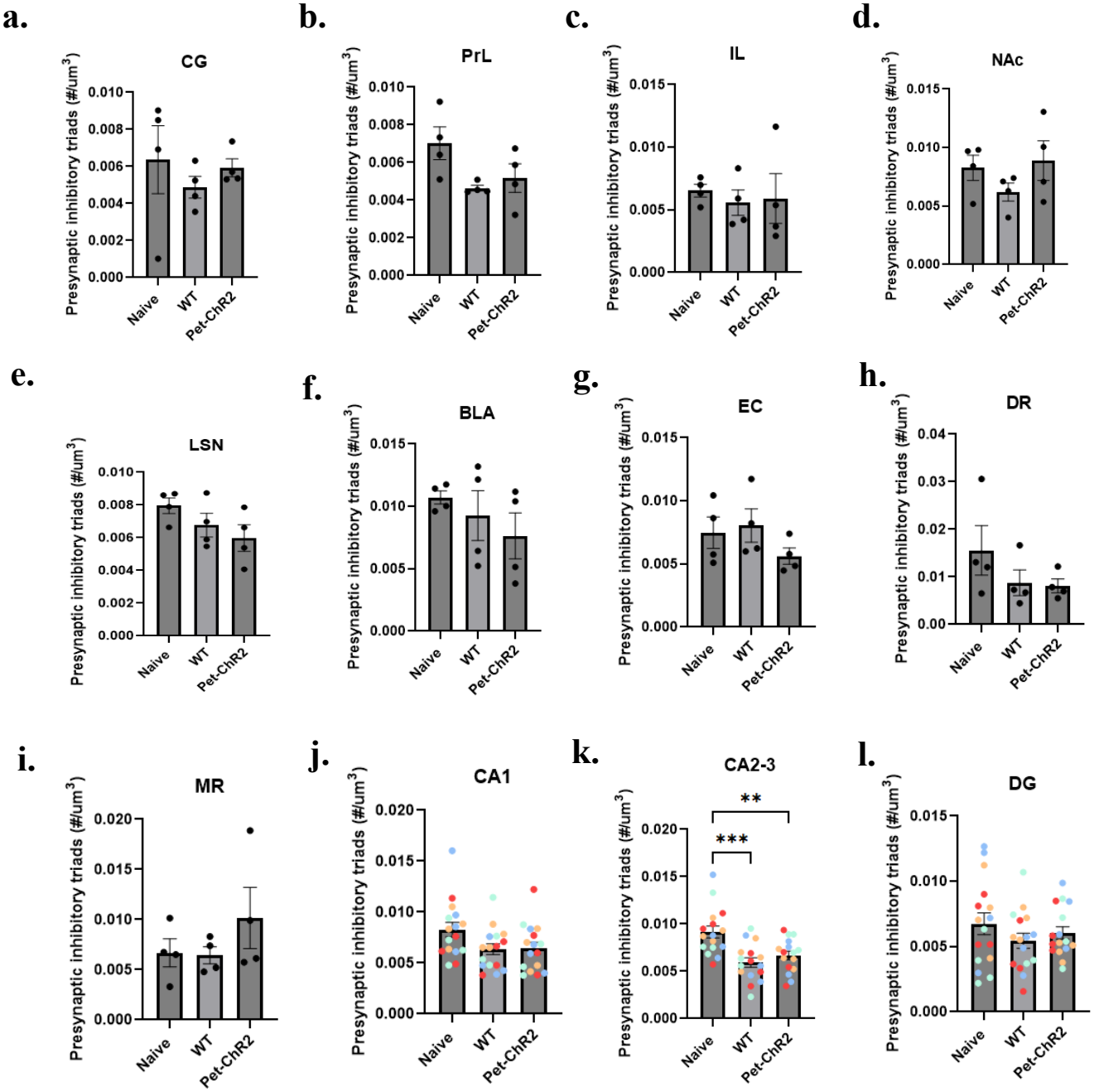

Figure 21. Changes in presynaptic inhibitory triads. Sections were stained with SERT, synaptophysin (synaptic marker), and postsynaptic marker GAD67 to visualize inhibitory triads. Presynaptic inhibitory 5-HT triads; identified through Syn in/SERT+ boutons within 0.6 µm of excitatory synapses (SERT-/synaptophysin+ boutons within 0.6 µm of GAD67+ puncta), were quantified and normalized to tissue volume. Data presented as mean ± SEM; n=4 per group. Hippocampus (CA1, CA2-3, DG) quantification was taken from 4 different levels of n=4 represented by four different colours, that showed no significant differences amongst levels. Significant differences were analysed using one-way ANOVA and post-hoc Tukey test; *$p < 0.05$, **$p < 0.01$, and ***$p < 0.001$.

Post-synaptic changes **(Figure 22 and 23)** of both excitatory and inhibitory triads are only significant in the CA2-3, LSN, and CA1 only in the post-synaptic excitatory triads **(Figure 22.k., e., j)** (the largest significant decrease is seen in the CA2-3 followed by the LSN). Where WT and Pet-ChR2 showed the same level of decrease compared to naïve.

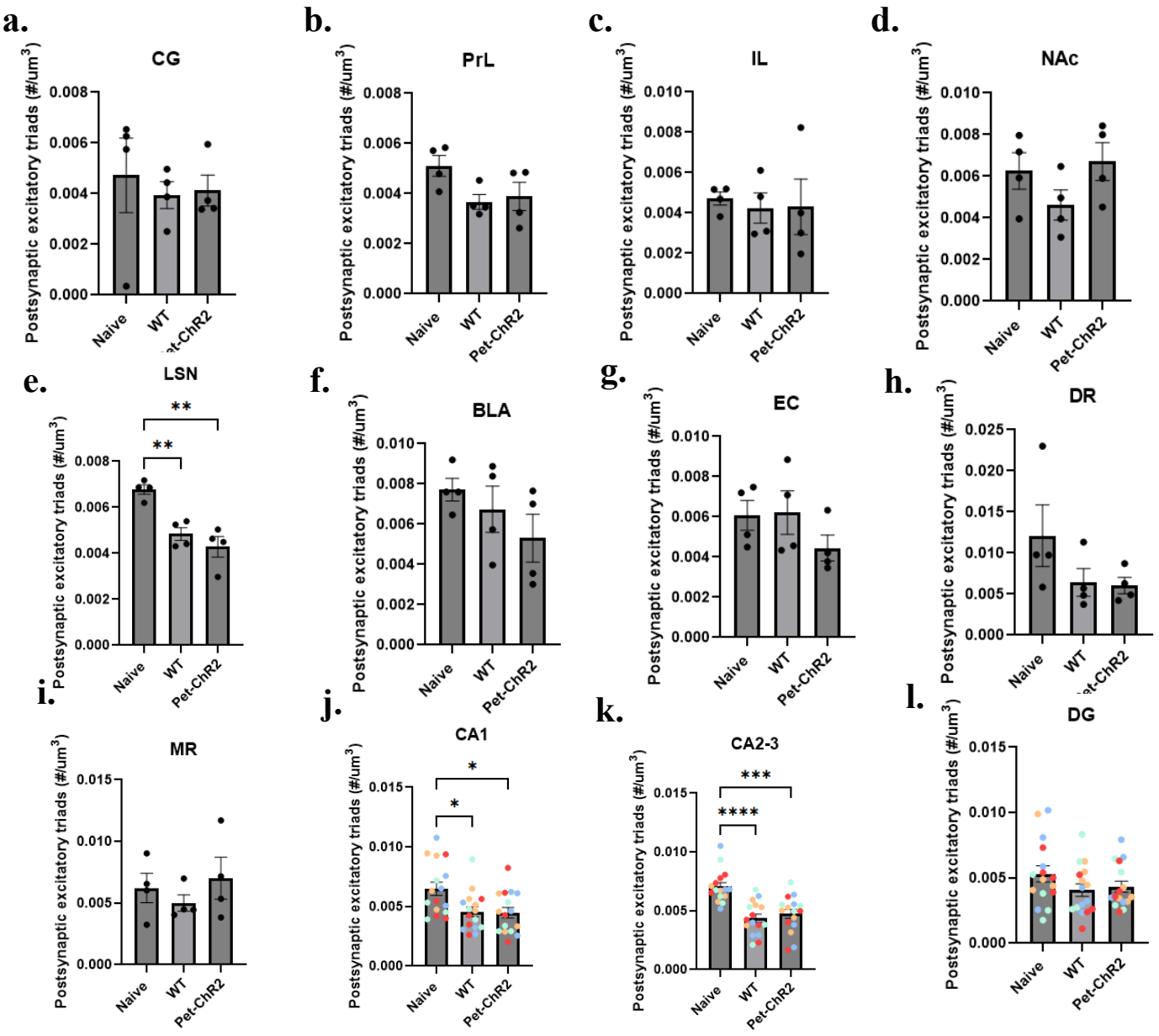

Figure 22. Changes in postsynaptic excitatory triads. Sections were stained with SERT, synaptophysin (synaptic marker), and postsynaptic marker PSD95 to visualize excitatory triads. Postsynaptic excitatory 5-HT triads; identified through Syn out/SERT+ boutons within 0.6 µm of excitatory synapses (SERT-/synaptophysin+ boutons within 0.6 µm of PSD95+ puncta), were quantified and normalized to tissue volume. Data presented as mean ± SEM; n=4 per group. Hippocampus (CA1, CA2-3, DG) quantification was taken from 4 different levels of n=4 represented by four different colours, that showed no significant differences amongst levels. Significant differences were analysed using one-way ANOVA and post-hoc Tukey test; *$p < 0.05$, **$p < 0.01$, ***$p < 0.001$, ****$p < 0.0001$.

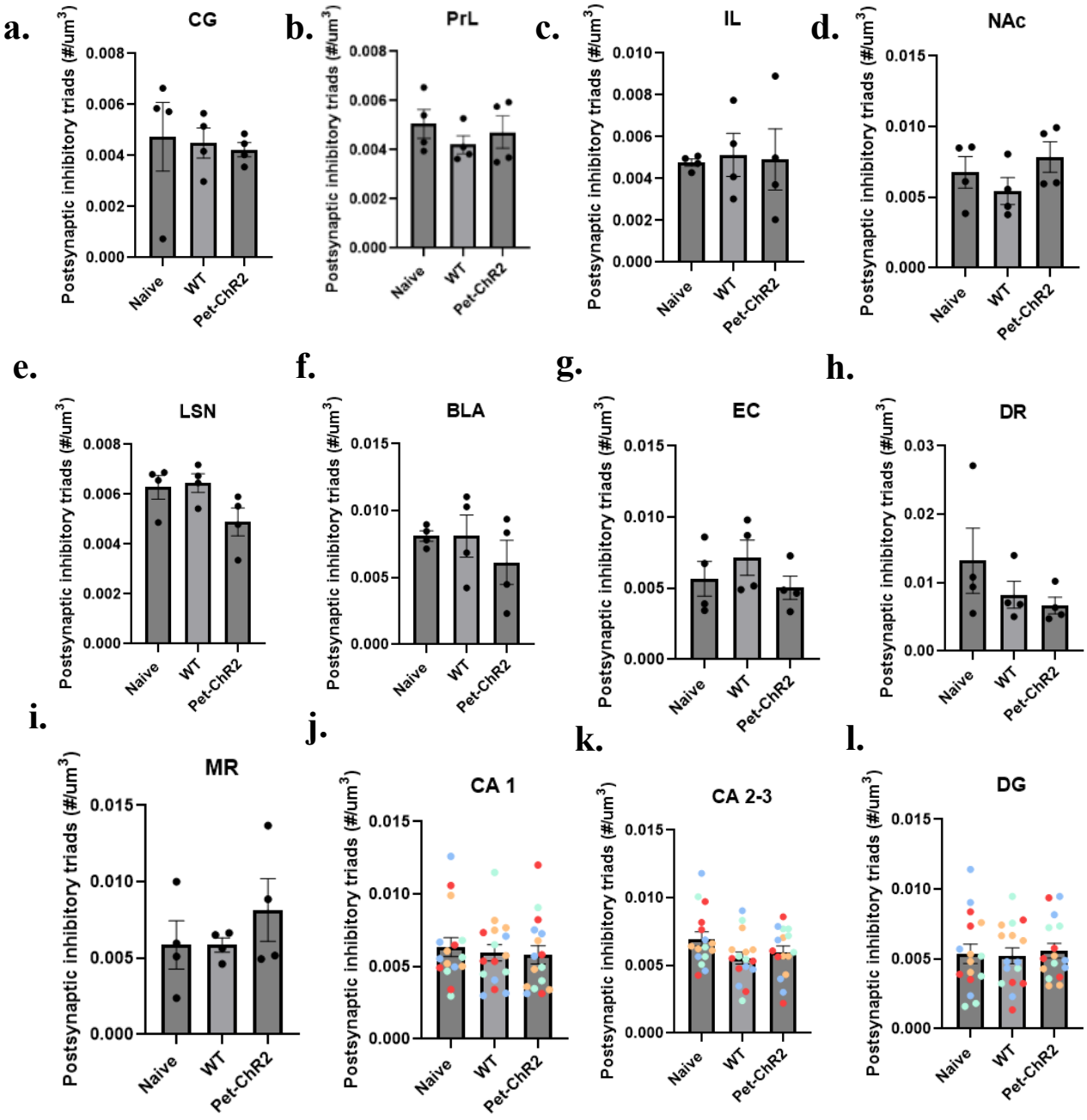

Figure 23. Changes in postsynaptic inhibitory triads. Sections were stained with SERT, synaptophysin (synaptic marker), and postsynaptic marker GAD67 to visualize inhibitory triads. Postsynaptic inhibitory 5-HT triads; identified through Syn out/SERT+ boutons within 0.6 µm of inhibitory synapses (SERT-/synaptophysin+ boutons within 0.6 µm of GAD67+ puncta), were quantified and normalized to tissue volume. Data presented as mean ± SEM; n=4 per group. Hippocampus (CA1, CA2-3, DG) quantification was taken from 4 different levels of n=4 represented by four different colours, that showed no significant differences amongst levels. Significant differences were analysed using one-way ANOVA and post-hoc Tukey test; *$p < 0.05$, **$p < 0.01$, ***$p < 0.001$, ****$p < 0.0001$.

4. Discussion

The burden imposed by MDD is increasing annually, both socially and economically. Unfortunately, the pathological etiology and the mechanisms behind pharmacological interventions are complex and still challenging to elucidate (Cui et al., 2024). Most symptoms are only partially addressed by current therapeutic options. Notably the first line of treatment is still SSRIs, which were invented in the early 1970s and entered medical use in the late 1980s (Wong et al., 2005). These therapies have been shown to lack efficacy and speed, and there is a large portion of MMD patients who do not respond to them. Consequently, it is imperative that 1) we further develop our understanding of MDD focusing on the effects that environmental risk factors, such as stress, have on both behaviour and brain function; and 2) assess the possibility of using alternative treatment options.

In this thesis I assessed the changes elicited by the UCMS protocol in the context of MDD and explored the potential benefits of optogenetic stimulation targeted to the serotonergic projections to the mPFC.

4.1 Chronic stress promoted behaviours changes associated with depressive and anxiety like phenotypes

Chronically stressed mice demonstrated depressive-like phenotypes, as seen in worsening of the coat state. Coat state measurement is related to a self-directed behaviour of auto-grooming in rodents (Nollet, 2021) that may be disturbed due to a loss of interest in self-care. The results seen in the UCMS mice are in line with what has been observed by others given that self-grooming is a very stress sensitive activity (Kalueff and Tuohimaa, 2004; Nollet, 2021). Changes in coat state have been reported as earlier as four weeks of UCMS (Burstein and Doron, 2018). This time point was also seen in our mice where scores started to shift from 0 (a normal coat) by week four. In

humans this would correlate to poor personal hygiene which is very often displayed by depressed patients (Nollet, 2021).

This observation of stress-induced behavioral change was confirmed by the OF test where mice showed decreased small and large center duration. This test relies on the common response in animals to specific stimuli where unstressed mice will be anxious to explore brightly lit and open areas, but will overcome anxiety due to curiousness (Seibenhener and Wooten, 2015). UCMS exposed animals showed an inability to overcome the anxiety and showed less exploratory behaviour than naïve mice. Interestingly, this was also seen in the EPM, where UCMS-exposed mice showed decreased open arm duration. Walz et al. (2016) demonstrated the translational validity of the OF test as it triggers thigmotaxis, the evolutionary response of remaining near the perimeter of unknown locations and avoiding the interior areas. This response is related to agoraphobia, pathologically defined as the anxiety of open spaces from which potential escape is difficult (Balaram and Marwaha, 2024). Anxiety driven by open spaces has also been reported in human patients. This demonstrates the ability of the UCMS protocol to induce behaviours seen in MDD.

Finally, UCMS induced increased immobility duration in the TST compared to naïve mice, related to depressive-like phenotypes in an inescapable stress situation.

These parameters demonstrated that UCMS induced behavioral changes associated with clinical depression and anxiety. Changes that validate the UCMS protocol in this research and support the ability of the UCMS protocol to mimic certain aspects of the human condition.

It is important to note that experimental lines both WT and Pet-ChR2 mice were always compared to basal levels set by the Naïve cohort. To have the best basal levels possible within the mouse line

the Naive cohort remained in their home cage during the extent of the stress. However, they participated during the behavioural testing period. These animals were examined after collecting brain tissues from the WT and Pet-ChR2 cohorts, and this was done in a different time as research has shown that exposure to other mice undergoing stress protocols may prompt stressogenic effects to animals that are themselves not directly exposed to stressors (Burstein and Doron, 2018). This has been denoted in the behaviour results with a dotted line separating Naive against WT and Pet-ChR2.

4.2 Optogenetic stimulation had antidepressant effects related to behavior in Pet-ChR2 mice

Chronically stressed mice showed antidepressant effects of repeated acute optogenetic stimulation of 5-HT projections to the mPFC in the TST. This observation comes in line with what other research groups have reported, although none have tested activation of 5-HT afferents specifically.

Papp et al. (2022) showed that non-selective neuronal optogenetic stimulation (using the hSyn promoter in an AAV induced ChR2 construct) during behaviour in the left PrL, part of the mPFC, restored lost sucrose intake in mice subjected to Chronic Mild Stress (CMS). Sucrose preference used as a measurement of stressed-induced anhedonia, a symptom of MDD (Papp et al., 2022). Additionally, this has been shown by others using different stress protocols. It has been shown that mice subjected to social defeat stress protocols can display normal levels of social interaction and recover deficits in sucrose preference (Covington et al., 2010) after optogenetic stimulation protocols within the mPFC. In these studies, ChR2 was overexpressed in the mPFC using a Herpes simplex virus (HSV) vector driven by the IE4/5 promoter, and opto-stimulation resulted in a burst pattern of cortical firing given the high stimulation pattern used (40 ms 100 Hz every 3 seconds).

Moreover, DBS during behavior in rats and mice in the ventro-medial prefrontal cortex (vm-PFC), the most clinically relevant current treatment equivalent to optogenetic stimulation, has shown rapid antidepressant characteristics in animal models of depression using CMS, and showed the ability to reverse anhedonia and other depression-related behaviours (Papp et al., 2018; Hamani et al., 2012). DBS has also been able to reverse anhedonic, anxiogenic, and dyscognitive effects of CMS in animals undergoing sucrose preference test, EPM and Novel Object Recognition (NOR) (Papp et al., 2018).

These studies mechanistically support what we saw in our behaviour tests; however, our approach is more precise in studying the effects. The optogenetic approach for the described studies uses an AAV and HSV mechanism to non-selectively implant ChR2 in every neuron in the mPFC, thus stimulation may alter many systems at the same time. This approach is more in line with what is seen in non-specific DBS. In turn, in our experiment we used the specific promoter Pet-1 to only express ChR2 in the serotonin system therefore the behavioral changes seen in our study are driven by serotonin neurons. Moreover, our experiment leads to a more physiological response of activation. We are using 20 Hz 10 ms LED pulses to drive the system towards activation and not induce burst-like patterns of cortical activation, which is seen in viral vector constructs that tend to lead to overexpression of opsin, in addition to most researchers using a higher and longer optogenetic stimulation pattern to overstimulate the system. This highlights the relevance of the serotonin system in 1) leading to a depressive phenotype when the system is dampened and 2) eliciting an antidepressant response upon activation via modulation of other systems.

The diagnosis of clinical depression and anxiety is done through a holistic medical history. Diagnosis encompasses medical interviews, that cover patient's health history and reported symptoms through clinical observation and tests, in addition to the medical history collected

through self-reports. In a preclinical setting of a mouse model, diagnostic criteria depend on brief observations of particular typical and atypical behaviors in controlled environments as validated by other researchers. It is, however, interesting to note that although behavioural tests are categorized between those assessing anxiety-like behaviours and depressive-like behaviors, clinical depression and anxiety are highly interconnected mental disorders which share high levels of co-morbidity (Can et al., 2012). Animal models highlight the co-morbidity between behaviours associated with each disorder. This may mimic the heterogeneity of symptoms between disorders and the blurry limits that exist in the diagnostic criteria (Can et al., 2012). Nonetheless, even when there are degrees of variance in the assessment of depressive and anxiety-like phenotypes in behavioral testing, the TST validity to assess antidepressant response from a treatment is still high (Cryan et al., 2005). Consequently, having a high degree of significance (after only three sessions of optogenetic stimulation) in the decrease of immobility duration in the Pet-ChR2 cohort when compared to chronically stressed mice (WT mice), strongly indicates that precise stimulation of 5-HT projections to the mPFC can by-pass the delayed effect seen in pharmaceutical antidepressant therapies.

4.3 Optogenetic stimulation induced anxiogenic like behaviours

The EPM test showed high levels of anxiety-like behavior in both WT and Pet-ChR2 mice after both cohorts underwent light exposure. Both cohorts showed very similar levels of closed arm duration in pre-stimulation period compared with the naive cohort, which suggests they all had similar basal levels of anxiety. When the light was turned on, the light-exposed stressed WT mice showed the highest level of closed arm duration possible which translated to 0 time spent in the open arm. This may be a result from the bright light bouncing off the white wall of the EPM

apparatus. It is not an effect of stimulating serotonergic projections itself, as both WT and Pet-ChR2 mice showed the effect, and WT mice do not express ChR2.

This was also seen to a lesser degree in the OF where both groups (WT and Pet-ChR2) showed low levels of small center and large center duration. However, unlike in the EPM the effect faded after light was turned off during the post-stimulatory period. One possible explanation is that by this point animals may have acclimated to the light, as this was the second time they were being stimulated. They showed mild anxiety-related phenotype while the light was on but were not affected after light was off. Interestingly Pet-ChR2 mice did not show the same level of avoidance of the center as did the WT mice during the post-stimulation period. This may indicate that opto-stimulation could already have been exerting an effect by the second stimulatory therapy. In the large center post-stimulation Pet-ChR2 mice already showed similar time spent in the large center to that of the naive animals.

Lastly the increased immobility duration shown by the FST may not be solely a parameter of increased depressive like phenotypes, but could in part reflect fatigue. During the behaviour test mice were not able to fully remain afloat, and we believe this to be the result of being too tired. The assay may be too prolonged, given that these are all female mice that spent 15 minutes in total inside the water tank. However, since both groups of mice, WT and Pet-ChR2, were connected to the optogenetic apparatus and showed the same velocity after 5 minutes of being in the water tank the comparison between them likely reflects the depression-like phenotype.

In addition, the anxiogenic response of both WT and Pet-ChR2 mice to light seen in two of the tests may be explained by the apparatus used. It would be important to completely rule out such observations for which the best strategy would be to try both anxiety focused test while using dark walls or trying to reduce the flare from the optic fiber tips.

4.4 Chronic stress attenuated chronic activity throughout the brain

Behavioral changes translated to neurochemical changes. Chronic stress resulted in a trend towards decreased expression of FosB throughout the brain, with decreased chronic activity in both excitatory and inhibitory neurons. This implies dampened chronic activity in the chronically stressed brain. It has been shown that deficits in markers of neuronal activity correlate to impaired cortical activity and translate to behavioural disturbances (Covington et al., 2010). Thus, impaired neuronal activity may explain the behavioral changes seen in our research.

Interestingly, there was significant attenuated chronic activity, as detected by FosB quantification, in the NAc. This region regulates emotional and reward stimuli by integrating signals from related regions within the limbic system (Xu et al., 2020). This may be due to the low levels of excitatory chronic activity seen in the mPFC, more specifically in the CG and PrL, which send dense projections to cortical and subcortical regions, including the NAc, that plays a crucial role in inhibitory behavioral control (Domingo-Rodriguez et al., 2020). Importantly there is also high degree of connectivity between the NAc and the hippocampus, particulalry within which the CA 2-3 and DG showed a decreasing trend of FosB expression in the stressed mice.

The DG is a major component of the hippocampal trisynaptic circuit that relays signals from the EC to the CA3 which targets the pyramidal neurons in the CA1 (Sun et al., 2023). The pyramidal neurons of the CA1 and the granule cells of the dorsal DG have been shown to be implicated in regulating emotional response, and exhibit a crucial role in emotional processing (Sun et al., 2023). The effect of chronic stress on the hippocampus is relevant in the context of depression as hippocampal excitatory neurons express high levels of glucocorticoid receptors (Kraus et al., 2022), which may explain the stress sensitivity of hippocampal activity, especially in the CA1, as shown by significant decreases in axonal volume and synaptic formations. The hippocampus also

showed morphological changes including decreased volume which may be a result of decreased density of dendrites and projections, as reported by McEwen (1999). Additionally, studies have also shown that FosB expression, especially in the hippocampal subgranular zone, is critical for neurogenesis (Cui et al., 2024). Decrease neurogenesis in the hippocampus has been shown to be directly linked to MDD. Hence, these findings suggest that chronic stress (in the form of UCMS) was able to weaken neuronal chronic activity in the mPFC and hippocampus which resulted in a depression-like phenotype.

Effects on the dorsal hippocampus are mainly associated with cognitive function; however, recent evidence suggests that it also plays a role in mood disorders like the ventral portion of the hippocampus (Sun et al., 2023), which is why it is important to assess changes within the dorsal part of the hippocampus. Considering other avenues of research, there is evidence to show that hippocampal subgranular zone deficits affect learning (Manning et al., 2019). Given the overlap in function between dorsal and ventral hippocampus in memory and mood regulation, our future research should aim to look at the cognitive variabilities in the UCMS mouse model. As research has shown that decreased expression of immediate early genes in the hippocampus and mPFC reflect deficits in the ability to encode new information (Covington et al., 2010). I saw significant decrease of excitatory and inhibitory synaptic contacts and pre- and post-synaptic triads in the hippocampus in stressed mice, where I also saw significant decrease of hippocampal volume in ventral and dorsal hippocampus together. Similar volume reductions have been seen in animal models (McEwen, 1999) and human patients of MDD (Boldrini et al., 2013). Our behavioural results suggest that these changes may contribute to mood-related disorders (depressive- and anxiety-phenotypes). Consequently, it would be interested to assess how chronic stress, acting at both ventral and dorsal hippocampus, disrupts memory and learning.

Additionally, the BLA and EC also showed decreased FosB expression after chronic stress compared to naïve mice. Both of these regions serve an important function in the pathophysiology of MDD. BLA dysfunction results in inhibition of the brain's reward system and ultimately affects dopamine release which is linked to depressive symptoms like anhedonia (Guo et al., 2024). Guo et al. (2024) commented on how the EC is responsible of regulating depressive-like phenotypes by relying on glutamatergic afferents from EC to hippocampus. Accordingly, attenuated function of the EC promotes depressive symptoms.

Interestingly, quantification of the co-localization of GAD67 and FosB showed decreases in IL, MO, CA 2-3, BLA and EC. These observations may be explained by the constant interplay between excitation and inhibition. Studies have shown that reduced excitatory input to interneurons results in reduced intrinsic excitability of such interneurons, that leads to a reduction of inhibitory synapses in turn into pyramidal cells (Selten et al., 2018). On this account, it is possible that the decrease inhibitory chronic activity seen in GAD67+/FosB+ quantification may be acting as a compensatory mechanism (Cameron and Schoenfeld, 2018) due to decrease in excitatory outputs. The brain itself may be trying to increase excitation to counteract the dampening of brain activity brought by chronic stress (Selten et al., 2018).

4.5 Chronic stress induced reduction in 5-HT synapses and reductions in excitatory and inhibitory 5-HT triadic synapses

Chronic stress induced loss of SERT+ axonal and varicosity density significantly in the mPFC and hippocampus. The same trend was seen all throughout the brain, including in the DR. Other studies have shown loss of axo-spinous synapses, where chronic stress reduced the general number of synapses (inhibitory and excitatory) and myelinated axons in the mPFC (Csabai et al., 2018). However, our study selectively shows that this loss of axonal material in the mPFC may be in part

due to serotonin axons. In our UCMS protocol, reduced axonal volume and dendritic spines of the serotonin system may have driven reduced network connectivity (as seen in reduced excitatory and inhibitory contacts and presynaptic triads). The loss of serotonin connectivity would ultimately impair the proper functioning of brain regions studied and could explain the loss of hippocampal volume. This deficiency may also explain the behavioural changes seen in UCMS-treated animals. Research has shown that persisting high levels of stress result in loss synapses in circuits that inhibit affective and cognitive processes (Holmes et al., 2019). This is confirmed by studies demonstrating that inhibition of synaptic protein synthesis, which results in a reduction in synapses, causes depressive-like behaviours in rodent models (Holmes et al., 2019; Ota et al., 2014)

4.6 Optogenetic stimulation increased serotonin activity and induced hippocampal activation

Optogenetic stimulation of serotonin projections to the CG was sufficient to significantly increase and potentiate serotonergic chronic activity throughout the DR as measured by TPH/FosB-labeled cells, with the highest effect in the DDR which has the highest concentration of TPH+ cells. This could result from either 1) the ability of the activation of the light sensitive protein (ChR2) in serotonergic axons and terminals to promote antidromic action potentials that traveled all the way to serotonergic cell bodies in the DR; this would, trigger orthodromic action potentials that plausibly resulted in serotonin release in DR-projecting areas within the limbic system (Veerakumar et al., 2014); 2) the activation of mPFC afferents to the DR that could have driven 5-HT neurons, thus tonically increasing their firing rate (Warden et al., 2012). Nonetheless, the top-down control exerted from the mPFC to the DR is evident from the chronic activation patterns.

To fully demonstrate the increase release of serotonin by opto-stimulation a future avenue of research would be to use serotonin sensors (Kubitschke et al., 2022) to measure in-vivo 5-HT

release. However, the indirect measurement showing a significant increase of FosB-TPH co-localization suggests that there is a chronic increase of serotonin neuronal activity. Strikingly, analysing the DR images of Pet-ChR2 mice it is not only possible to observe the usual FosB nuclear staining, there also appears to be FosB signal within projections **(Figure 24.a. and b.)** (resulting in staining patterns like 5-HT axons) of 5-HT neurons suggesting that opto-stimulation greatly intensified chronic activity that chronic activity marker signal was still mobilizing to the nucleus of the 5-HT cells.

Axonal-like FosB signal was also observable in the LSN and MSN, just like what was seen in the DR. These nuclei serve as projection channels that communicate to the hippocampus formation. This suggests that optogenetic stimulation of 5-HT projections to the mPFC could be evoking intensified chronic activity brain-wide, as seen in extended increase in FosB signal even outside the nucleus of the cells.

Noticeable excitatory chronic activity was significantly increased in two areas: the MSN and CA1. These areas showed potentiated excitatory activity with higher levels of CamKIIα+/FosB+ cell quantification than naive animals after opto-stimulation. Studies have shown that potentiation of excitatory synapses through CamKIIα activation in hippocampus, more specifically in the stratum lacunosum-moleculare region of the CA1 where the axons of layer III neurons in the EC form excitatory synapses with the distal apical dendrites of the pyramidal cells of CA1 (temporoamonic pathway), is essential in antidepressant response (Cai et al., 2013). Cai et al. (2013) showed that this effect is regulated by 5-HT through the 5-HT1B heteroreceptor, that is postsynaptically activated to produce facilitation in the excitatory synaptic transmission through the temporoammonic pathway in a mouse model of depression. The Cai et al. (2013) study measured activity through field excitatory postsynaptic potentials, thus electrophysiological studies suggest

the same conclusions that were reached by immunohistochemistry protocols in our research. This local potentiation of excitatory neurons in the hippocampus was seen through the effect of the commonly used SSRI fluoxetine after this medication reached therapeutic effects in mice following the period it takes for the 5-HT1A autoreceptor to be desensitized (Albert et al., 1994). The effect of fluoxetine on hippocampal activity was mimicked by only five sessions of optogenetic stimulation in our research. Most importantly the molecular changes observed were accompanied by antidepressant-like actions on behaviour.

The synaptic features of 5-HT innervation did not show recovery after optogenetic stimulation. However, the CG and MR showed a trend towards recovery of SERT+ axonal density and excitatory contacts. This partial recovery may suggest that more extensive optogenetic stimulation is necessary to have a significant effect on excitatory synaptic communication. It should be noted that the stimulation protocol we used (stimulation was only administered during one third of the behavioural tests, using 20 Hz 10 ms LED pulses) was brief and less potent compared to other studies. Nonetheless, increased glutamatergic synaptic communication has been shown to be essential for antidepressant response, as rapid increase in the number and function of glutamate neurons synaptic connections is part of the mechanism of action that aids ketamine in producing rapid antidepressant-like effects (Holmes et al., 2019). According to trends in recovery of excitatory triads in our study, optogenetic stimulation of 5-HT projections in the mPFC could be trying to increase excitatory synaptic volumetric transmission in its efforts to lead to a full antidepressant response.

5. Conclusion

Our study demonstrates that UCMS induced behavioural changes associated with clinical depression in an all-female mouse cohort. This was shown by worsening of the coat state,

decreased large center duration in the OF, and increased immobility duration in the FST. Phenotypic changes were associated with neuronal activity changes. In particular, there were brain-wide decreases in FosB-labelled cells both excitatory CaMKIIα+/FosB+ cells and inhibitory GAD67+/FosB+ labeled cells. There was also reductions in innervation as reflected by decreased hippocampal volume, decreased SERT+ axonal and varicosity density, and decreased serotonin innervation including excitatory and inhibitory contacts and pre- and post-synaptic triads.

All together chronic stress impaired neuronal activity of the NAc and showed strong effects in the mPFC, more specifically in the PrL and CG. Reduced FosB expression in these regions came mainly from impairments in pyramidal activity. On the other hand, the IL, EC, MO, and to a lesser extent the CA2-3 and BLA showed reduced FosB expression that directly affected inhibitory neural activity. These results suggests that depression, as a result of UCMS exposure, is elicited by changes that are region- and function-specific, that ultimately disrupt the excitatory/inhibitory interplay.

Interestingly, optogenetic stimulation of 5-HT projections to the mPFC was able to reverse behavioural changes associated with chronic stress-induced depression, as seen in decreased immobility duration in TST in opto-stimulated mice.

This behavioral change induced by opto-stimulation was accompanied by the potentiation of serotonin chronic activity in the DR, as shown by increase TPH+/FosB+ co-localization. Opto-stimulation also strongly increased excitatory chronic activity in the CA1 shown by increased CaMKIIα+/FosB+ cell quantification. Additionally, opto-stimulation increased PrL, IL, and CG excitatory neuronal activity, where the PrL showed the biggest effect. There was also an increase

in inhibitory neural activity in the NAc and to a lesser extent in the PrL. These observations suggest that the optic fiber that lies in the CG may be mainly directing light stimulation mostly towards the PrL, as it the region with the strongest effect. It also suggests that opto-stimulation is mainly targeting pyramidal neurons in the mPFC and CA1. Notably there is a trend in several other brain regions towards increased excitatory neural activity after opto-stimulation, which may suggest that stimulation was too acute (only 1 week) to observe its full potential. This could explain why opto-stimulation was unable to induce recovery of the chronic stressed-induced loss of 5-HT axonal volume and synaptic formations.

Antidepressants have been shown to recover lost 5-HT axonal volume and promote triadic recovery (Zahrai et al., 2020) in a post-stroke depression model. However, this stroke study used chronic exposure (5-6 weeks) to fluoxetine to gain full recovery. In our UCMS model, brain tissue was collected within the same week of the last behavioral test (**Figure 1.a.)** after only five stimulation sessions, which may not be enough time or stimulation to promote full 5-HT axonal reconstruction and subsequently recover 5-HT synaptic communication. Nonetheless, even when opto-stimulation and tissue collection were accelerated compared to other studies, we still observed a robust effect both behaviorally and neuronally to suggest that opto-stimulation of 5-HT projections in the mPFC promotes antidepressant-like effects.

From the molecular data obtained we must hypothesize that the antidepressant response from optogenetic stimulation may be a result of a microcircuitry between the mPFC-DR-Hippocampus **(Figure 24.c.)**. Respectively functioning through two different paths 1) the activation of 5-HT mPFC projections that directly activates the DR and increases 5-HT firing to serotonergic projecting regions, and 2) the activation of mPFC neurons that can activate pyramidal neurons in

the hippocampus which in turn synergize with DR activity to activate the hippocampal pyramidal neurons.

Overall, this research provides evidence that sub-chronic stimulation of serotonergic projections is sufficient to activate depression-associated brain areas inhibited by chronic stress and elicit an antidepressant response, bypassing the lag period normally associated with SSRIs.

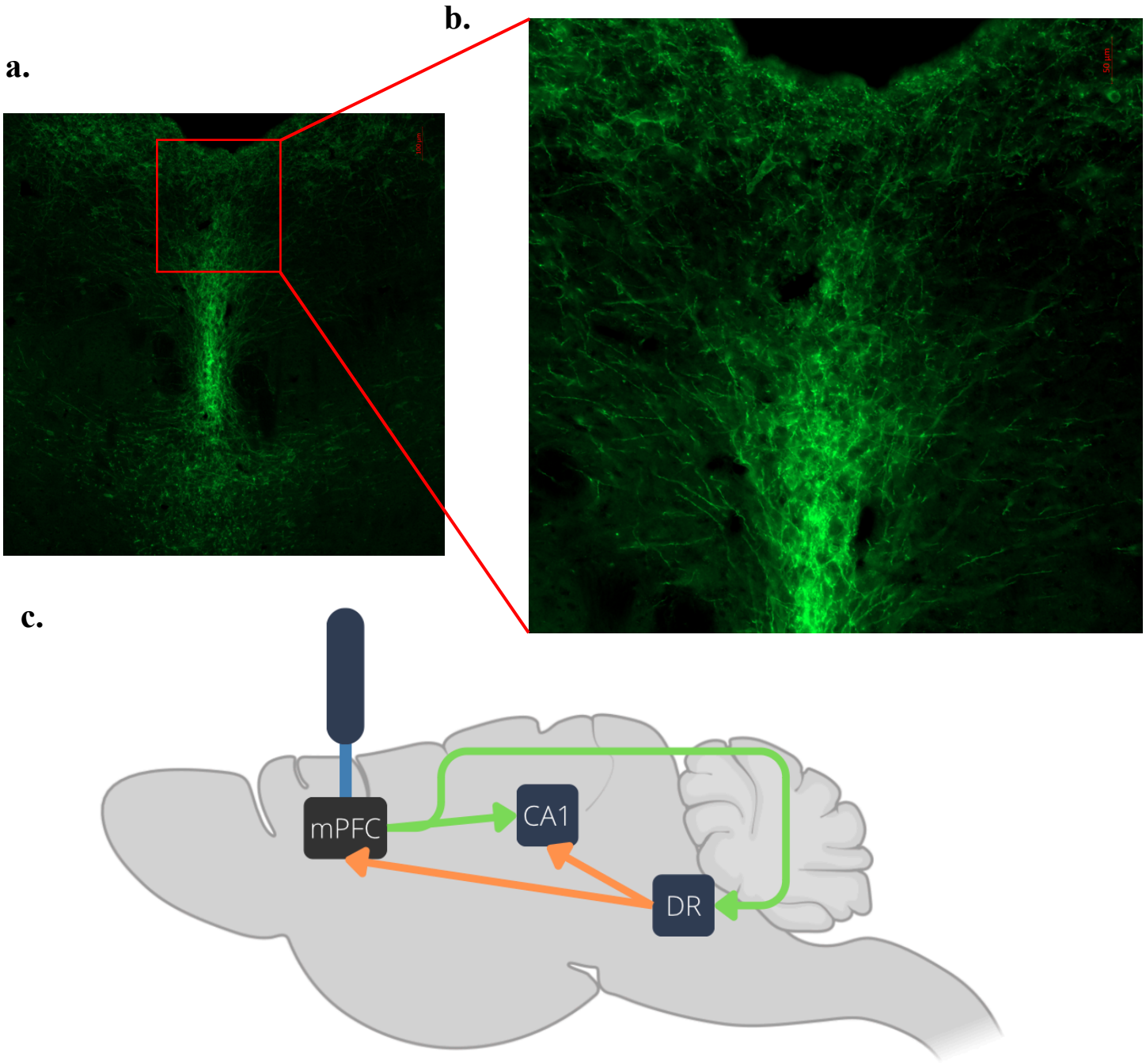

Figure 24. Optogenetic stimulation microcircuitry. FosB staining shown in DR through what appears to be 5-HT processes in **a.** 10x epifluorescent microscopy and a zoomed in **b.** 20x image. **c.** shows the microcircuitry involved in the antidepressant response of opto-stimulation of 5-HT projection to the CG.

6. Future steps

It would be important to explore functional cognitive changes elicited by stress due to the high evidence of hippocampal remodeling, in both literature and our research. This can be done through cognitive specific behavioural tests like novel object recognition, Y-maze, and Morris watermaze (Tanila, 2018), which have been assessed in other studies. Our model suggests that there is a high level of excitatory chronic activity increase specifically in CA1 after optogenetic stimulation of 5-HT projections to mPFC, thus it would also be important to assess the possible recovery in cognitive function in case stress disrupt memory consolidation. It has been suggested that local potentiation of the CA1 through the temporoammonic pathway is essential in SSRIs' antidepressant mechanism of action; however, it is the same pathway used for long term potentiation (LTP) for memory consolidation (Cai et al., 2013). Consequently, if LTP is also disrupted in this model it may suggest that optogenetic stimulation is using the same mechanism than SSRIs, with the added caveat of showing earlier antidepressant effects.

Additionally, it will be important to address a limitation in this research. We will need to address the effect of stimulation without the added effect of stress, consequently we would need to add a cohort of naïve mice that goes through opto-stimulation without UCMS exposure. Along this line of reasoning we would also need to explore the effects of stimulation prior to behavioural testing.

Supplemental figures

Supplemental table 1. F and P values of all statistical comparisons

	One-way ANOVA												
Coat state	Interaction	**coat state**											
		F = 155.4											
		P < 0.0001											
EPM	Interaction	**Open arm**	**Closed arm**	**Distance moved**									
		F = 5.343	F = 5.29	F = 9.462									
		P = 0.0124	P = 0.0129	P = 0.001									
OF	Interaction	**Small center**	**Large center**	**Distance moved**									
		F = 18.38	F = 13.16	F = 7.597									
		P < 0.0001	P = 0.0002	P = 0.0029									
TST	Interaction	**Immobility**											
		F = 11.77											
		P = 0.0003											
NSF	Interaction	**Open field**	**Home cage**										
		F = 0.2469	F = 2.939										
		P = 0.7832	P = 0.073										
FST	Interaction	**Immobility**	**Velocity**										
		F = 1.321	F = 20.92										
		P = 0.2883	P < 0.0001										
Dorsal raphe	Interaction	**DDR**	**VDR**	**LDR**									
FosB		F = 18.82	F = 8.411	F = 1.085									
		P = 0.0006	P = 0.0087	P = 0.3783									
TPH		F = 5.85	F = 8.232	F = 2.921									
		P = 0.0236	P = 0.0093	P = 0.1053									
TPH-FosB		F = 10.35	F = 7.587	F = 7.126									
		P = 0.0046	P = 0.0117	P = 0.014									
Chronic activity	Interaction	**CG**	**PrL**	**IL**	**MO**	**NAc**	**LSN**	**MSN**	**CA1**	**CA2-3**	**DG**	**BLA**	**EC**
(FosB)		F = 4.007	F = 1.138	F = 4.643	F = 4.108	F = 4.807	F = 1.418	F = 0.01766	F = 12.47	F = 4.029	F = 4.127	F = 1.72	F = 1.448
		P = 0.0569	P = 0.3627	P = 0.0459	P = 0.0540	P = 0.038	P = 0.3041	P = 0.9825	P = 0.0025	P = 0.0563	P = 0.0535	P = 0.233	P = 0.2849
Excitatory activity	Interaction	**CG**	**PrL**	**IL**	**MO**	**NAc**	**MSN**	**CA1**	**CA2-3**	**DG**	**BLA**	**EC**	
(CamkIIα-FosB)		F = 3.067	F = 5.739	F = 2.1	F = 1.395	F = 1.723	F = 7.561	F = 8.462	F = 0.6649	F = 0.3322	F = 0.2622	F = 1.123	
		P = 0.0964	P = 0.0335	P = 0.2035	P = 0.3092	P = 0.2386	P = 0.0178	P = 0.0106	P = 0.5485	P = 0.732	P = 0.7793	P = 0.3955	
Inhibitory activity	Interaction	**CG**	**PrL**	**IL**	**MO**	**NAc**	**LSN**	**MSN**	**CA1**	**CA2-3**	**DG**	**BLA**	**EC**
(GAD67-FosB)		F = 1.889	F = 2.056	F = 14.86	F = 9.085	F = 1.75	F = 2.216	F = 0.235	F = 3.98	F = 6.646	F = 4.265	F = 5.484	F = 8.571
		P = 0.2066	P = 0.1839	P = 0.002	P = 0.0113	P = 0.2281	P = 0.1796	P = 0.7965	P = 0.0578	P = 0.0169	P = 0.0498	P = 0.0277	P = 0.0082
MRI	Interaction	**Volume**											
		P = 0.0387											
5-HT Axonal	Interaction	**CG**	**PrL**	**IL**	**NAc**	**LSN**	**CA1**	**CA2-3**	**DG**	**BLA**	**EC**	**DR**	**MR**
Volume		F = 5.545	F = 19.41	F = 2.792	F = 4.775	F = 23.24	F = 81.18	F = 101.3	F = 19.75	F = 17.38	F = 7.401	F = 14.24	F = 4.703
		P = 0.027	P = 0.0005	P = 0.114	P = 0.0386	P = 0.0003	P < 0.0001	P < 0.0001	P < 0.0001	P = 0.0008	P = 0.0126	P = 0.0016	P = 0.04
5-HT Varicosity	Interaction	**CG**	**PrL**	**IL**	**NAc**	**LSN**	**CA1**	**CA2-3**	**DG**	**BLA**	**EC**	**DR**	**MR**
Density		F = 3.44	F = 5.039	F = 0.9746	F = 4.89	F = 23.67	F = 37.39	F = 38.39	F = 6.242	F = 13.31	F = 8.836	F = 9.32	F = 5.985
		P = 0.0777	P = 0.034	P = 0.4139	P = 0.0365	P = 0.0003	P < 0.0001	P < 0.0001	P = 0.0041	P = 0.002	P = 0.0075	P = 0.0064	P = 0.0222
5-HT Excitatory	Interaction	**CG**	**PrL**	**IL**	**NAc**	**LSN**	**CA1**	**CA2-3**	**DG**	**BLA**	**EC**	**DR**	**MR**
Synapses		F = 3.278	F = 52.08	F = 2.039	F = 3.666	F = 18.29	F = 32.4	F = 38.18	F = 8.863	F = 3.423	F = 3.245	F = 3.773	F = 1.151
		P = 0.0852	P < 0.0001	P = 0.186	P = 0.0684	P = 0.0007	P < 0.0001	P < 0.0001	P = 0.0006	P = 0.0784	P = 0.0869	P = 0.0646	P = 0.3588
5-HT Inhibitory	Interaction	**CG**	**PrL**	**IL**	**NAc**	**LSN**	**CA1**	**CA2-3**	**DG**	**BLA**	**EC**	**DR**	**MR**
Synapses		F = 5.527	F = 35.97	F = 1.216	F = 2.288	F = 4.946	F = 21.37	F = 28.59	F = 5.69	F = 3.332	F = 3.303	F = 2.97	F = 0.8465
		P = 0.0272	P < 0.0001	P = 0.3408	P = 0.1572	P = 0.0356	P < 0.0001	P < 0.0001	P = 0.0063	P = 0.0826	P = 0.084	P = 0.1022	P = 0.4604
5-HT Excitatory	Interaction	**CG**	**PrL**	**IL**	**NAc**	**LSN**	**CA1**	**CA2-3**	**DG**	**BLA**	**EC**	**DR**	**MR**
Presynaptic triad		F = 0.4462	F = 5.826	F = 0.3528	F = 1.998	F = 11	F = 9.936	F = 21.61	F = 3.317	F = 0.774	F = 1.437	F = 1.731	F = 1.041
		P = 0.6535	P = 0.0238	P = 0.712	P = 0.1913	P = 0.0038	P = 0.0003	P < 0.0001	P = 0.0453	P = 0.4896	P = 0.2874	P = 0.2312	P = 0.392
5-HT Inhibitory	Interaction	**CG**	**PrL**	**IL**	**NAc**	**LSN**	**CA1**	**CA2-3**	**DG**	**BLA**	**EC**	**DR**	**MR**
Presynaptic triad		F = 0.4443	F = 3.478	F = 0.1343	F = 1.285	F = 2.081	F = 3.15	F = 10.26	F = 1.015	F = 0.9166	F = 1.287	F = 1.393	F = 1.091
		P = 0.6546	P = 0.076	P = 0.876	P = 0.323	P = 0.1807	P = 0.0524	P = 0.0002	P = 0.3704	P = 0.4342	P = 0.3224	P = 0.2972	P = 0.3764
5-HT Excitatory	Interaction	**CG**	**PrL**	**IL**	**NAc**	**LSN**	**CA1**	**CA2-3**	**DG**	**BLA**	**EC**	**DR**	**MR**
Postynaptic triad		F = 0.1781	F = 3.115	F = 0.07824	F = 1.713	F = 15.79	F = 5.716	F = 16.5	F = 1.648	F = 1.452	F = 1.349	F = 1.932	F = 0.6467
		P = 0.8397	P = 0.0937	P = 0.9254	P = 0.2342	P = 0.0011	P = 0.0061	P < 0.0001	P = 0.2039	P = 0.2841	P = 0.3073	P = 0.2004	P = 0.5465
5-HT Inhibitory	Interaction	**CG**	**PrL**	**IL**	**NAc**	**LSN**	**CA1**	**CA2-3**	**DG**	**BLA**	**EC**	**DR**	**MR**
Postynaptic triad		F = 0.08664	F = 0.5936	F = 0.032	F = 1.322	F = 3.225	F = 0.2041	F = 2.311	F = 0.09379	F = 0.7219	F = 0.9532	F = 1.246	F = 0.7660
		P = 0.9178	P = 0.5726	P = 0.9686	P = 0.3139	P = 0.0879	P = 0.8161	P = 0.1108	P = 0.9106	P = 0.512	P = 0.4212	P = 0.3329	P = 0.4929

References

Albert, P.R., Blier, P., 2023. Does serotonin matter in depression? Journal of Psychiatry and Neuroscience 48, E400–E403. https://doi.org/10.1503/jpn.230130

Albert, P.R., Lembo, P., Storring, J.M., Charest, A., Saucier, C., 1994. The 5-HTIA Receptor: Signaling;, Desensitization, and Gene Transcription. 1996 American College of Neuropsychopharmacology Elsevier Science Inc VOL. 14.

Albert, P.R., Lemonde, S., 2004. 5-HT1A Receptors, Gene Repression, and Depression: Guilt by Association. Neuroscientist 10, 575–593. https://doi.org/10.1177/1073858404267382

Bains, N., Abdijadid, S., 2023. Major Depressive Disorder, in: StatPearls [Internet]. StatPearls Publishing.

Balaram, K., Marwaha, R., 2024. Agoraphobia, in: StatPearls. StatPearls Publishing, Treasure Island (FL).

Berger, M., Gray, J.A., Roth, B.L., 2009. The Expanded Biology of Serotonin. Annual review of medicine 60, 355. https://doi.org/10.1146/annurev.med.60.042307.110802

Berger, S., Gureczny, S., Reisinger, S.N., Horvath, O., Pollak, D.D., 2019. Effect of Chronic Corticosterone Treatment on Depression-Like Behavior and Sociability in Female and Male C57BL/6N Mice. Cells 8, 1018. https://doi.org/10.3390/cells8091018

Beyer, C.E., Cremers, T.I.F.H., 2008. Do selective serotonin reuptake inhibitors acutely increase frontal cortex levels of serotonin? European Journal of Pharmacology 580, 350–354. https://doi.org/10.1016/j.ejphar.2007.11.028

Blumberger, D.M., Hsu, J.H., Daskalakis, Z.J., 2015. A Review of Brain Stimulation Treatments for Late-Life Depression. Curr Treat Options Psych 2, 413–421. https://doi.org/10.1007/s40501-015-0059-0

Boldrini, M., Santiago, A.N., Hen, R., Dwork, A.J., Rosoklija, G.B., Tamir, H., Arango, V., John Mann, J., 2013. Hippocampal Granule Neuron Number and Dentate Gyrus Volume in Antidepressant-Treated and Untreated Major Depression. Neuropsychopharmacol 38, 1068–1077. https://doi.org/10.1038/npp.2013.5

Boyden, E.S., Zhang, F., Bamberg, E., Nagel, G., Deisseroth, K., 2005. Millisecond-timescale, genetically targeted optical control of neural activity. Nat Neurosci 8, 1263–1268. https://doi.org/10.1038/nn1525

Burstein, O., Doron, R., 2018. The Unpredictable Chronic Mild Stress Protocol for Inducing Anhedonia in Mice. J Vis Exp 58184. https://doi.org/10.3791/58184

Cai, H., Xie, X.-M., Zhang, Q., Cui, X., Lin, J.-X., Sim, K., Ungvari, G.S., Zhang, L., Xiang, Y.-T., 2021. Prevalence of Suicidality in Major Depressive Disorder: A Systematic Review and Meta-Analysis of Comparative Studies. Front Psychiatry 12, 690130. https://doi.org/10.3389/fpsyt.2021.690130

Cai, X., Kallarackal, A.J., Kvarta, M.D., Goluskin, S., Gaylor, K., Bailey, A.M., Lee, H.-K., Huganir, R.L., Thompson, S.M., 2013. Local potentiation of excitatory synapses by serotonin and its alteration in rodent models of depression. Nat Neurosci 16, 464–472. https://doi.org/10.1038/nn.3355

Cameron, H.A., Schoenfeld, T.J., 2018. Behavioral and structural adaptations to stress. Frontiers in Neuroendocrinology, Stress and the Brain 49, 106–113. https://doi.org/10.1016/j.yfrne.2018.02.002

Can, A., Dao, D.T., Terrillion, C.E., Piantadosi, S.C., Bhat, S., Gould, T.D., 2012. The Tail Suspension Test. J Vis Exp 3769. https://doi.org/10.3791/3769

Canadian Stroke Congress 2019 Abstract Supplement, 2019. . International Journal of Stroke 14, 3–52. https://doi.org/10.1177/1747493019872147

Cardin, J.A., Carlén, M., Meletis, K., Knoblich, U., Zhang, F., Deisseroth, K., Tsai, L.-H., Moore, C.I., 2010. Targeted optogenetic stimulation and recording of neurons in vivo using cell-type-specific expression of Channelrhodopsin-2. Nat Protoc 5, 247–254. https://doi.org/10.1038/nprot.2009.228

Cipriani, A., Brambilla, P., Furukawa, T.A., Geddes, J., Gregis, M., Hotopf, M., Malvini, L., Barbui, C., 2005. Fluoxetine versus other types of pharmacotherapy for depression. Cochrane Database Syst Rev CD004185. https://doi.org/10.1002/14651858.CD004185.pub2

Cipriani, A., Furukawa, T.A., Salanti, G., Chaimani, A., Atkinson, L.Z., Ogawa, Y., Leucht, S., Ruhe, H.G., Turner, E.H., Higgins, J.P.T., Egger, M., Takeshima, N., Hayasaka, Y., Imai, H., Shinohara, K., Tajika, A., Ioannidis, J.P.A., Geddes, J.R., 2018. Comparative efficacy and acceptability of 21 antidepressant drugs for the acute treatment of adults with major depressive disorder: a systematic review and network meta-analysis. The Lancet 391, 1357–1366. https://doi.org/10.1016/S0140-6736(17)32802-7

Cohen, S., Janicki-Deverts, D., Miller, G.E., 2007. Psychological Stress and Disease. JAMA 298, 1685–1687. https://doi.org/10.1001/jama.298.14.1685

Covington, H.E., Lobo, M.K., Maze, I., Vialou, V., Hyman, J.M., Zaman, S., LaPlant, Q., Mouzon, E., Ghose, S., Tamminga, C.A., Neve, R.L., Deisseroth, K., Nestler, E.J., 2010. Antidepressant Effect of Optogenetic Stimulation of the Medial Prefrontal Cortex. J Neurosci 30, 16082–16090. https://doi.org/10.1523/JNEUROSCI.1731-10.2010

Cryan, J.F., Mombereau, C., Vassout, A., 2005. The tail suspension test as a model for assessing antidepressant activity: Review of pharmacological and genetic studies in mice. Neuroscience & Biobehavioral Reviews, Animal Models of Depression and Antidepressant Activity 29, 571–625. https://doi.org/10.1016/j.neubiorev.2005.03.009

Csabai, D., Wiborg, O., Czéh, B., 2018. Reduced Synapse and Axon Numbers in the Prefrontal Cortex of Rats Subjected to a Chronic Stress Model for Depression. Front. Cell. Neurosci. 12, 24. https://doi.org/10.3389/fncel.2018.00024

Cui, L., Li, S., Wang, S., Wu, X., Liu, Y., Yu, W., Wang, Y., Tang, Y., Xia, M., Li, B., 2024. Major depressive disorder: hypothesis, mechanism, prevention and treatment. Sig Transduct Target Ther 9, 30. https://doi.org/10.1038/s41392-024-01738-y

Cui, Y., Cao, K., Lin, H., Cui, S., Shen, C., Wen, W., Mo, H., Dong, Z., Bai, S., Yang, L., Shi, Y., Zhang, R., 2020. Early-Life Stress Induces Depression-Like Behavior and Synaptic-Plasticity Changes in a Maternal Separation Rat Model: Gender Difference and Metabolomics Study. Front. Pharmacol. 11. https://doi.org/10.3389/fphar.2020.00102

David, D.J., Samuels, B.A., Rainer, Q., Wang, J.-W., Marsteller, D., Mendez, I., Drew, M., Craig, D.A., Guiard, B.P., Guilloux, J.-P., Artymyshyn, R.P., Gardier, A.M., Gerald, C., Antonijevic, I.A., Leonardo, E.D., Hen, R., 2009. Neurogenesis-Dependent and -Independent Effects of Fluoxetine in an Animal Model of Anxiety/Depression. Neuron 62, 479–493. https://doi.org/10.1016/j.neuron.2009.04.017

Delgado, P.L., 2000. Depression: The Case for a Monoamine Deficiency. J Clin Psychiatry.

Deng, Z.-D., Robins, P.L., Regenold, W., Rohde, P., Dannhauer, M., Lisanby, S.H., 2024. How electroconvulsive therapy works in the treatment of depression: is it the seizure, the electricity, or both? Neuropsychopharmacol. 49, 150–162. https://doi.org/10.1038/s41386-023-01677-2

Dieterich, A., Srivastava, P., Sharif, A., Stech, K., Floeder, J., Yohn, S.E., Samuels, B.A., 2019. Chronic corticosterone administration induces negative valence and impairs positive valence behaviors in mice. Transl Psychiatry 9, 1–13. https://doi.org/10.1038/s41398-019-0674-4

Domingo-Rodriguez, L., Ruiz de Azua, I., Dominguez, E., Senabre, E., Serra, I., Kummer, S., Navandar, M., Baddenhausen, S., Hofmann, C., Andero, R., Gerber, S., Navarrete, M., Dierssen, M., Lutz, B., Martín-García, E., Maldonado, R., 2020. A specific prelimbic-nucleus accumbens pathway controls resilience versus vulnerability to food addiction. Nat Commun 11, 782. https://doi.org/10.1038/s41467-020-14458-y

Flint, J., 2023. The genetic basis of major depressive disorder. Mol Psychiatry 28, 2254–2265. https://doi.org/10.1038/s41380-023-01957-9

Flügge, G., van Kampen, M., Mijnster, M.J., 2004. Perturbations in brain monoamine systems during stress. Cell Tissue Res 315, 1–14. https://doi.org/10.1007/s00441-003-0807-0

Frisbee, J.C., Brooks, S.D., Stanley, S.C., d'Audiffret, A.C., 2015. An Unpredictable Chronic Mild Stress Protocol for Instigating Depressive Symptoms, Behavioral Changes and Negative Health Outcomes in Rodents. J Vis Exp 53109. https://doi.org/10.3791/53109

Frontiers | Reduced Synapse and Axon Numbers in the Prefrontal Cortex of Rats Subjected to a Chronic Stress Model for Depression [WWW Document], 2024. URL https://www.frontiersin.org/journals/cellular-neuroscience/articles/10.3389/fncel.2018.00024/full (accessed 7.29.24).

Guo, H., Guo, J., Gao, Z., Luo, F., Zhang, E., 2024. The role of amygdala-ventral pallidum pathway in depression-like behaviors in male mice. J Neurosci Res 102, e25258. https://doi.org/10.1002/jnr.25258

Hamani, C., Machado, D.C., Hipólide, D.C., Dubiela, F.P., Suchecki, D., Macedo, C.E., Tescarollo, F., Martins, U., Covolan, L., Nobrega, J.N., 2012. Deep Brain Stimulation Reverses Anhedonic-Like Behavior in a Chronic Model of Depression: Role of Serotonin and Brain Derived Neurotrophic Factor. Biological Psychiatry, Molecular Substrates of Neuroplasticity in Depression 71, 30–35. https://doi.org/10.1016/j.biopsych.2011.08.025

Hamani, C., Mayberg, H., Stone, S., Laxton, A., Haber, S., Lozano, A.M., 2011. The Subcallosal Cingulate Gyrus in the Context of Major Depression. Biological Psychiatry, Bipolar Disorder: Genes and Brain Development 69, 301–308. https://doi.org/10.1016/j.biopsych.2010.09.034

Hassamal, S., 2023. Chronic stress, neuroinflammation, and depression: an overview of pathophysiological mechanisms and emerging anti-inflammatories. Front. Psychiatry 14. https://doi.org/10.3389/fpsyt.2023.1130989

Healy, D., Leonard, B.E., 1987. Monoamine transport in depression: Kinetics and dynamics. Journal of Affective Disorders 12, 91–103. https://doi.org/10.1016/0165-0327(87)90001-2

Holmes, S.E., Scheinost, D., Finnema, S.J., Naganawa, M., Davis, M.T., DellaGioia, N., Nabulsi, N., Matuskey, D., Angarita, G.A., Pietrzak, R.H., Duman, R.S., Sanacora, G., Krystal, J.H., Carson, R.E., Esterlis, I., 2019. Lower synaptic density is associated with depression severity and network alterations. Nat Commun 10, 1529. https://doi.org/10.1038/s41467-019-09562-7

Jans, L.A.W., Riedel, W.J., Markus, C.R., Blokland, A., 2007. Serotonergic vulnerability and depression: assumptions, experimental evidence and implications. Mol Psychiatry 12, 522–543. https://doi.org/10.1038/sj.mp.4001920

Jin, Y., Dougherty, S.E., Wood, K., Sun, L., Cudmore, R.H., Abdalla, A., Kannan, G., Pletnikov, M., Hashemi, P., Linden, D.J., 2016. Regrowth of Serotonin Axons in the Adult Mouse Brain Following Injury. Neuron 91, 748–762. https://doi.org/10.1016/j.neuron.2016.07.024

Kalueff, A.V., Tuohimaa, P., 2004. Contrasting grooming phenotypes in C57Bl/6 and 129S1/SvImJ mice. Brain Research 1028, 75–82. https://doi.org/10.1016/j.brainres.2004.09.001

Karrouri, R., Hammani, Z., Benjelloun, R., Otheman, Y., 2021. Major depressive disorder: Validated treatments and future challenges. World Journal of Clinical Cases 9, 9350. https://doi.org/10.12998/wjcc.v9.i31.9350

Kim, C.K., Adhikari, A., Deisseroth, K., 2017. Integration of optogenetics with complementary methodologies in systems neuroscience. Nat Rev Neurosci 18, 222–235. https://doi.org/10.1038/nrn.2017.15

Kraus, K.L., Chordia, A.P., Drake, A.W., Herman, J.P., Danzer, S.C., 2022. Hippocampal interneurons are direct targets for circulating glucocorticoids. J Comp Neurol 530, 2100–2112. https://doi.org/10.1002/cne.25322

Kritzer, M.D., Peterchev, A.V., Camprodon, J.A., 2023. Electroconvulsive Therapy: Mechanisms of Action, Clinical Considerations, and Future Directions. Harv Rev Psychiatry 31, 101–113. https://doi.org/10.1097/HRP.0000000000000365

Kubitschke, M., Müller, M., Wallhorn, L., Pulin, M., Mittag, M., Pollok, S., Ziebarth, T., Bremshey, S., Gerdey, J., Claussen, K.C., Renken, K., Groß, J., Gneiße, P., Meyer, N., Wiegert, J.S., Reiner, A., Fuhrmann, M., Masseck, O.A., 2022. Next generation genetically encoded fluorescent sensors for serotonin. Nat Commun 13, 7525. https://doi.org/10.1038/s41467-022-35200-w

Lan, M.J., Chhetry, B.T., Liston, C., Mann, J.J., Dubin, M., 2016. Transcranial Magnetic Stimulation of Left Dorsolateral Prefrontal Cortex Induces Brain Morphological Changes in Regions Associated with a Treatment Resistant Major Depressive Episode; an Exploratory Analysis. Brain Stimul 9, 577–583. https://doi.org/10.1016/j.brs.2016.02.011

Leyton, M., Young, S.N., Blier, P., Ellenbogen, M.A., Palmour, R.M., Ghadirian, A.-M., Benkelfat, C., 1997. The effect of tryptophan depletion on mood in medication-free, former patients with major affective disorder. Neuropsychopharmacology 16, 294–297. https://doi.org/10.1016/S0893-133X(96)00262-X

Lohoff, F.W., 2010. Overview of the Genetics of Major Depressive Disorder. Current psychiatry reports 12, 539. https://doi.org/10.1007/s11920-010-0150-6

Lynall, M.-E., McIntosh, A.M., 2023. The Heterogeneity of Depression. AJP 180, 703–704. https://doi.org/10.1176/appi.ajp.20230574

Maes, M., Kubera, M., Obuchowiczwa, E., Goehler, L., Brzeszcz, J., 2011. Depression's multiple comorbidities explained by (neuro)inflammatory and oxidative & nitrosative stress pathways.

Mann, S.K., Malhi, N.K., 2024. Repetitive Transcranial Magnetic Stimulation, in: StatPearls. StatPearls Publishing, Treasure Island (FL).

Manning, C.E., Eagle, A.L., Kwiatkowski, C.C., Achargui, R., Woodworth, H., Potter, E., Ohnishi, Y., Leinninger, G.M., Robison, A.J., 2019. Hippocampal subgranular zone FosB expression is critical for neurogenesis and learning. Neuroscience 406, 225–233. https://doi.org/10.1016/j.neuroscience.2019.03.022

Mayberg, H.S., Lozano, A.M., Voon, V., McNeely, H.E., Seminowicz, D., Hamani, C., Schwalb, J.M., Kennedy, S.H., 2005. Deep Brain Stimulation for Treatment-Resistant Depression. Neuron 45, 651–660. https://doi.org/10.1016/j.neuron.2005.02.014

McEwen, B.S., 2017. Neurobiological and Systemic Effects of Chronic Stress. Chronic Stress (Thousand Oaks) 1, 2470547017692328. https://doi.org/10.1177/2470547017692328

McEwen, B.S., 1999. STRESS AND HIPPOCAMPAL PLASTICITY. Annual Review of Neuroscience 22, 105–122. https://doi.org/10.1146/annurev.neuro.22.1.105

Meaney, M.J., Diorio, J., Francis, D., Weaver, S., Yau, J., Chapman, K., Seckl, J.R., 2000. Postnatal Handling Increases the Expression of cAMP-Inducible Transcription Factors in the Rat

Hippocampus: The Effects of Thyroid Hormones and Serotonin. J Neurosci 20, 3926–3935. https://doi.org/10.1523/JNEUROSCI.20-10-03926.2000

Meaney, M.J., Diorio, J., Francis, D., Widdowson, J., LaPlante, P., Caldji, C., Sharma, S., Seckl, J.R., Plotsky, P.M., 2010. Early Environmental Regulation of Forebrain Glucocorticoid Receptor Gene Expression: Implications for Adrenocortical Responses to Stress; pp. 49–60. Developmental Neuroscience 18, 49–60. https://doi.org/10.1159/000111395

Mei, Y., Zhang, F., 2012. Molecular Tools and Approaches for Optogenetics. Biological Psychiatry 71, 1033–1038. https://doi.org/10.1016/j.biopsych.2012.02.019

Moncrieff, J., Cooper, R.E., Stockmann, T., Amendola, S., Hengartner, M.P., Horowitz, M.A., 2023. The serotonin theory of depression: a systematic umbrella review of the evidence. Mol Psychiatry 28, 3243–3256. https://doi.org/10.1038/s41380-022-01661-0

Moraczewski, J., Awosika, A.O., Aedma, K.K., 2024. Tricyclic Antidepressants, in: StatPearls. StatPearls Publishing, Treasure Island (FL).

Nemeroff, C.B., Owens, M.J., 2009. The Role of Serotonin in the Pathophysiology of Depression: As Important As Ever. Clinical Chemistry 55, 1578–1579. https://doi.org/10.1373/clinchem.2009.123752

Nestler, E.J., Hyman, S.E., 2010. Animal models of neuropsychiatric disorders. Nat Neurosci 13, 1161–1169. https://doi.org/10.1038/nn.2647

Nollet, M., 2021. Models of Depression: Unpredictable Chronic Mild Stress in Mice. Current Protocols 1, e208. https://doi.org/10.1002/cpz1.208

Ohmura, Y., Tanaka, K.F., Tsunematsu, T., Yamanaka, A., Yoshioka, M., 2014. Optogenetic activation of serotonergic neurons enhances anxiety-like behaviour in mice. International Journal of Neuropsychopharmacology 17, 1777–1783. https://doi.org/10.1017/S1461145714000637

Ohmura, Y., Tsutsui-Kimura, I., Sasamori, H., Nebuka, M., Nishitani, N., Tanaka, K.F., Yamanaka, A., Yoshioka, M., 2020. Different roles of distinct serotonergic pathways in anxiety-like behavior, antidepressant-like, and anti-impulsive effects. Neuropharmacology 167, 107703. https://doi.org/10.1016/j.neuropharm.2019.107703

Ota, K.T., Liu, R.-J., Voleti, B., Maldonado-Aviles, J.G., Duric, V., Iwata, M., Dutheil, S., Duman, C., Boikess, S., Lewis, D.A., Stockmeier, C.A., DiLeone, R.J., Rex, C., Aghajanian, G.K., Duman, R.S., 2014. REDD1 is essential for stress-induced synaptic loss and depressive behavior. Nat Med 20, 531–535. https://doi.org/10.1038/nm.3513

Papp, M., Gruca, P., Lason, M., Litwa, E., Solecki, W., Willner, P., 2022. Optogenetic stimulation of medial prefrontal cortex excites GABAergic cells in the nucleus accumbens and hippocampus of Wistar-Kyoto rats exposed to chronic mild stress. Psychopharmacology 239, 2299–2307. https://doi.org/10.1007/s00213-022-06116-6

Papp, M., Gruca, P., Lason, M., Tota-Glowczyk, K., Niemczyk, M., Litwa, E., Willner, P., 2018. Rapid antidepressant effects of deep brain stimulation of the pre-frontal cortex in an animal model

of treatment-resistant depression. J Psychopharmacol 32, 1133–1140. https://doi.org/10.1177/0269881118791737

Pariante, C.M., Lightman, S.L., 2008. The HPA axis in major depression: classical theories and new developments. Trends in Neurosciences 31, 464–468. https://doi.org/10.1016/j.tins.2008.06.006

Piñeyro, G., Blier, P., 1999. Autoregulation of Serotonin Neurons: Role in Antidepressant Drug Action. Pharmacol Rev 51, 533–591.

Ren, J., Friedmann, D., Xiong, J., Liu, C.D., Ferguson, B.R., Weerakkody, T., DeLoach, K.E., Ran, C., Pun, A., Sun, Y., Weissbourd, B., Neve, R.L., Huguenard, J., Horowitz, M.A., Luo, L., 2018. Anatomically Defined and Functionally Distinct Dorsal Raphe Serotonin Sub-systems. Cell 175, 472-487.e20. https://doi.org/10.1016/j.cell.2018.07.043

Richter-Levin, G., Xu, L., 2018. How could stress lead to major depressive disorder? IBRO Rep 4, 38–43. https://doi.org/10.1016/j.ibror.2018.04.001

Risold, P.Y., 2004. CHAPTER 20 - The Septal Region, in: Paxinos, G. (Ed.), The Rat Nervous System (Third Edition). Academic Press, Burlington, pp. 605–632. https://doi.org/10.1016/B978-012547638-6/50021-3

Rolls, E.T., Cheng, W., Feng, J., 2020. The orbitofrontal cortex: reward, emotion and depression. Brain Commun 2, fcaa196. https://doi.org/10.1093/braincomms/fcaa196

Seibenhener, M.L., Wooten, M.C., 2015. Use of the Open Field Maze to Measure Locomotor and Anxiety-like Behavior in Mice. J Vis Exp 52434. https://doi.org/10.3791/52434

Selective Serotonin Reuptake Inhibitors (SSRIs) [WWW Document], 2024. URL https://elsevier.health/en-US/preview/selective-serotonin-reuptake-inhibitors-ssris (accessed 8.6.24).

Selten, M., van Bokhoven, H., Nadif Kasri, N., 2018. Inhibitory control of the excitatory/inhibitory balance in psychiatric disorders. F1000Res 7, 23. https://doi.org/10.12688/f1000research.12155.1

Sub Laban, T., Saadabadi, A., 2024. Monoamine Oxidase Inhibitors (MAOI), in: StatPearls. StatPearls Publishing, Treasure Island (FL).

Sun, D., Mei, L., Xiong, W.-C., 2023. Dorsal Dentate Gyrus, a Key Regulator for Mood and Psychiatric Disorders. Biological Psychiatry 93, 1071–1080. https://doi.org/10.1016/j.biopsych.2023.01.005

Tanila, H., 2018. Testing cognitive functions in rodent disease models: Present pitfalls and future perspectives. Behavioural Brain Research, Animal Model of the Year 2036: Novel Perspectives in Behavioral Neuroscience 352, 23–27. https://doi.org/10.1016/j.bbr.2017.05.040

Ting, J.T., Feng, G., 2013. Development of transgenic animals for optogenetic manipulation of mammalian nervous system function: Progress and prospects for behavioral neuroscience. Behav Brain Res 255, 3–18. https://doi.org/10.1016/j.bbr.2013.02.037

Turcotte-Cardin, V., Vahid-Ansari, F., Luckhart, C., Daigle, M., Geddes, S.D., Tanaka, K.F., Hen, R., James, J., Merali, Z., Béïque, J.-C., Albert, P.R., 2019. Loss of Adult 5-HT1A Autoreceptors Results in a Paradoxical Anxiogenic Response to Antidepressant Treatment. J. Neurosci. 39, 1334–1346. https://doi.org/10.1523/JNEUROSCI.0352-18.2018

Vahid-Ansari, F., Albert, P.R., 2021. Rewiring of the Serotonin System in Major Depression. Front. Psychiatry 12, 802581. https://doi.org/10.3389/fpsyt.2021.802581

Vahid-Ansari, F., Albert, P.R., 2018. Chronic Fluoxetine Induces Activity Changes in Recovery From Poststroke Anxiety, Depression, and Cognitive Impairment. Neurotherapeutics 15, 200–215. https://doi.org/10.1007/s13311-017-0590-3

Vahid-Ansari, F., Zhang, M., Zahrai, A., Albert, P.R., 2019. Overcoming Resistance to Selective Serotonin Reuptake Inhibitors: Targeting Serotonin, Serotonin-1A Receptors and Adult Neuroplasticity. Front. Neurosci. 13. https://doi.org/10.3389/fnins.2019.00404

Van Der Wal, J.M., Bergfeld, I.O., Lok, A., Mantione, M., Figee, M., Notten, P., Beute, G., Horst, F., Van Den Munckhof, P., Schuurman, P.R., Denys, D., 2020. Long-term deep brain stimulation of the ventral anterior limb of the internal capsule for treatment-resistant depression. J Neurol Neurosurg Psychiatry 91, 189–195. https://doi.org/10.1136/jnnp-2019-321758

Veerakumar, A., Challis, C., Gupta, P., Da, J., Upadhyay, A., Beck, S.G., Berton, O., 2014. Antidepressant-like Effects of Cortical Deep Brain Stimulation Coincide With Pro-neuroplastic Adaptations of Serotonin Systems. Biological Psychiatry, Neurostimulation Treatments for Depression 76, 203–212. https://doi.org/10.1016/j.biopsych.2013.12.009

Walz, N., Mühlberger, A., Pauli, P., 2016. A Human Open Field Test Reveals Thigmotaxis Related to Agoraphobic Fear. Biological Psychiatry, Corticotropin-Releasing Factor, FKBP5, and Posttraumatic Stress Disorder 80, 390–397. https://doi.org/10.1016/j.biopsych.2015.12.016

Wang, Q., Timberlake, M.A., Prall, K., Dwivedi, Y., 2017. The Recent Progress in Animal Models of Depression. Prog Neuropsychopharmacol Biol Psychiatry 77, 99–109. https://doi.org/10.1016/j.pnpbp.2017.04.008

Warden, M.R., Selimbeyoglu, A., Mirzabekov, J.J., Lo, M., Thompson, K.R., Kim, S.-Y., Adhikari, A., Tye, K.M., Frank, L.M., Deisseroth, K., 2012. A prefrontal cortex–brainstem neuronal projection that controls response to behavioural challenge. Nature 492, 428–432. https://doi.org/10.1038/nature11617

Warner-Schmidt, J., 2013. Treating the Brain Deep Down: Short-circuiting depression. Nat Med 19, 680–681. https://doi.org/10.1038/nm.3215

Wong, D.T., Perry, K.W., Bymaster, F.P., 2005. The Discovery of Fluoxetine Hydrochloride (Prozac). Nat Rev Drug Discov 4, 764–774. https://doi.org/10.1038/nrd1821

Wyler, S.C., Spencer, W.C., Green, N.H., Rood, B.D., Crawford, L., Craige, C., Gresch, P., McMahon, D.G., Beck, S.G., Deneris, E., 2016. Pet-1 Switches Transcriptional Targets Postnatally

to Regulate Maturation of Serotonin Neuron Excitability. J Neurosci 36, 1758–1774. https://doi.org/10.1523/JNEUROSCI.3798-15.2016

Xu, L., Nan, J., Lan, Y., 2020. The Nucleus Accumbens: A Common Target in the Comorbidity of Depression and Addiction. Front. Neural Circuits 14. https://doi.org/10.3389/fncir.2020.00037

Yang, L., Zhao, Y., Wang, Y., Liu, L., Zhang, X., Li, B., Cui, R., 2015. The Effects of Psychological Stress on Depression. Curr Neuropharmacol 13, 494–504. https://doi.org/10.2174/1570159X1304150831150507

Yaribeygi, H., Panahi, Y., Sahraei, H., Johnston, T.P., Sahebkar, A., 2017. The impact of stress on body function: A review. EXCLI J 16, 1057–1072. https://doi.org/10.17179/excli2017-480

Young, S.N., Ervin, F.R., Pihl, R.O., Finn, P., 1989. Biochemical aspects of tryptophan depletion in primates [WWW Document]. CoLab. URL https://colab.ws/articles/10.1007%2Fbf00441950 (accessed 8.6.24).

Zahrai, A., Vahid-Ansari, F., Daigle, M., Albert, P.R., 2020. Fluoxetine-induced recovery of serotonin and norepinephrine projections in a mouse model of post-stroke depression. Transl Psychiatry 10, 334. https://doi.org/10.1038/s41398-020-01008-9

Zeng, H., Madisen, L., 2012. Mouse transgenic approaches in optogenetics. Prog Brain Res 196, 193–213. https://doi.org/10.1016/B978-0-444-59426-6.00010-0

Zolfaghari, F.S., Pirri, F., Gauvin, E., Peeri, M., Amiri, S., 2021. Exercise and fluoxetine treatment during adolescence protect against early life stress-induced behavioral abnormalities in adult rats. Pharmacology Biochemistry and Behavior 205, 173190. https://doi.org/10.1016/j.pbb.2021.173190